The Planetary and Lunar Ephemerides DE430 and DE431

**William M. Folkner,* James G. Williams,† Dale H. Boggs,†
Ryan S. Park,* and Petr Kuchynka***

ABSTRACT. — The planetary and lunar ephemerides DE430 and DE431 are generated by fitting numerically integrated orbits of the Moon and planets to observations. The present-day lunar orbit is known to submeter accuracy through fitting lunar laser ranging data with an updated lunar gravity field from the Gravity Recovery and Interior Laboratory (GRAIL) mission. The orbits of the inner planets are known to subkilometer accuracy through fitting radio tracking measurements of spacecraft in orbit about them. Very long baseline interferometry measurements of spacecraft at Mars allow the orientation of the ephemeris to be tied to the International Celestial Reference Frame with an accuracy of 0″.0002. This orientation is the limiting error source for the orbits of the terrestrial planets, and corresponds to orbit uncertainties of a few hundred meters. The orbits of Jupiter and Saturn are determined to accuracies of tens of kilometers as a result of fitting spacecraft tracking data. The orbits of Uranus, Neptune, and Pluto are determined primarily from astrometric observations, for which measurement uncertainties due to the Earth's atmosphere, combined with star catalog uncertainties, limit position accuracies to several thousand kilometers. DE430 and DE431 differ in their integrated time span and lunar dynamical modeling. The dynamical model for DE430 included a damping term between the Moon's liquid core and solid mantle that gives the best fit to lunar laser ranging data but that is not suitable for backward integration of more than a few centuries. The ephemeris DE431 is similar to DE430 but was fit without the core/mantle damping term, so the lunar orbit is less accurate than in DE430 for times near the current epoch, but is more suitable for times more than a few centuries in the past. DE431 is a longer integration (covering years –13,200 to +17,191) than DE430 (covering years 1550 to 2650).

I. Introduction

The planetary and lunar ephemeris DE430 succeeds the ephemeris DE421 [1] and its precursor DE405 [2] as a general purpose ephemeris. Several interim ephemerides have been released since DE421 with specific improvements in estimates of the orbits of Mercury, Mars, and Saturn intended primarily to support the Mercury Surface, Space Environment,

* Mission Design and Navigation Section.
† Tracking Systems and Applications Section.

The research described in this publication was carried out by the Jet Propulsion Laboratory, California Institute of Technology, under a contract with the National Aeronautics and Space Administration.

Geochemistry, and Ranging (MESSENGER), Mars Science Laboratory, and Cassini missions. These interim ephemerides had small deficiencies in other areas, particularly the lunar librations. DE430 has been updated for all bodies, including the Moon.

The positions and velocities of the Sun, Earth, Moon, and planets, along with the orientation of the Moon, result from a numerically integrated dynamical model. They are stored as Chebyshev polynomial coefficients fit in 32-day-long segments [3]. DE430 also includes Chebyshev polynomial coefficients fit to a numerically integrated difference between ephemeris coordinate time and terrestrial time. Parameters of the dynamical model have been adjusted to fit measurements of the relative positions of the planets and Moon with respect to Earth. The dynamical model is similar to that used for DE405 [4], but includes a model for the fluid core of the Moon [5,6] and an updated treatment of asteroids. The coordinate system and units are similar to those used for DE421 and DE405, but include changes to the definition of coordinate time and the astronomical unit.

Perturbations from 343 asteroids have been included in the dynamical model. The asteroid orbits were iteratively integrated with the positions of the planets, the Sun, and the Moon. The set of 343 asteroids is identical to the set used in DE421. The set represents 90 percent of the total mass of the main belt and contains the asteroids with the most significant effects on the orbit of Mars in terms of perturbation amplitude and frequency [7]. For DE421, a limited number of individual asteroid mass parameters were estimated, with the rest of the asteroid mass parameters determined by dividing them into three taxonomic classes, estimating a constant density for each class, and using volumes estimated from Infrared Astronomical Satellite (IRAS) observations [8]. For DE430, we estimated the mass parameter for each asteroid individually subject to a priori values and uncertainties for volume and density derived from the Wide-field Infrared Survey Explorer (WISE) and the Supplemental IRAS Minor Planet Survey (SIMPS) [9,10].

The lunar dynamical model for DE430 includes interaction between the rotation of the fluid core and the mantle. The effect of this interaction is clearly seen in lunar laser ranging (LLR) data and characterizes a damping in the differential rotation between the core and mantle. Because the initial conditions of the lunar core cannot be determined perfectly, error grows in backward integrations when this interaction model is included. Consequently, the DE430 time span has been limited to the years 1550 to 2650. Further information on the lunar coordinate system and data reduction is available elsewhere.[1]

In order to provide a general ephemeris covering several thousand years, a lunar model without the core–mantle interaction term has been used for the ephemeris DE431. DE430 and DE431 have been fit to the same data. The difference in the orbits of the planets between DE430 and DE431 is less than 1 m over the DE430 time span, which is well below the estimated uncertainties from the fit. The difference in the orbit of the Moon between DE430 and DE431 is less than 1 m during the time span of the LLR data, 1970 to 2012, but grows over longer times primarily due to a difference in estimated tidal acceleration. Figure 1 shows a plot of the difference between the lunar orbit in DE430 and DE431.

[1] J. G. Williams, D. H. Boggs, and W. M. Folkner, "DE430 Lunar Orbit, Physical Librations and Surface Coordinates," JPL Interoffice Memorandum 335-JW,DB,WF-20130722-016 (internal document), Jet Propulsion Laboratory, Pasadena, California, July 22, 2013.

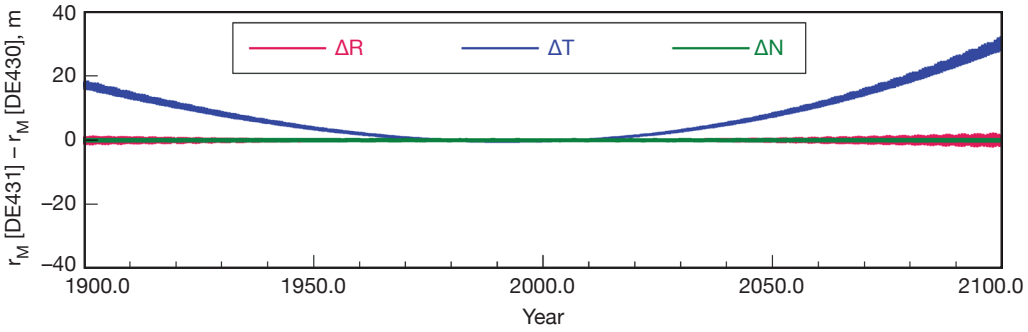

Figure 1. Difference in lunar orbit of DE431 and DE430 in radial (R), along-track (T), and normal (N) components.

DE430 should be used to analyze modern data. DE431 is suitable for the analysis of earlier historical observations of the Sun, Moon, and planets. The DE431 time span from the year –13,200 to the year 17,191 extends far beyond historical times and caveats are offered. For the planets, uncertainties in the initial conditions of the orbits will cause errors in the along-track directions that increase at least linearly with time away from the present. Resonances including, but not limited to, those between Jupiter and Saturn, and between Uranus, Neptune, and Pluto, may complicate the propagation of errors. Typically, the along-track component will degrade faster than the other two components. For the Moon, the uncertainty given for the tidal acceleration causes a 28 m/century^2 along-track uncertainty. But there are other concerns, e.g., the theory for the orientation of Earth includes polynomial expressions that are adequate for thousands of years, but are not designed for much longer times.

Compared with DE421, DE430 and DE431 have been fit to additional data for the Moon and planets. The lunar orbit has been improved through use of additional LLR data, and an improved gravity field of the Moon from the Gravity Recovery and Interior Laboratory (GRAIL) mission. The orbit of Mercury has been improved through use of range measurements to the MESSENGER spacecraft after it entered orbit about Mercury. The orbits of Venus, Earth, and Mars have been improved though additional very long baseline interferometry (VLBI) observations and additional range measurements to Venus Express, Mars Express, Mars Odyssey, and Mars Reconnaissance Orbiter. A more accurate orbit of Saturn has been achieved primarily due to improved treatment of range measurements to the Cassini spacecraft. The orbit of Pluto has been improved through additional observations from several observatories. The orbits of Jupiter, Uranus, and Neptune are not significantly different from those in DE421, although additional astrometric observations have been included.

Improvements for the orbits of Mercury and Pluto are expected in the next year. The MESSENGER data used for DE430 and DE431 are from the first year in orbit about Mercury. During that time, the spacecraft orbit pericenter was always over the northern hemisphere. Lack of Doppler measurements at low altitude over the southern hemisphere limited the accuracy of the estimated Mercury gravity field and spacecraft trajectory. Data from a second year with the pericenter over the southern hemisphere are available but had not been processed at the time of the DE430 and DE431 fit. An improved orbit for Pluto is needed for

the New Horizons mission. Additional measurements and improved processing of existing data are in progress.

The coordinate system for DE430 and DE431 is described in Section II. The dynamical model for translation is described in Section III. The dynamical model for the orientation of the Moon is described in Section IV. Section V describes the data to which the dynamical parameters have been adjusted. The initial conditions and dynamical constants are given in Section VI.

II. Planetary Ephemeris Coordinates

A. Orientation of Axes

The coordinate system is defined by axes aligned with the International Celestial Reference System (ICRS), with the *XY* plane close to the mean equator of epoch J2000.0 and the *X*-axis close to the intersection of the mean equator of J2000.0 with the mean ecliptic plane.[2] The ICRS is currently realized by the positions of extragalactic radio sources given in the Second Realization of the International Celestial Reference Frame (ICRF2) [11] adopted by the International Astronomical Union (IAU) in 2009.[3] The orbits of the inner planets are aligned with ICRF2 with an accuracy of 0″.0002 through use of VLBI observations of spacecraft in orbit about Mars.[4]

Analysis of VLBI observations relative to ICRF2 indicates a secular drift in aberration consistent with the solar system orbiting about the center of the galaxy [12]. This effect is not modeled in ICRF2 or in the ephemerides DE430 and DE431. It may need to be taken into account in future ephemerides as measurement accuracies improve.

B. Solar System Barycenter

The origin of the ICRS is the solar system barycenter.[5] For DE430 and DE431, the barycenter is approximated using the invariant quantities of the *n*-body metric used to model the point mass interactions of the Sun, Moon, planets, and asteroids (see Section III.A). The mass/energy of the system $\mathcal{M}$ is a conserved quantity where $\mathcal{M}$ is defined by[6]

$$\mathcal{M} = \sum_A \mu_A^* \tag{1}$$

where the summation is over all bodies (Sun, Moon, planets, and asteroids) and

$$\mu_A^* = GM_A \left\{ 1 + \frac{1}{2c^2} v_A^2 - \frac{1}{2c^2} \sum_{B \neq A} \frac{GM_B}{r_{AB}} \right\} \tag{2}$$

---

[2] 21st International Astronomical Union General Assembly, Resolution B2, 1991.

[3] 27th International Astronomical Union General Assembly, Resolution B3, 2009.

[4] W. M. Folkner and J. S. Border, "Linking the Planetary Ephemeris to the International Celestial Reference Frame," *Highlights of Astronomy,* vol. 16 (in press).

[5] 24th International Astronomical Union General Assembly, Resolution B1.3, 2000.

[6] F. B. Estabrook, "Derivation of Relativistic Lagrangian for *n*-body Equations Containing Relativity Parameters β and γ," JPL Interoffice Memorandum (internal document), Jet Propulsion Laboratory, Pasadena, California, 1971.

where GM_A is the mass parameter of body A, $r_{AB} = |\mathbf{r}_A - \mathbf{r}_B|$ is the distance between body A at position $\mathbf{r}_A$ and body B at position $\mathbf{r}_A$, $v_A = |\mathbf{v}_\mathbf{A}|$ is the magnitude of the velocity of body A, and c is the speed of light. The momentum $\mathbf{P}$ is also conserved where $\mathbf{P}$ is given by

$$\mathbf{P} = \frac{d}{dt}\left[\sum_A \mu_A^* \mathbf{r}_\mathbf{A}\right]. \tag{3}$$

The position of the center of mass/energy $\mathbf{R}$ is given by

$$\mathbf{R} = \left(\sum_A \mu_A^* \mathbf{r}_A\right) / \left(\sum_A \mu_A^*\right). \tag{4}$$

The velocity of the center of mass/energy $\mathbf{V} = d\mathbf{R}/dt = \mathbf{P}/\mathcal{M}$ is invariant for the n-body metric since $\mathbf{P}$ and $\mathcal{M}$ are invariant.

For DE430 and DE431, the initial positions and velocities of the Moon and planets with respect to the Sun were estimated, and the positions and velocities of the asteroids with respect to the Sun were estimates from the Horizons online solar system data service [13]. The initial position and velocity of the Sun were computed by setting $\mathbf{R}$ and $\mathbf{V}$ to zero. The positions of the Sun, Moon, planets, and asteroids were then integrated using the equations of motion given in Sections III and IV. Because the equations of motion include extended body effects not included in the n-body metric, the center of mass/energy as defined by Equation (4) is not an exact invariant. The position of the center of mass/energy moves with respect to the origin of the coordinate system by less than 1 mm/century, as shown in Figure 2. This motion is near the numerical noise of the stored ephemeris and is small compared with current measurement accuracy.

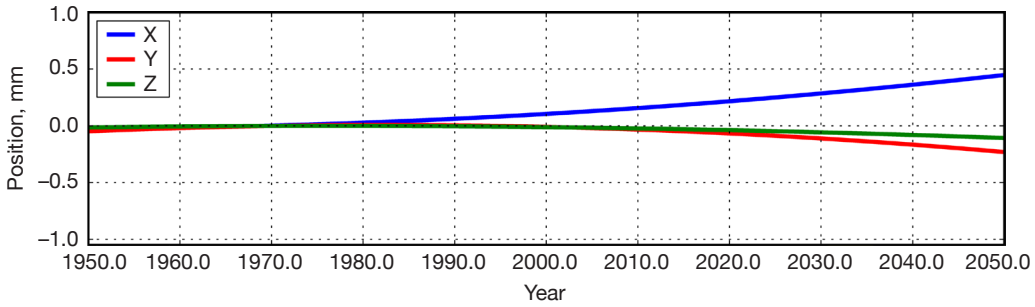

Figure 2. Coordinates of the solar system barycenter of DE430 computed using a translational invariant for the *n*-body metric.

Previous JPL ephemerides have implemented the barycenter in different manners. For DE421, the positions of the Moon and planets were integrated using the equations of motion while the position and velocity of the Sun were computed at each integration time step such that $\mathbf{R}$ and $\mathbf{V}$ remained zero. For DE405, the position of the Sun was integrated, with the initial position and velocity of the Sun computed by setting $\mathbf{R}$ and $\mathbf{V}$ to zero, except that the rate of change of μ_A^* was neglected in computing the initial velocity of the Sun. As a consequence, the position of the barycenter as computed using Equation (4) for

DE405 changed with time by approximately 0.5 m/century [14]. This drift has no measurable consequences on the relative motions of the Sun, Moon, and planets.

The location of the barycenter relative to the Sun, Moon, and planets depends on the set of bodies modeled. In particular, inclusion of trans-Neptunian objects such as Sedna and Eris in the ephemerides from the Institute of Applied Astronomy [15] causes a difference of the location of the barycenter with respect to the Sun of about 100 km. The change in barycenter does not significantly affect the relative positions of the Sun, Moon, and planets.

C. Ephemeris Coordinate Time

The coordinate time scale used for DE430 and DE431 is Barycentric Dynamical Time (TDB) as defined in terms of Barycentric Coordinate Time (TCB).[7,8] For purposes of measurement reduction, the difference between International Atomic Time (TAI) and TDB is needed at the point the measurement is made. An intermediate time, Terrestrial Time (TT), is introduced, where $TT = TAI + 32.184s$. The quantity TDB–TT as a function of TDB is given by

$$\begin{aligned} TDB - TT = {} & \frac{L_G - L_B}{1 - L_B}(TDB - T_0) + \frac{1 - L_G}{1 - L_B} TDB_0 \\ & + \frac{1 - L_G}{1 - L_B} \int_{T_0 + TDB_0}^{TDB} \frac{1}{c^2}\left(\frac{v_E^2}{2} + w_{0E} + w_{LE} \right) dt + \frac{1}{c^2} \mathbf{v}_\mathbf{E} \cdot \left(\mathbf{r}_S - \mathbf{r}_E \right) \\ & - \frac{1 - L_G}{1 - L_B} \int_{T_0 + TDB_0}^{TDB} \frac{1}{c^4}\left(-\frac{v_e^4}{8} - \frac{3}{2} v_E^2 w_{0E} + 4 \mathbf{v}_E \cdot \mathbf{w}_{AE} + \frac{1}{2} w_{0E}^2 + \Delta_E \right) dt \\ & + \frac{1}{c^4}\left(3 w_{0E} + \frac{v_E^2}{2} \right) \mathbf{v}_E \cdot (\mathbf{r}_S - \mathbf{r}_E) \end{aligned} \tag{5}$$

where, for this expression, TDB and TT are measured in Julian days, T_0 is the Julian day 2443144.5003725, $TDB_0 = 65.5 \times 10^{-6}/86400$ days, c is the speed of light, $L_G = 6.969290134 \times 10^{-10}$ defines the rate of TT with respect to Geocentric Coordinate Time (TCG), $L_B = 1.550519768 \times 10^{-8}$ defines the rate of TDB with respect to TCB, $\mathbf{v}_\mathbf{E}$ is the velocity of the Earth, $\mathbf{r}_\mathbf{S}$ is the position of the measurement station, and $\mathbf{r}_\mathbf{E}$ is the position of the Earth. Positions and velocities are all with respect to the solar system barycenter. w_{0E} is the potential at the geocenter due to external point masses that is given by

$$w_{0E} = \sum_{A \neq E} \frac{GM_A}{r_{AE}} \tag{6}$$

with the summation over all modeled bodies A other than the Earth. w_{LE} is the potential at the Earth due to external oblate figures of external bodies, where for computation of TDB–TT for DE430 and DE431, only the effect of the oblateness of the Sun is included, as given by

---

[7] 21st International Astronomical Union General Assembly, Resolution B2, 1991.

[8] 24th International Astronomical Union General Assembly, Resolution B1.3, 2000.

$$w_{LE} = -\frac{GM_{\odot} J_{2\odot}}{|\boldsymbol{r}_{\odot} - \boldsymbol{r}_E|^3} R_{\odot}^2 \frac{1}{2}\left(3\sin\varphi_{E,\odot}^2 - 1\right) \tag{7}$$

where $J_{2\odot}$ is the unnormalized second-degree zonal harmonic of the Sun's gravitational potential, $R_{\odot}$ is the radius of the Sun, and $\varphi_{E,\odot}$ is the latitude of the Earth relative to the Sun's equator. $\mathbf{w}_{AE}$ is the sum of the product of the potential of external point masses times their velocities given by

$$\mathbf{w}_{AE} = \sum_{A \neq E} \frac{GM_A \mathbf{v}_A}{r_{AE}} \tag{8}$$

and Δ_E is given by

$$\Delta_E = \sum_{A \neq E} \frac{GM_A}{r_{AE}} \left[-2v_A^2 + \sum_{B \neq A} \frac{GM_B}{r_{AB}} + \frac{1}{2}\left(\frac{\mathbf{v}_A \cdot (\mathbf{r}_E - \mathbf{r}_A)}{r_{AE}} \right)^2 + \frac{1}{2}\mathbf{a}_A \cdot \left(\mathbf{r}_E - \mathbf{r}_A\right) \right] \tag{9}$$

where $\mathbf{a}_A$ is the acceleration of body A. Equation (5) is based on [16]. It is essentially the same as used in [17]. The relations between the various time scales are summarized in the IERS 2010 Conventions [18]. Several of the terms included, specifically the contributions of the asteroids and the solar oblateness, are small compared with current measurement accuracies.

For DE430 and DE431, the negative of the quantity TDB–TT from Equation (5) evaluated at the geocenter has been numerically integrated and saved as a set of Chebyshev polynomial coefficients in a format similar to the positions and velocities of the bodies. For measurement reduction, TT–TDB as a function of TT is also needed; it can be computed by a simple iterative technique.

Figure 3 shows the difference in the integrated value of TT–TDB and the numerically integrated time ephemeris based on DE405 (TE405) [19]. A constant difference of 65.5 μs was introduced in the current definition of TDB and has been subtracted from the difference. The slope of ~5.7 ns/century is another consequence of the current definition of TDB. At the time TE405 was integrated, the definition of TDB was different and not strictly suitable for use as ephemeris coordinate time. The ephemeris coordinate time was labeled T_{eph} and the definition of T_{eph} included an adjusted constant to ensure no average rate of T_{eph} with respect to TAI. The slope in the difference between TT–TDB for DE430 and TE405 seen in Figure 3 is similar to the results for the INPOP08 ephemeris [17]. This slope causes differences in the reduction of planetary data that are small compared with current measurement accuracies. The small "ripple" about the mean slope of the difference is due to inclusion of the effects of asteroids in Equation (5) that are small and were not included in TE405.

D. Astronomical Unit

The JPL planetary ephemerides have been integrated with position coordinates in astronomical units. For ephemerides prior to DE430, the astronomical unit (au) was estimated

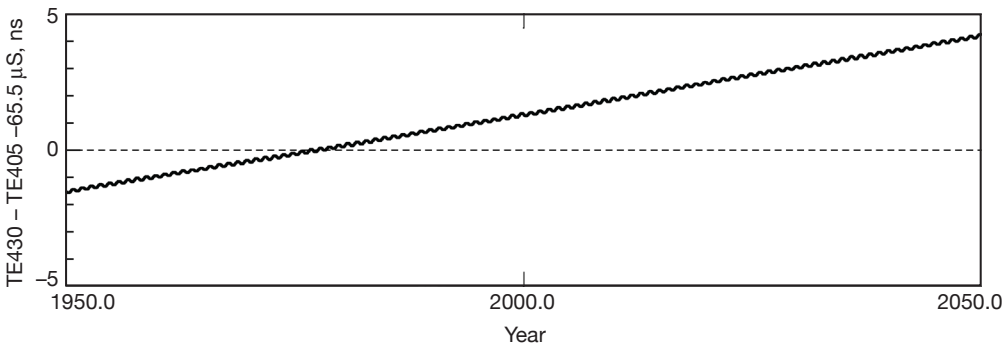

Figure 3. Difference between TT–TDB at the geocenter integrated from DE430 (TE430) and the comparable quantity integrated from DE405 [19] after removing a constant 65.5 μs.

(in km) for each ephemeris, basically enabling conversion of the mass parameter of the Sun from units of au^3/day^2 to units of km^3/s^2. The mass parameter of the Sun was defined by $GM_\odot = k^2$, where Gauss's constant $k = 0.01720209895$ is a defined value. With the introduction of the TCB time scale, and with modern data nearly accurate enough to measure the rate of change of $GM_\odot$, the astronomical unit is now defined to be 149597870.700 km in all time scales.[9] $GM_\odot$ in units of au^3/day^2 is now an estimated quantity. For DE430 and DE431, $GM_\odot$ has been set to k^2 since our current estimate is consistent with this value given the current value of the au [20].

While the JPL ephemerides have been integrated with coordinates given in au, the positions for each ephemeris have been scaled by the appropriate value of the au to units of km and fit to Chebyshev polynomials for distribution to users. Many programs that read the JPL ephemerides automatically convert the interpolated values of coordinates from units of km to au. Users should now be aware of the value of the au they prefer to be used for this conversion.

E. Orientation of the Moon

The orientation of the lunar exterior (mantle and crust, hereafter referred to by mantle) is parameterized by Euler angles, ϕ_m, θ_m, and ψ_m, that relate the Moon-centered, rotating lunar mantle to the inertial frame. The Moon is distorted by tides and rotation. The mantle coordinate system is defined by the principal axes of the undistorted mantle in which the moment of inertia matrix of the undistorted mantle is diagonal. The directions of the principal axes are estimated from analysis of LLR data. The Euler angles that define the rotation from the principal axis (PA) frame to the inertial ICRF2 frame are: ϕ_m, the angle from the X-axis of the inertial frame along the XY plane to the intersection of the mantle equator; θ_m, the inclination of the mantle equator from the inertial XY plane; and ψ_m, the longitude from the intersection of the inertial XY plane with the mantle equator along the mantle equator to the prime meridian.

Position vectors expressed in coordinates along the principal axes, $\mathbf{r}_{PA}$, can be expressed as coordinate vectors in inertial space $\mathbf{r}_I$ using the relation

[9] 28th International Astronomical Union General Assembly, Resolution B2, 2012.

$$\mathbf{r}_I = \mathcal{R}_z(-\phi_m)\mathcal{R}_x(-\theta_m)\mathcal{R}_z(-\psi_m)\mathbf{r}_{PA} \tag{10}$$

where the rotation matrices $\mathcal{R}_x$, $\mathcal{R}_y$, and $\mathcal{R}_z$ are right-handed rotations of frame orientations defined by

$$\mathcal{R}_x(\alpha) = \begin{pmatrix} 1 & 0 & 0 \\ 0 & \cos\alpha & \sin\alpha \\ 0 & -\sin\alpha & \cos\alpha \end{pmatrix} \tag{11}$$

$$\mathcal{R}_y(\alpha) = \begin{pmatrix} \cos\alpha & 0 & -\sin\alpha \\ 0 & 1 & 0 \\ \sin\alpha & 0 & \cos\alpha \end{pmatrix} \tag{12}$$

$$\mathcal{R}_z(\alpha) = \begin{pmatrix} \cos\alpha & \sin\alpha & 0 \\ -\sin\alpha & \cos\alpha & 0 \\ 0 & 0 & 1 \end{pmatrix}. \tag{13}$$

The mantle Euler angles are numerically integrated along with the positions of the bodies. Instead of integrating the Euler angles using second-order equations, they are integrated using first-order equations with time derivatives computed in terms of the angular velocity of the mantle. The angular velocity of the mantle is integrated using its time derivative that is computed from the torques acting on the Moon, as described in Section IV. The time derivatives of the Euler angles are related to the angular velocity of the mantle expressed in the mantle frame, $\boldsymbol{\omega}_m$, by

$$\begin{aligned} \dot{\phi}_m &= (\omega_{m,x}\sin\psi_m + \omega_{m,y}\cos\psi_m)/\sin\theta_m \\ \dot{\theta}_m &= \omega_{m,x}\cos\psi_m - \omega_{m,y}\sin\psi_m \\ \dot{\psi}_m &= \omega_{m,z} - \dot{\phi}_m\cos\theta_m. \end{aligned} \tag{14}$$

The model for the Moon includes a fluid core. The orientation of the core with respect to the inertial frame is described by the Euler angles ϕ_c, θ_c, and ψ_c that are defined and numerically integrated in the same manner as the Euler angles for the mantle. As was done for the mantle, the Euler angles for the core are integrated using coupled first-order equations along with the core angular velocity. However, since the shape of the core is modeled as fixed to the frame of the mantle, it is more convenient to express and integrate the core angular velocity expressed in the mantle frame. The time derivatives of the core Euler angles are then computed by

$$\begin{aligned} \dot{\phi}_c &= \omega^{\dagger}_{c,z} - \dot{\psi}_c\cos\theta_c \\ \dot{\theta}_c &= \omega^{\dagger}_{c,x} \\ \dot{\psi}_c &= -\omega^{\dagger}_{c,y}/\sin\theta_c \end{aligned} \tag{15}$$

where the coordinate vector of core angular velocity in the mantle frame $\boldsymbol{\omega}_c$ is related to the coordinate vector $\boldsymbol{\omega}^{\dagger}_c$ in a frame defined by the intersection of the core equator with the inertial XY plane by

$$\boldsymbol{\omega}_c^{\dagger} = \mathcal{R}_z(\phi_c - \phi_m)\mathcal{R}_x(-\theta_m)\mathcal{R}_z(-\psi_m)\boldsymbol{\omega}_c. \tag{16}$$

Alternatively, the time derivatives of the core Euler angles can be computed using the angular velocity of the core expressed in the core frame $\boldsymbol{\omega}_c^{\ddagger}$ by

$$\begin{aligned}
\dot{\phi}_c &= \left(\omega_{c,x}^{\ddagger}\sin\psi_c + \omega_{c,y}^{\ddagger}\cos\psi_c\right)/\sin\theta_c \\
\dot{\theta}_c &= \omega_{c,x}^{\ddagger}\cos\psi_c - \omega_{c,y}^{\ddagger}\sin\psi_c \\
\dot{\psi}_c &= \omega_{c,z}^{\ddagger} - \dot{\phi}_c\cos\theta_c
\end{aligned} \tag{17}$$

and the core angular velocity expressed in the core frame is given by

$$\boldsymbol{\omega}_c^{\ddagger} = \mathcal{R}_z(\psi_c)\mathcal{R}_x(\theta_c)\mathcal{R}_z(\phi_c)\mathcal{R}_z(-\phi_m)\mathcal{R}_x(-\theta_m)\mathcal{R}_z(-\psi_m)\boldsymbol{\omega}_c. \tag{18}$$

While the orientation for the mantle and core are both numerically integrated, only the mantle Euler angles and mantle angular velocity are distributed with the planetary ephemerides. The initial values for the core Euler angles and the core angular velocity, with the latter expressed in the mantle frame, are given in Table 7 (see page 49).

The locations of features on the lunar crust are usually given by coordinates expressed in the mean-Earth/mean-rotation (MER) frame, where the *X* axis is defined by the body-fixed axis that points toward the mean Earth direction and the *Z* axis points toward the mean rotation axis direction. Coordinate vectors in the MER frame are related to coordinate vectors in the PA frame by a fixed rotation. However, the definition of the MER frame depends on the approximations used to estimate the *X* and *Z* directions. For DE430, an updated estimate of the MER frame has been made. Coordinate vectors in the DE430 PA frame are converted to the DE430 MER frame by[10]

$$\mathbf{r}_{MER,DE430} = \mathcal{R}_x(-0.285")\mathcal{R}_y(-78.580")\mathcal{R}_z(-67.573")\mathbf{r}_{PA,DE430}. \tag{19}$$

Several recent lunar missions have been producing cartographic data products in the MER frame as estimated from DE421. It may be convenient for continuity to retain that coordinate system. Coordinate vectors in the DE430 PA frame are converted to the DE421 MER frame by

$$\mathbf{r}_{MER,DE421} = \mathcal{R}_x(-0.295")\mathcal{R}_y(-78.627")\mathcal{R}_z(-67.737")\mathbf{r}_{PA,DE430}. \tag{20}$$

F. Orientation of the Earth

Only the long-term change of the Earth's orientation is modeled in the ephemeris integration. The Earth orientation model used for the DE430 and DE431 integration is based on the International Astronomical Union (IAU) 1976 precession model [21,22] with an estimated linear correction and on a modified IAU 1980 nutation model [23] including only terms with a period of 18.6 years.

---

[10] J. G. Williams, D. H. Boggs, and W. M. Folkner, "DE430 Lunar Orbit, Physical Librations, and Surface Coordinates," JPL Interoffice Memorandum 335-JW,DB,WF-20130722-016 (internal document), Jet Propulsion Laboratory, Pasadena, California, July 22, 2013.

The mean longitude of the ascending node of the lunar orbit measured on the ecliptic plane from the mean equinox of date is calculated by

$$\Omega = 125°02'40''.280 - 1934°08'10''.549T + 7''.455T^2 + 0''.008T^3 \tag{21}$$

where T is the TDB time in Julian centuries (36525 days) from J2000.0. The nutations in longitude $\Delta\psi$ and obliquity $\Delta\epsilon$ are given by

$$\begin{aligned} \Delta\psi &= -17''.206262 \sin(\Omega) \\ \Delta\epsilon &= 9''.205348 \cos(\Omega). \end{aligned} \tag{22}$$

The true pole of date unit vector, $\mathbf{p}_d$, is computed by rotating the Earth-fixed pole vector by the effect of the 18.6-year nutation term to give

$$\mathbf{p}_d = \begin{pmatrix} \sin(\Delta\psi)\sin(\bar{\epsilon} + \Delta\epsilon) \\ \cos(\Delta\psi)\sin(\bar{\epsilon} + \Delta\epsilon)\cos(\bar{\epsilon}) - \cos(\bar{\epsilon} + \Delta\epsilon)\sin(\bar{\epsilon}) \\ \cos(\Delta\psi)\sin(\bar{\epsilon} + \Delta\epsilon)\sin(\bar{\epsilon}) + \cos(\bar{\epsilon} + \Delta\epsilon)\cos(\bar{\epsilon}) \end{pmatrix} \tag{23}$$

where the mean obliquity $\bar{\epsilon}$ is given by

$$\bar{\epsilon} = 84381.''448 - 46.''815T - 0.''00059T^2 + 0.''001813T^3. \tag{24}$$

The pole unit vector in the inertial frame $\mathbf{p}_E$ is computed by precessing the pole of date with an estimated linear correction,

$$\mathbf{p}_E = \mathcal{R}_z(\zeta)\mathcal{R}_y(-\Theta)\mathcal{R}_z(z)\mathcal{R}_x(-\Phi_x)\mathcal{R}_y(-\Phi_y)\mathbf{p}_d \tag{25}$$

where $\Phi_x = \Phi_{x_0} + 100T \times d\Phi_x/dt$ and $\Phi_y = \Phi_{y_0} + 100T \times d\Phi_y/dt$ are estimated linear corrections with offsets and rates listed in Table 10 (see page 50) and the precession angles are given by

$$\begin{aligned} \zeta &= 2306''.2181T + 0''.30188T^2 + 0''.017998T^3 \\ \Theta &= 2004''.3109T - 0'.42665T^2 - 0''.041833T^3 \\ z &= 2306''.2181T + 1''.09468T^2 + 0''.018203T^3. \end{aligned} \tag{26}$$

III. Translational Equations of Motion

The translational equations of motion include contributions from: (a) the point mass interactions among the Sun, Moon, planets, and asteroids; (b) the effects of the figure of the Sun on the Moon and planets; (c) the effects of the figures of the Earth and Moon on each other and on the Sun and planets from Mercury through Jupiter; (d) the effects upon the Moon's motion caused by tides raised upon the Earth by the Moon and Sun; and (e) the effects on the Moon's orbit of tides raised on the Moon by the Earth.

The point mass interactions are described in Section III.A. The effects of the static figures of bodies are described in Section III.B. Also in Section III.B, the effects of the Moon's static

figure plus its time-varying figure due to tides are included. The effects of tides raised on the Earth acting on the Moon are described in Section III.C.

A. Point Mass Mutual Interaction

The gravitational acceleration of each body due to external point masses is derived from the isotropic, parametrized post-Newtonian (PPN) *n*-body metric [24–26]. For each body A, the acceleration due to interaction with other point masses, $\mathbf{a}_{A,pm-pm}$, is given by

$$\begin{aligned}\mathbf{a}_{A,pm-pm} = \sum_{B\neq A} \frac{GM_B(\mathbf{r}_B-\mathbf{r}_A)}{r_{AB}^3}\Bigg\{1 &- \frac{2(\beta+\gamma)}{c^2}\sum_{C\neq A}\frac{GM_C}{r_{AC}} - \frac{2\beta-1}{c^2}\sum_{C\neq B}\frac{GM_C}{r_{BC}} \\ &+ \gamma\left(\frac{v_A}{c}\right)^2 + (1+\gamma)\left(\frac{v_B}{c}\right)^2 - \frac{2(1+\gamma)}{c^2}\mathbf{v}_A\cdot\mathbf{v}_B \\ &- \frac{3}{2c^2}\left[\frac{(\mathbf{r}_A-\mathbf{r}_B)\cdot\mathbf{v}_B}{r_{AB}}\right]^2 + \frac{1}{2c^2}(\mathbf{r}_B-\mathbf{r}_A)\cdot\mathbf{a}_B\Bigg\} \\ &+ \frac{1}{c^2}\sum_{B\neq A}\frac{GM_B}{r_{AB}^3}\Big[\big[\mathbf{r}_A-\mathbf{r}_B\big]\cdot\big[(2+2\gamma)\mathbf{v}_A-(1+2\gamma)\mathbf{v}_B\big]\Big](\mathbf{v}_A-\mathbf{v}_B) \\ &+ \frac{(3+4\gamma)}{2c^2}\sum_{B\neq A}\frac{GM_B\mathbf{a}_B}{r_{AB}}\end{aligned} \tag{27}$$

where β is the PPN parameter measuring the nonlinearity in superposition of gravity and γ is the PPN parameter measuring space curvature produced by unit rest mass. The summation is over all bodies: Sun, Moon, planets and asteroids. The acceleration $\mathbf{a}_B$ of body B appears in two terms on the right-hand side of Equation (27). Since these terms are multiplied by c^{-2}, using the Newtonian acceleration for these terms is accurate to $O(c^{-2})$.

B. Point Mass Interaction with Extended Bodies

The modeled accelerations of bodies due to interactions of point masses with the gravitational field of nonspherical bodies include: (a) the interaction of the zonal harmonics of the Earth (through fourth degree) and the point mass Moon, Sun, Mercury, Venus, Mars, and Jupiter; (b) the interaction between the zonal, sectoral, and tesseral harmonics of the Moon (through sixth degree) and the point mass Earth, Sun, Mercury, Venus, Mars, and Jupiter; (c) the second-degree zonal harmonic of the Sun (J_2) interacting with all other bodies.

The contribution to the inertial acceleration of an extended body arising from the interaction of its own figure with an external point mass is expressed in the $\xi\eta\zeta$ coordinate system, where the ξ-axis is directed outward from the extended body to the point mass, the $\xi\zeta$-plane contains the figure (rotational) pole of the extended body, and the η-axis completes the right-handed system.

In that system, the acceleration due to the extended body is given by[11]

[11] T. D. Moyer, *Mathematical Formulation of the Double-Precision Orbit Determination Program*, Technical Report 32-1527 (internal document), Jet Propulsion Laboratory, Pasadena, California, 1971.

$$\begin{bmatrix}\ddot{\xi}\\ \ddot{\eta}\\ \ddot{\zeta}\end{bmatrix}=-\frac{GM}{r^2}\left\{\sum_{n=2}^{n_1}J_n\left(\frac{R}{r}\right)^n\begin{bmatrix}(n+1)P_n(\sin\varphi)\\ 0\\ -\cos\varphi P_n'(\sin\varphi)\end{bmatrix}\right.$$
$$\left.+\sum_{n=2}^{n_2}\left(\frac{R}{r}\right)^n\sum_{m=1}^{n}\begin{bmatrix}-(n+1)P_n^m(\sin\varphi)[+C_{nm}\cos m\lambda+S_{nm}\sin m\lambda]\\ m\sec\varphi P_n^m(\sin\varphi)[-C_{nm}\sin m\lambda+S_{nm}\cos m\lambda]\\ \cos\varphi P'^m_n(\sin\varphi)[+C_{nm}\cos m\lambda+S_{nm}\sin m\lambda]\end{bmatrix}\right\} \tag{28}$$

where r is the center-of-mass separation between the two bodies; n_1 and n_2 are the maximum degrees of the zonal and tesseral expansions, respectively; $P_n(\sin\varphi)$ is the Legendre polynomial of degree n; $P_n^m(\sin\varphi)$ is the associated Legendre function of degree n and order m; J_n is the zonal harmonic coefficient for the extended body; C_{nm}, S_{nm} are the tesseral harmonic coefficients for the extended body; R is the equatorial radius of the extended body; φ is the latitude of the point mass relative to the body-fixed coordinate system in which the harmonics are expressed; and λ is the east longitude of the point mass in the same body-fixed coordinate system. The primes denote differentiation with respect to the argument $\sin\varphi$. The accelerations are transformed into the inertial frame by application of the appropriate rotation matrix.

The interaction between the figure of an extended body A and a point mass B also induces an acceleration of the point mass. If $\mathbf{a}_{A,figA-pmB}$ denotes the acceleration of extended body A interacting with point mass external body B given by Equation (28) when expressed in inertial coordinates, then the corresponding acceleration of the point mass, $\mathbf{a}_{B,figA-pmB}$, is given by

$$\mathbf{a}_{B,figA-pmB}=-\frac{m_A}{m_B}\mathbf{a}_{A,figA-pmB}. \tag{29}$$

For the Moon, the second-degree gravity field is time varying due to distortion by tides and spin and the spherical harmonic coefficients of the gravity field are computed from the moment of inertia tensor, which in turn is computed as a function of time, as described in Section IV.B. The coefficients are given by

$$\begin{aligned}J_{2,M}(t)&=\frac{I_{33,T}(t)-\frac{1}{2}[I_{11,T}(t)+I_{22,T}(t)]}{m_M R_M^2}\\ C_{22,M}(t)&=\frac{I_{22,T}(t)-I_{11,T}(t)}{4m_M R_M^2}\\ C_{21,M}(t)&=-I_{13,T}(t)/m_M R_M^2\\ S_{21,M}(t)&=-I_{32,T}(t)/m_M R_M^2\\ S_{22,M}(t)&=-I_{21,T}(t)/2m_M R_M^2\end{aligned} \tag{30}$$

where the $I_{ij,T}$ are the elements of the total lunar moment of inertia matrix (defined in Section IV); m_M is the lunar mass, and R_M is the lunar radius.

C. Acceleration of the Moon from Earth Tides

The tides raised upon the Earth by the Sun and Moon affect the motion of the Moon. The distortion of the Earth by the Sun and Moon are characterized by the degree-2 Love numbers $k_{2j,E}$, where order $j = 0$, 1, and 2 correspond to tides with long-period, diurnal, and semi-diurnal periods, respectively.

We apply a time-delay tidal model to account for dissipation. The distorted response of the Earth is delayed with respect to the tide-raising forces from the Moon or Sun. The appropriate time delay depends on the period of each tidal component. Consequently, we employ different time delays for each order j. To allow for time delays shifting across the diurnal and semidiurnal frequency bands, separate time delays are associated with the Earth's rotation and the lunar orbit.

The acceleration of the Moon due to the Earth tides is evaluated separately for the tides raised by the Sun and the tides raised by the Moon. The Earth tides depend on the position of the tide-raising body with respect to Earth $\mathbf{r}_T$, where T can denote either the Sun or the Moon. The position of the tide-raising body is evaluated at an earlier time $t - \tau_j'$ for long-period, diurnal, and semi-diurnal responses. The distortion of the Earth is delayed by a response time τ_j, so that the distortion leads the direction to the tide-raising body by an angle $\dot{\theta}\tau_j$, where $\dot{\theta}$ is the rotation rate of the Earth. The long-period zonal tides ($j = 0$) do not depend on the rotation of the Earth, so $\tau_0 = 0$. The acceleration of the Moon due to the distorted Earth depends on the position of the Moon with respect to the Earth $\mathbf{r}$ and on the modified position vector for the tide-raising body $\mathbf{r}_j^*$, which is given for each order j by

$$\boldsymbol{r}_j^* = \mathcal{R}_z\left(-\dot{\theta}\tau_j\right)\mathbf{r}_T\left(t-\tau_j'\right) \tag{31}$$

where $\mathcal{R}_z(-\dot{\theta}\tau_j)$ here means a right-handed rotation of the vector $\mathbf{r}_T(t-\tau_j')$ by the angle $\dot{\theta}\tau_j$ about the Earth's rotation axis with $\mathcal{R}_z$, as defined in Equation (13).

The vectors $\mathbf{r}$ and $\mathbf{r}_j^*$ are expressed in cylindrical coordinates with the Z axis perpendicular to the Earth's equator, so that $\mathbf{r} = \boldsymbol{\rho} + \mathbf{z}$ and the time-delayed position of the tide-raising body is given by $\mathbf{r}_j^* = \boldsymbol{\rho}_j^* + \mathbf{z}_j^*$. The acceleration of the Moon with respect to Earth, $\mathbf{a}_{M,tide}$, for each tide-raising body is then given by

$$\begin{aligned}\mathbf{a}_{M,tide} = \frac{3}{2}\left(\frac{m_E+m_M}{m_E}\right)\frac{Gm_T R_E^5}{r^5}\Bigg\{&\frac{k_{20,E}}{r_0^{*5}}\left(\left[2z_0^{*2}\mathbf{z}+\rho_0^{*2}\boldsymbol{\rho}\right]-\frac{5\left[\left(zz_0^*\right)^2+\frac{1}{2}\left(\rho\rho_0^*\right)^2\right]\mathbf{r}}{r^2}+r_0^{*2}\mathbf{r}\right)\\&+\frac{k_{21,E}}{r_1^{*5}}\left(2\left[\left(\boldsymbol{\rho}\cdot\boldsymbol{\rho}_1^*\right)\mathbf{z}_1^*+zz_1^*\boldsymbol{\rho}_1^*\right]-\frac{10zz_1^*\left(\boldsymbol{\rho}\cdot\boldsymbol{\rho}_1^*\right)\mathbf{r}}{r^2}\right)\\&+\frac{k_{22,E}}{r_2^{*5}}\left(\left[2\left(\boldsymbol{\rho}\cdot\boldsymbol{\rho}_2^*\right)\boldsymbol{\rho}_2^*-\rho_2^{*2}\boldsymbol{\rho}\right]-\frac{5\left[\left(\boldsymbol{\rho}\cdot\boldsymbol{\rho}_2^*\right)^2-\frac{1}{2}\left(\rho\rho_2^*\right)^2\right]\mathbf{r}}{r^2}\right)\Bigg\}\end{aligned} \tag{32}$$

where m_T is the mass of the tide-raising body.

The tidal acceleration due to tidal dissipation is implicit in the above acceleration. Tides raised on the Earth by the Moon do not influence the motion of the Earth–Moon barycenter. The effect of Sun-raised tides on the barycentric motion is not considered.

The tidal bulge leads the Moon and its gravitational attraction accelerates the Moon forward and retards the Earth's spin. Energy and angular momentum are transferred from the Earth's rotation to the lunar orbit. Consequently, the Moon moves away from the Earth, the lunar orbit period lengthens, and the Earth's day becomes longer. Some energy is dissipated in the Earth rather than being transferred to the orbit.

The estimated tidal acceleration in orbital mean longitude is –25.82 ± 0.03″/century^2 for DE430 and –25.80 ± 0.03″/century^2 for DE431. The semimajor axis recession rates are 38.08 ± 0.04 mm/yr and 38.05 ± 0.04 mm/yr for DE430 and DE431, respectively. The uncertainties reflect an uncertainty in extrapolating the lunar position beyond the span of the fit. The uncertainty in converting the Love numbers and time delays to tidal acceleration and recession rate might be as large as 0.5 percent.

IV. Evolution of the Lunar Orientation

The Moon is modeled as an anelastic mantle with a liquid core. The orientation of the core and mantle are integrated from the differential equations for the core and mantle angular velocities. The angular momentum vectors of the mantle and core are the product of the angular velocities and the moments of inertia. The angular momentum vectors change with time due to torques and due to distortion of the mantle.

A. Rate of Change of Lunar Angular Velocities

In a rotating system, the change in angular velocity $\boldsymbol{\omega}$ is related to torques N by

$$\mathrm{N} = \frac{d}{dt}(\mathbf{I}\boldsymbol{\omega}) + \boldsymbol{\omega} \times \mathbf{I}\boldsymbol{\omega} \tag{33}$$

where $\mathbf{I}$ is the moment of inertia tensor. The second term on the right side puts the time derivative into the rotating system. The total lunar moment of inertia $\mathbf{I}_T$, which is the sum of the moment of inertia of the mantle $\mathbf{I}_m$ and the moment of inertia of the core $\mathbf{I}_c$, is proportional to the mass m_M times the square of the radius R_M. Because the fractional uncertainty in the constant of gravitation G is much larger than that for the lunar mass parameter Gm_M, Equation (33) is evaluated in the integration with both sides multiplied by G.

The components of vectors can be given in the inertial frame, mantle frame, or other frames. Since the moment of inertia matrices are nearly diagonal in the mantle frame, there is great convenience to inverting matrices and performing the matrix multiplications in the mantle frame. The resulting vector components can then be rotated to other frames if desired.

The moment of inertia of the mantle varies with time due to tidal distortions. The distortions are functions of the lunar position and rotational velocities computed at time $t-\tau_m$, where τ_m is a time lag determined from the fits to the LLR data. The time delay allows for dissipation when flexing the Moon [5]. The time derivative of the angular velocity of the mantle is given by

$$\dot{\boldsymbol{\omega}}_m = \mathbf{I}_m^{-1}\left\{\sum_{A\neq M}\mathbf{N}_{M,figM-pmA} + \mathbf{N}_{M,figM-figE} - \dot{\mathbf{I}}_m\boldsymbol{\omega}_m - \boldsymbol{\omega}_m\times\mathbf{I}_m\boldsymbol{\omega}_m + \mathbf{N}_{cmb}\right\} \tag{34}$$

where $\mathbf{N}_{M,figM-pmA}$ is the torque on the lunar mantle from the point mass of body A, $\mathbf{N}_{M,figM-figE}$ is the torque on the mantle due to the extended figure of the Moon interacting with the extended figure of the Earth, and $\mathbf{N}_{cmb}$ is the torque due to interaction between the mantle and core. The torques are given in Section IV.C.

The fluid core is assumed to be rotating like a solid and constrained by the shape of the core–mantle boundary at the interior of the mantle, with moment of inertia constant in the frame of the mantle [6]. The time derivative of the angular velocity of the core expressed in the mantle frame is given by

$$\dot{\boldsymbol{\omega}}_c = \mathbf{I}_c^{-1}\left\{-\boldsymbol{\omega}_m\times\mathbf{I}_c\boldsymbol{\omega}_c - \mathbf{N}_{cmb}\right\}. \tag{35}$$

B. Lunar Moments of Inertia

In the mantle frame, the undistorted moment of inertia of the mantle and the moment of inertia of the core are diagonal. The undistorted total moment of inertia $\tilde{\mathbf{I}}_T$ is given by

$$\tilde{\mathbf{I}}_T = \begin{bmatrix} A_T & 0 & 0 \\ 0 & B_T & 0 \\ 0 & 0 & C_T \end{bmatrix} \tag{36}$$

with A_T, B_T, and C_T given by

$$\begin{aligned} A_T &= \frac{2(1-\beta_L\gamma_L)}{(2\beta_L-\gamma_L+\beta_L\gamma_L)} m_M R_M^2 \tilde{J}_{2,M} \\ B_T &= \frac{2(1+\gamma_L)}{(2\beta_L-\gamma_L+\beta_L\gamma_L)} m_M R_M^2 \tilde{J}_{2,M} \\ C_T &= \frac{2(1+\beta_L)}{(2\beta_L-\gamma_L+\beta_L\gamma_L)} m_M R_M^2 \tilde{J}_{2,M} \end{aligned} \tag{37}$$

where $\tilde{J}_{2,M}$ is the second-degree zonal harmonic of the undistorted Moon and β_L and γ_L are ratios of the undistorted moments of inertia given by

$$\begin{aligned} \beta_L &= (C_T - A_T)/B_T \\ \gamma_L &= (B_T - A_T)/C_T. \end{aligned} \tag{38}$$

The undistorted total moment of inertia and the second-degree zonal harmonic of the undistorted Moon are not the same as the mean values since the tidal distortions have non-zero averages.

The moment of inertia of the core $\mathbf{I}_c$ is given by

$$\mathbf{I}_c = \alpha_c C_T \begin{bmatrix} 1-f_c & 0 & 0 \\ 0 & 1-f_c & 0 \\ 0 & 0 & 1 \end{bmatrix} = \begin{bmatrix} A_c & 0 & 0 \\ 0 & B_c & 0 \\ 0 & 0 & C_c \end{bmatrix} \tag{39}$$

where $\alpha_c = C_c/C_T$ is the ratio of the core polar moment of inertia to the undistorted total polar moment of inertia and f_c is the core oblateness. Distortion of the core moment of inertia is not considered.

The undistorted moment of inertia of the mantle is the difference between the undistorted total moment of inertia and the core moment of inertia,

$$\tilde{\mathbf{I}}_m = \tilde{\mathbf{I}}_T - \mathbf{I}_c. \tag{40}$$

The moment of inertia of the mantle varies with time due to tidal distortion by the Earth and spin distortion,

$$\mathbf{I}_m(t) = \tilde{\mathbf{I}}_m - \frac{k_{2,M} m_E R_M^5}{r^5} \begin{bmatrix} x^2 - \frac{1}{3}r^2 & xy & xz \\ xy & y^2 - \frac{1}{3}r^2 & yz \\ xz & yz & z^2 - \frac{1}{3}r^2 \end{bmatrix}$$

$$+ \frac{k_{2,M} R_M^5}{3G} \begin{bmatrix} \omega_{m,x}^2 - \frac{1}{3}(\omega_m^2 - n^2) & \omega_{m,x}\omega_{m,y} & \omega_{m,x}\omega_{m,z} \\ \omega_{m,x}\omega_{m,y} & \omega_{m,y}^2 - \frac{1}{3}(\omega_m^2 - n^2) & \omega_{m,y}\omega_{m,z} \\ \omega_{m,x}\omega_{m,z} & \omega_{m,y}\omega_{m,z} & \omega_{m,z}^2 - \frac{1}{3}(\omega_m^2 + 2n^2) \end{bmatrix} \tag{41}$$

where the position of the Moon relative to Earth $\mathbf{r}$ and the angular velocity of the mantle $\boldsymbol{\omega}_m$, are evaluated at time $t - \tau_m$; $k_{2,M}$ is the lunar potential Love number; m_E is the mass of the Earth; R_M is the equatorial radius of the Moon; r is the Earth-Moon distance; x, y, z are the components of the position of the Moon relative to Earth referred to the mantle frame; $\omega_{m,x}, \omega_{m,y}, \omega_{m,z}$ are the components of $\boldsymbol{\omega}_m$ in the mantle frame; and n is the lunar mean motion.

The rate of change of the mantle's moment of inertia is given by

$$\dot{\mathbf{I}}_m = \frac{5k_{2,M}m_E R_M^5 \mathbf{r}\cdot\dot{\mathbf{r}}}{r^7}\begin{bmatrix} x^2-\frac{1}{3}r^2 & xy & xz \\ xy & y^2-\frac{1}{3}r^2 & yz \\ xz & yz & z^2-\frac{1}{3}r^2 \end{bmatrix}$$
$$-\frac{k_{2,M}m_E R_M^5}{r^5}\begin{bmatrix} 2(x\dot{x}-\frac{1}{3}\mathbf{r}\cdot\dot{\mathbf{r}}) & x\dot{y}+\dot{x}y & x\dot{z}+\dot{x}z \\ x\dot{y}+\dot{x}y & 2(y\dot{y}-\frac{1}{3}\mathbf{r}\cdot\dot{\mathbf{r}}) & y\dot{z}+\dot{y}z \\ x\dot{z}+\dot{x}z & y\dot{z}+\dot{y}z & 2(z\dot{z}-\frac{1}{3}\mathbf{r}\cdot\dot{\mathbf{r}}) \end{bmatrix}$$
$$+\frac{k_{2,M}R_M^5}{3G}\begin{bmatrix} 2(\omega_{m,x}\dot{\omega}_{m,x}-\frac{1}{3}\boldsymbol{\omega}_m\cdot\dot{\boldsymbol{\omega}}_m) & \omega_{m,x}\dot{\omega}_{m,y}+\dot{\omega}_{m,x}\omega_{m,y} & \omega_{m,x}\dot{\omega}_{m,z}+\dot{\omega}_{m,x}\omega_{m,z} \\ \omega_{m,x}\dot{\omega}_{m,y}+\dot{\omega}_{m,x}\omega_{m,y} & 2(\omega_{m,y}\dot{\omega}_{m,y}-\frac{1}{3}\boldsymbol{\omega}_m\cdot\dot{\boldsymbol{\omega}}_m) & \omega_{m,y}\dot{\omega}_{m,z}+\dot{\omega}_{m,y}\omega_{m,z} \\ \omega_{m,x}\dot{\omega}_{m,z}+\dot{\omega}_{m,x}\omega_{m,z} & \omega_{m,y}\dot{\omega}_{m,z}+\dot{\omega}_{m,y}\omega_{m,z} & 2(\omega_{m,z}\dot{\omega}_{m,z}-\frac{1}{3}\boldsymbol{\omega}_m\cdot\dot{\boldsymbol{\omega}}_m) \end{bmatrix}. \tag{42}$$

C. Lunar Torques

The torque on the Moon due to an external point mass A is given by

$$\mathbf{N}_{M,figM-pmA} = M_M \mathbf{r}_{AM} \times \mathbf{a}_{M,figM-pmA} \tag{43}$$

where $\mathbf{r}_{AM}$ is the position of the point mass relative to the Moon and $\mathbf{a}_{M,figM-pmA}$ is the acceleration of the Moon due to the interaction of the extended figure of the Moon with the point mass A, as described in Section III.B. Torques are computed for the figure of the Moon interacting with the Earth, Sun, Mercury, Venus, Mars, and Jupiter.

Yoder [27] and Eckhardt [28] showed that torques due to the interaction of the figure of the Moon with the figure of the Earth are important for the orientation of the Moon. The three most significant terms of the torque are

$$\mathbf{N}_{M,figM-figE} = \frac{15GM_E R_E^2 J_{2,E}}{2r_{EM}^5}\Big\{\big(1-7\sin^2\varphi_{M,E}\big)\big[\hat{\mathbf{r}}_{\mathbf{EM}}\times\mathbf{I}_M\hat{\mathbf{r}}_{\mathbf{EM}}\big] + 2\sin\varphi_{M,E}\big[\hat{\mathbf{r}}_{EM}\times\mathbf{I}_M\hat{\mathbf{p}}_{\mathbf{E}}+\hat{\mathbf{p}}_{\mathbf{E}}\times\mathbf{I}_M\hat{\mathbf{r}}_{\mathbf{EM}}\big] - \frac{2}{5}\big[\hat{\mathbf{p}}_{\mathbf{E}}\times\mathbf{I}_M\hat{\mathbf{p}}_{\mathbf{E}}\big]\Big\} \tag{44}$$

where $\hat{\mathbf{p}}_E$ is the direction vector of the Earth's pole and $\hat{\mathbf{r}}_{EM}$ is the direction vector of the Earth from the Moon; $\mathbf{I}$ is the lunar moment of inertia tensor; R_E is the equatorial radius of the Earth; and $\varphi_{M,E}$ is defined by $\sin\varphi_{M,E} = \hat{\mathbf{r}}_{EM}\cdot\hat{\mathbf{p}}_E$.

The torque on the mantle due to the interaction between the core and mantle is evaluated in the mantle frame and is given by

$$\mathbf{N}_{cmb} = k_v\big(\boldsymbol{\omega}_c-\boldsymbol{\omega}_m\big)+\big(C_c-A_c\big)\big(\hat{\mathbf{z}}_m\cdot\boldsymbol{\omega}_c\big)\big(\hat{\mathbf{z}}_m\times\boldsymbol{\omega}_c\big) \tag{45}$$

where $\hat{\mathbf{z}}_m$ is a unit vector in the mantle frame aligned with the polar axis. The torque on the core is the negative of the torque on the mantle.

V. Observational Data Fit by the Planetary and Lunar Ephemerides

The observations that have been used to estimate the dynamical parameters for DE430 and DE431 are summarized in Tables 1, 2, and 3. The observations are sorted by body, classification, and type.

LLR data are measurements of the round-trip light-time from an observatory to retroreflectors on the Moon at the Apollo 11, 14, or 15 landing sites or the Lunokhod 1 and 2 rovers. These measurements began in 1970 following the first landings of astronauts and continue to the present (e.g. [29,30]). Residuals between the measured round-trip light-time t_{meas} and the value computed from the model t_{comp} are typically expressed as one-way range residuals $\Delta\rho = (t_{meas} - t_{comp})c/2$. The measurement accuracy has improved with time as technology for producing short-duration high-energy laser pulses and timing measurements has advanced. The earliest measurements have root-mean-square (rms) residuals of ~ 25 cm while the most recent measurements have rms residuals of ~ 2 cm. The most accurate measurement residuals are limited by dynamical modeling and by ambiguity in knowledge of which corner cube in the retroreflector array returned the photon that was timed [31]. LLR data are the only data used for estimation of the orbit and orientation of the Moon. The majority of LLR measurements are from McDonald Observatory (e.g., [32,33]), Observatoire de la Côte d'Azur (e.g., [34]) and Apache Point Observatory (e.g., [35]). The LLR measurement residuals for DE430 are shown in Figure 4.

Spacecraft measurements are based on radio range, Doppler, and VLBI measurements. For spacecraft in orbit about the planet, the Doppler measurements are used to estimate the position of the spacecraft with respect to the planet and range and VLBI measurements are then used to estimate the orbit of the planet. For spacecraft flying by a planet, the range, Doppler, and VLBI data, as available, are used to estimate both the trajectory of the spacecraft and a 3-dimensional (3–D) position of the planet, given as range, right ascension, and declination.

Range measurements to spacecraft are usually made at regular intervals during a tracking pass, typically every 10 min, while Doppler measurements are made more frequently, typically every minute. Both range and Doppler measurements are based on measurement of the phase of a radio signal, with the carrier signal used for Doppler and a ranging modulation signal used for range. Since the carrier signal is at a much higher frequency and usually has much higher signal strength, Doppler measures changes in range much more accurately than the range measurements. Because of the shorter wavelength associated with the higher frequency, the integer number of carrier wavelengths cannot be resolved, so Doppler measurements do not allow estimation of absolute range. Range measurements are more correctly measurements of round-trip light-time. For plotting residuals, the residual light time (measured minus computed) is multiplied by the speed of light, and divided by two to give approximate residual distance in meters. The range measurement accuracy is often limited by a calibration of the signal path delay in the tracking station prior to each tracking pass [20,36]. Since this calibration error is common to all range measurements in the tracking pass, there is only one statistically independent range point per pass. We therefore use only one range point per tracking pass in our data reduction, and the number of range measurements per spacecraft in Tables 1–3 reflects this.

Table 1. Observational data for the Moon and inner planets. The columns contain the observatory/source, the time coverage, and the number of observations.

Planet	Class	Type	Observatory/Spacecraft	Span	Number
Moon					
	LLR	Range	McDonald 2.7 m	1969–1985	3451
			MLRS/saddle	1984–1988	275
			MLRS/Mt Fowlkes	1988–2007	2746
			Haleakala	1984–1990	694
			Observatoire de la Côte d'Azur	1984–2012	9635
			Matera	2004	11
			Apache Point	2006–2012	1557
Mercury					
	Spacecraft	Range	Mariner 10	1974–1975	2
			MESSENGER	2011	242
	Spacecraft	3–D	MESSENGER	2008–2009	3
	Radar	Range	Arecibo	1967–1982	242
			Goldstone	1972–1997	283
			Haystack	1966–1971	217
			Eupatoria	1980–1995	75
	Radar	Closure	Goldstone	1989–1997	39
Venus					
	Spacecraft	Range	Venus Express	2006–2013	2158
	Spacecraft	VLBI	Venus Express	2007–2013	54
			Magellan	1990–1994	18
	Radar	Range	Arecibo	1967–1970	227
			Goldstone	1970–1990	512
			Haystack	1966–1971	330
			Eupatoria	1962–1995	1134
Mars					
	Spacecraft	Range	Viking Lander 1	1976–1982	1178
			Viking Lander 2	1976–1977	80
			Mars Pathfinder	1997	90
			Mars Global Surveyor	1999–2006	3067
			Mars Odyssey	2002–2012	6009
			Mars Reconnaissance Orbiter	2006–2012	1475
			Mars Express	2005–2013	5321
	Spacecraft	VLBI	Mars Global Surveyor	2001–2003	15
			Mars Odyssey	2002–2013	77
			Mars Reconnaissance Orbiter	2006–2013	59

Table 2. Observational data for Jupiter and Saturn. The columns contain the observatory/source, the time coverage, and the number of observations.

Planet	Class	Type	Observatory/Spacecraft	Span	Number
Jupiter					
	Spacecraft	3–D	Pioneer 10	1973	1
			Pioneer 11	1974	1
			Voyager 1	1979	1
			Voyager 2	1979	1
			Ulysses	1992	1
			Cassini	2000	1
	Spacecraft	VLBI	Galileo	1996–1997	24
	Astrometric	CCD	Flagstaff	1998–2012	342
			Nikolaev	1962–1998	2586
	Astrometric	Transit	La Palma	1986–1997	658
			Washington	1914–1994	1705
Saturn					
	Spacecraft	Range	Cassini	2004–2013	131
	Spacecraft	VLBI	Cassini	2004–2011	12
	Spacecraft	3–D	Voyager 1	1980	1
			Voyager 2	1981	1
	Astrometric	CCD	Flagstaff	1998–2012	5635
			Table Mountain	2002–2009	1374
			Nikolaev	1972–1994	1176
	Astrometric	Relative	Yerkes	1910–1921	18
	Astrometric	Transit	Bordeaux	1987–1993	119
			La Palma	1986–1997	730
			Washington	1926–1993	1422

Table 3. Observational data for Uranus, Neptune, and Pluto. The columns contain the observatory/source, the time coverage, and the number of observations.

Planet	Class	Type	Observatory/Spacecraft	Span	Number
Uranus					
	Spacecraft	3–D	Voyager 2	1986	1
	Astrometric	CCD	Flagstaff	1995–2012	3892
			Table Mountain	1998–2009	645
			Nikolaev	1961–1998	430
	Astrometric	Relative	Yerkes	1908–1922	21
	Astrometric	Transit	Bordeaux	1985–1993	238
			La Palma	1984–1997	1030
			Washington	1926–1993	2043
Neptune					
	Spacecraft	3–D	Voyager 2	1989	1
	Astrometric	CCD	Flagstaff	1995–2012	4259
			Table Mountain	1999–2012	832
			Nikolaev	1961–1998	436
	Astrometric	Relative	Yerkes	1904–1922	33
	Astrometric	Transit	Bordeaux	1985–1993	183
			La Palma	1984–1998	1106
			Washington	1926–1993	1838
Pluto					
	Astrometric	CCD	Flagstaff	1995–2012	995
			Table Mountain	2001–2012	365
			Pico dos Dias	1995–2012	5489
	Astrometric	Photographic	Pulkovo	1930–1992	53
	Occultation		Various	2005–2012	19

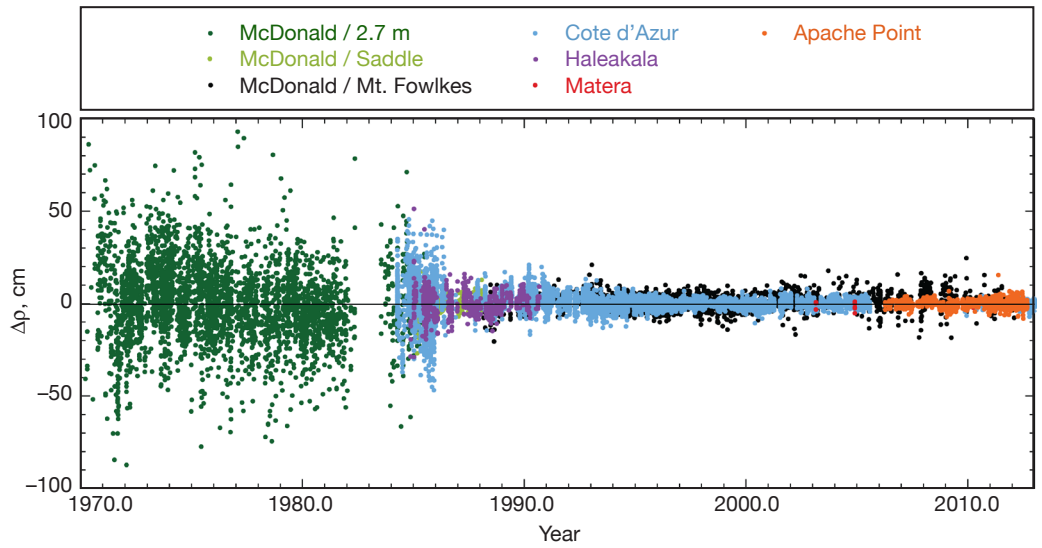

Figure 4. Lunar laser ranging measurement residuals.

Spacecraft *VLBI* measurements are usually made using two widely separated tracking stations. The measurements are made using a modulation on the carrier signal (delta-differential one-way range) and give one component of the direction to the spacecraft [37]. The angular component direction depends on the baseline used. The baseline from Goldstone, California, to Madrid, Spain, is nearly parallel to the Earth's equator, so measurements on that baseline measure an angular component that is close to right ascension. The baseline from Goldstone to Canberra, Australia, has an angle of about 45 deg relative to the equator and so measures an angular component that is approximately mid-way between the right ascension and declination directions. Residuals for single-baseline measurements are given for each baseline. For Cassini, the Very Long Baseline Array (VLBA) was used, where the difference in time of arrival of the spacecraft carrier signal was used to determine both components of the direction to the spacecraft [38].

Radar measurements are measurements of the round-trip light-time from a radio telescope to the surface of the inner planets. The topography of the planet was originally a significant error source. Radar closure measurements are the difference in range measurements to the same point on the surface made at different times in order to cancel the error in topography. The topography of the inner planets is now well known from radio and laser altimetry measurements from spacecraft. However, the radio range and VLBI measurements of those spacecraft determine the orbits of the inner planets much more accurately than the planetary radar measurements, so the planetary radar data are included here primarily for historical comparison.

Astrometric measurements record the direction to the planet, namely, right ascension and declination, based on imaging relative to a star field. The accuracy of the star catalog is often the largest source of measurement error. We here use *CCD* to indicate more modern observations using electronic detectors, generally referred to star catalogs based on the Hipparcos mission launched in 1991 [39] that are referred to the ICRF2 through estimation of the positions of radio stars using VLBI [40]. Older measurements were taken using *photographic* plates or *transit* methods, often referred to older star catalogs, though corrected to the Hipparcos catalog in some fashion. Barnard [41–57] measured the angular separation between the outer planets and some of their satellites *relative* to angularly nearby stars at Yerkes Observatory. The positions of those stars are taken from modern star catalogs, with accuracies limited by knowledge of stellar proper motion.[12] *Transit* observations cover a longer time span than the more modern spacecraft and astrometric measurements. Since the measurement noise is relatively large for the transit measurements, they do not contribute significantly to the ephemeris solution. The transit measurements are included mainly for historical comparison.

Occultation measurements of Pluto are included here, where the right ascension and declination are determined from the timed disappearance and reappearance of a star by Pluto [58].

[12] R. A. Jacobson, "Visual Observations of the Outer Planets by E. E. Barnard," American Astronomical Society, Division of Planetary Sciences meeting, Puerto Rico, 2009.

A. Mercury

For DE430 and DE431, the orbit of Mercury is primarily determined by range measurements to the MESSENGER spacecraft after entering orbit in early 2011 [59]. The residuals for measurements processed are shown in Figure 5. The measurement residuals show some signature at the Mercury orbit period that cannot be removed by the ephemeris dynamical model. The signature is due to limitations in the estimated spacecraft orbits relative to Mercury. This will be improved with data from the second year of MESSENGER operations that includes orbits with pericenter over the southern hemisphere.

Previously, the orbit of Mercury was best determined by range measurements to the Mariner 10 spacecraft during its first two flybys in 1974 and 1975 [60], radar range from 1967 to 1997 [61–64], and radio tracking of MESSENGER for three flybys in 2008 and 2009. Residuals for these measurements are shown in Figures 6–8.

B. Venus

The orbit of Venus is primarily determined by range measurements to the Venus Express spacecraft since 2006. Range residuals are shown in Figure 9. VLBI measurement of the Magellan spacecraft from 1991 to 1995 and of the Venus Express spacecraft help determine the orientation of the orbits of Earth and Venus with respect to the ICRF2 frame. These VLBI data are less accurate than the Mars spacecraft VLBI measurements, primarily because the modulation signal used on Magellan and Venus Express has a narrower bandwidth than the signal used on the Martian orbiters. The Magellan and Venus Express VLBI residuals are shown in Figures 10–11. Radar range measurements [61,65–67] were the primary data for determining the orbit of Venus prior to Venus Express mission. The radar measurement residuals are shown in Figure 12.

C. Mars

VLBI measurements of Mars Global Surveyor, Mars Odyssey, and Mars Reconnaissance Orbiter provide the best determination of the orientation of the solar system with respect to the ICRF2.[13] The current accuracy is approaching the accuracy of the knowledge of the positions of the radio sources used to define the frame. VLBI measurement accuracy has been improved from 2001 to 2013 through digitization of signals at the radio telescopes at intermediate frequencies and the availability of wider digital data bandwidths that allow an improved signal-to-noise ratio. Residuals for the VLBI measurements are shown in Figures 13–14.

Radio tracking of spacecraft landed on Mars or in orbit about Mars extends from 1976 to the present. The large amount of data available and the proximity of the Mars orbit to the asteroid belt provide a continuously increasing sensitivity to asteroid mass parameters [7,17,20,68–70]. Although the increasing set of range measurements is improving the ability to predict the orbit of Mars, continued tracking is required to maintain the current orbit accuracy. Residuals for range measurements to Martian landers and orbiters are shown in Figures 15–20.

---

[13] W. M. Folkner and J. S. Border, "Linking the Planetary Ephemeris to the International Celestial Reference Frame," *Highlights of Astronomy,* vol. 16 (in press).

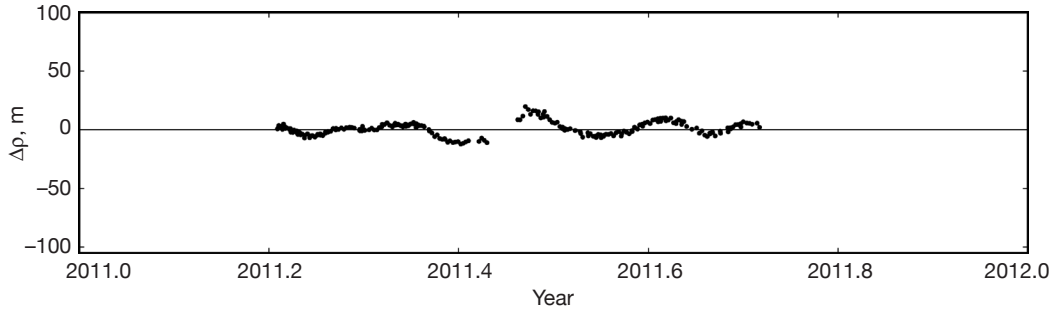

Figure 5. Range measurement residuals for MESSENGER spacecraft in orbit about Mercury.

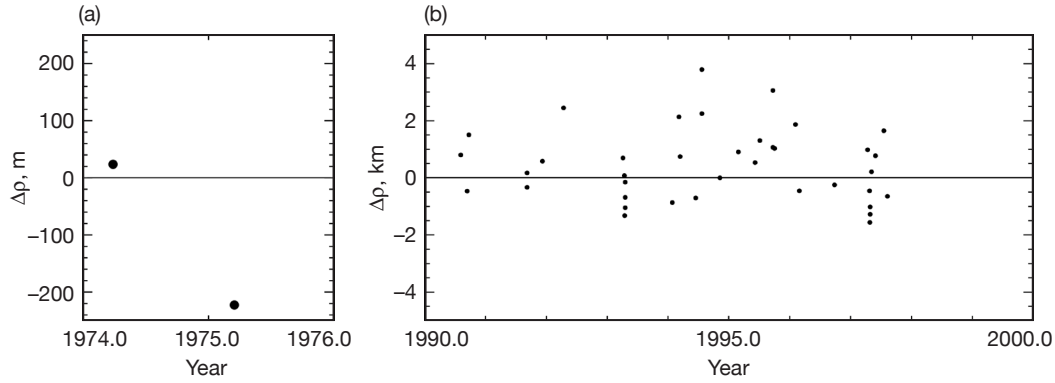

Figure 6. (a) Range residuals for Mariner 10 spacecraft; (b) Mercury radar closure residuals.

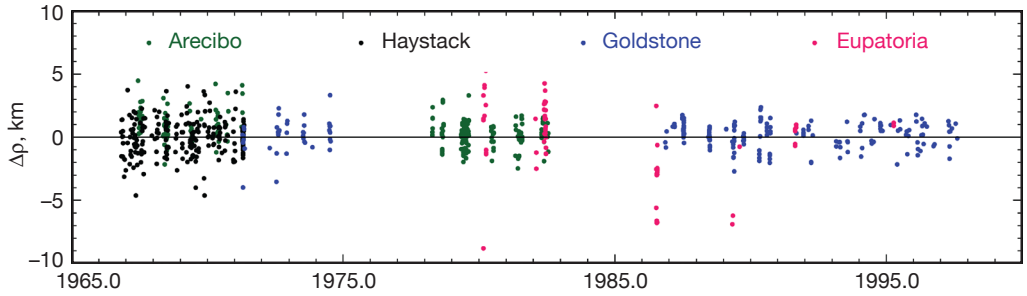

Figure 7. Residuals for radar range measurements for Mercury.

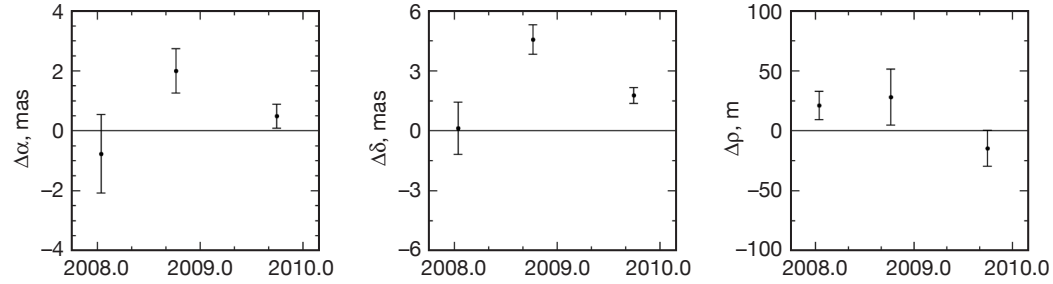

Figure 8. Residuals for MESSENGER flybys of Mercury.

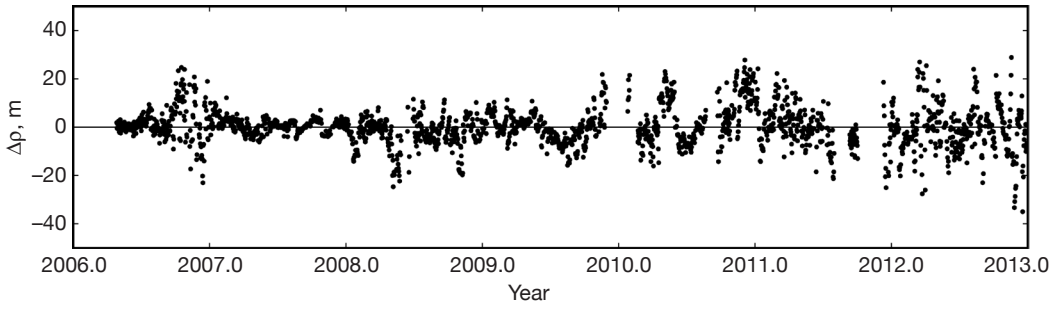

Figure 9. Residuals for range measurement to Venus Express.

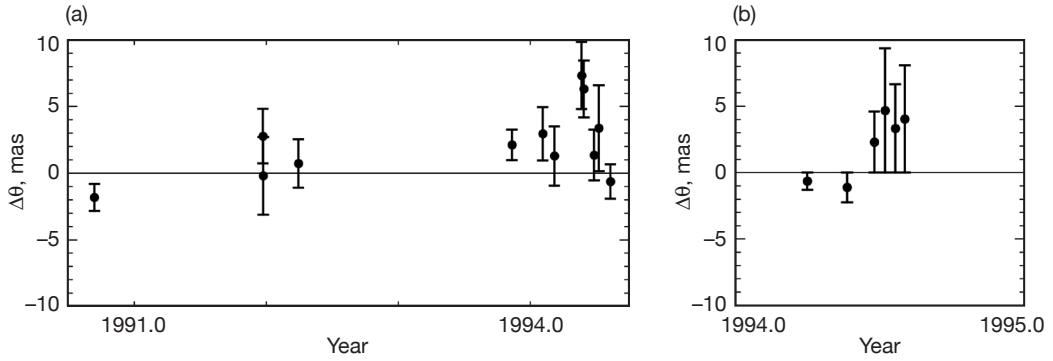

Figure 10. VLBI residuals for Magellan. (a) Goldstone–Canberra baseline; (b) Goldstone–Madrid baseline.

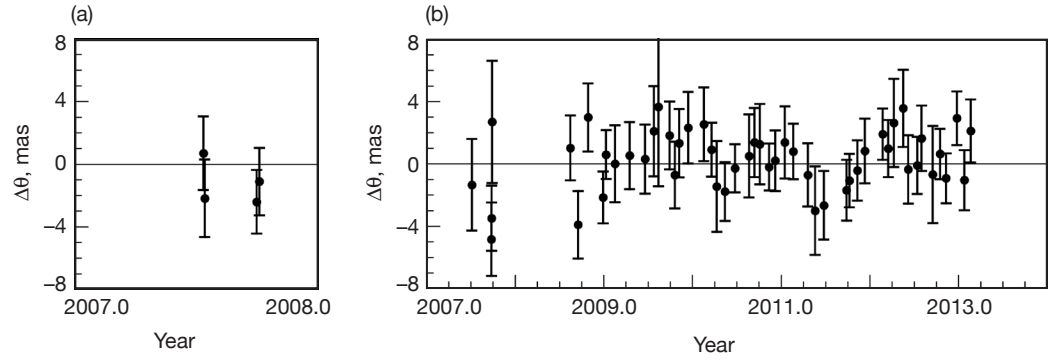

Figure 11. VLBI residuals for Venus Express. (a) Goldstone–Canberra baseline; (b) New Norcia–Cebreros baseline.

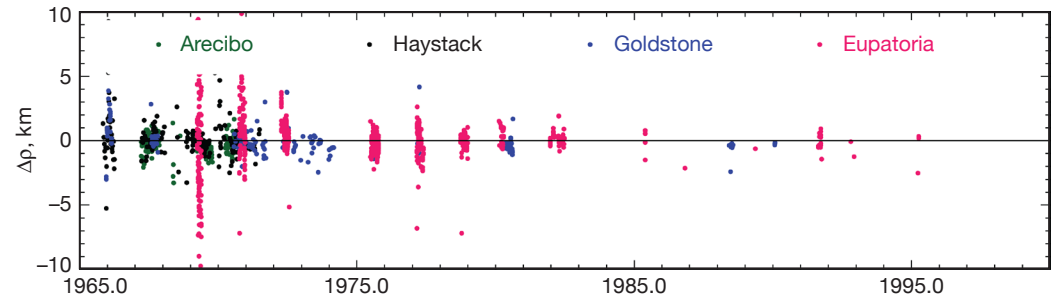

Figure 12. Residuals for radar range measurements for Venus.

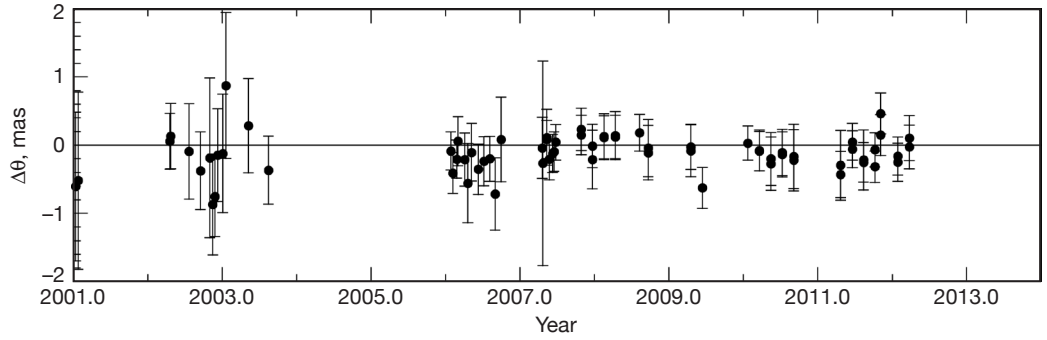

Figure 13. Mars orbiter VLBI residuals on Goldstone-Madrid baseline.

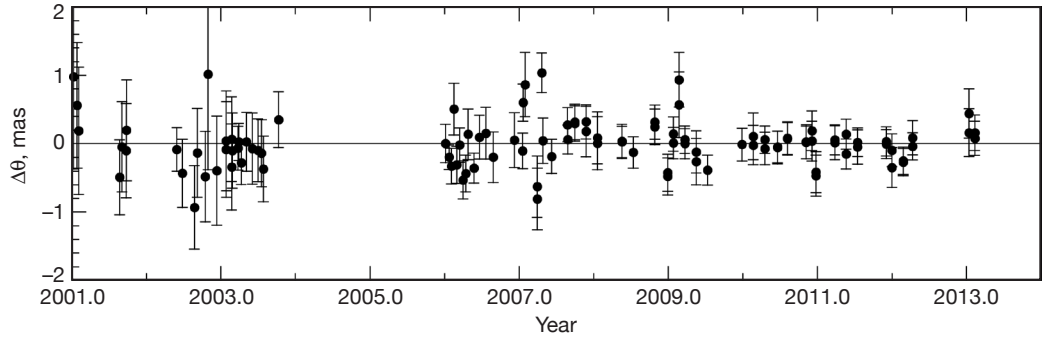

Figure 14. Mars orbiter VLBI residuals on Goldstone-Canberra baseline.

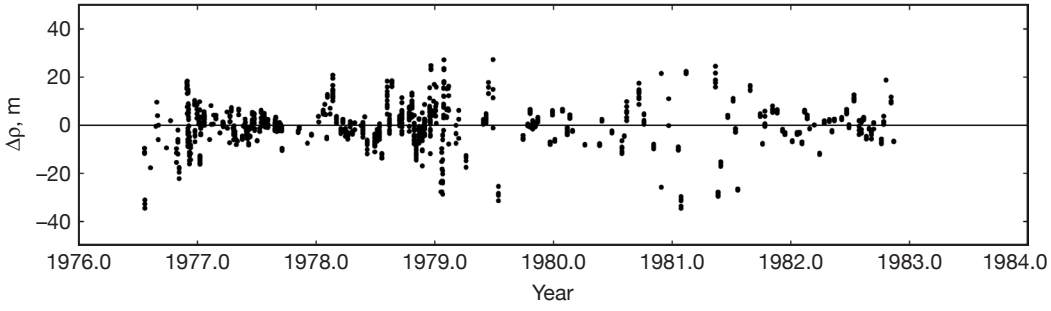

Figure 15. Viking Lander 1 range residuals.

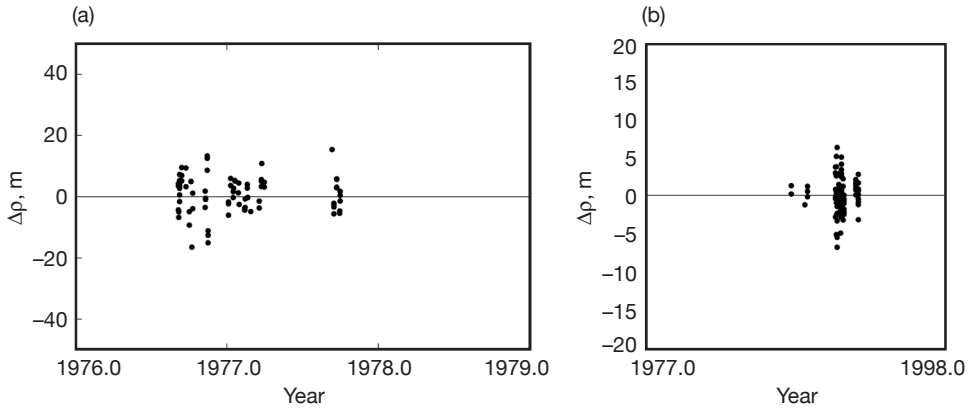

Figure 16. (a) Viking Lander 2 and (b) Mars Pathfinder range residuals.

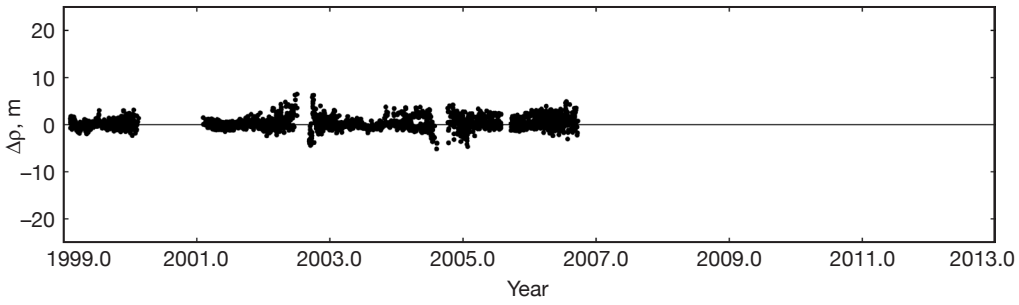

Figure 17. Residuals for range measurement to Mars Global Surveyor.

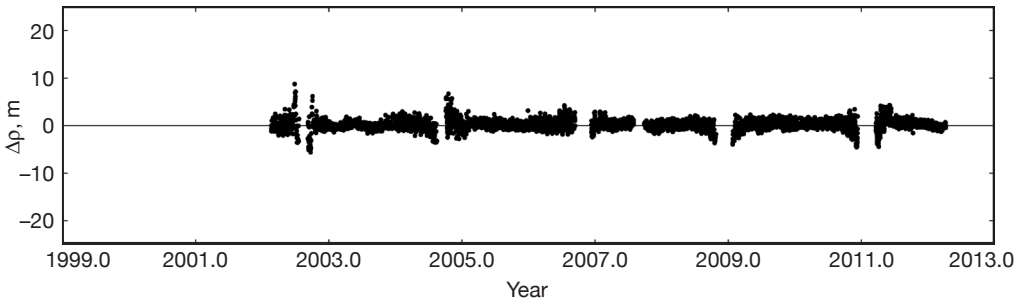

Figure 18. Residuals for range measurement to Mars Odyssey.

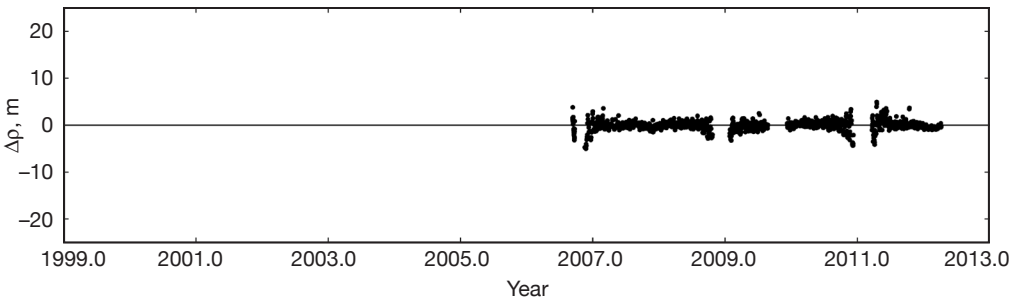

Figure 19. Residuals for range measurement to Mars Reconnaissance Orbiter.

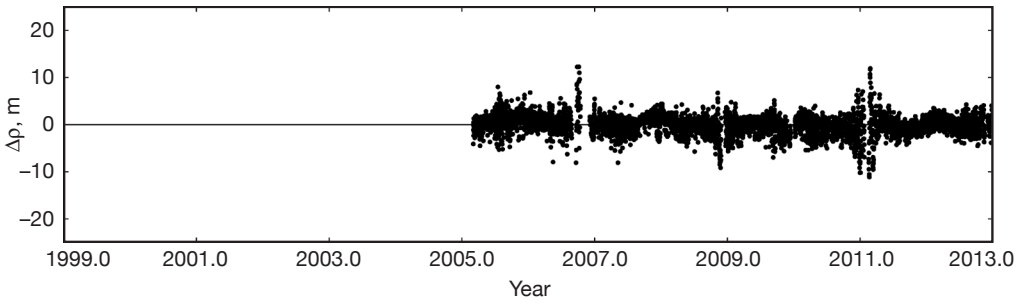

Figure 20. Residuals for range measurement to Mars Express.

D. Jupiter

The orbit of Jupiter is less well determined than the orbits of the inner planets and Saturn. The only spacecraft to orbit Jupiter, Galileo, was not able to use the high-gain antenna and so was not able to support range measurements. VLBI measurements of the Galileo spacecraft were made, but with relatively low accuracy due to limitations on the modulations available on the low-gain antenna. The orbit of Jupiter is determined by radio tracking of spacecraft that flew past Jupiter, and by astrometric data, with each of these data sets contributing approximately equally. Residuals for the spacecraft flyby data are shown in Figures 21–23 and for the Galileo VLBI data in Figure 24. Because Jupiter is resolved by telescopes, its astrometric position is better determined by observations of its satellites. We include measurements of the four Galilean satellites, which have orbits with respect to Jupiter that are most accurately determined. Residuals for CCD astrometric measurements are shown in Figures 25–32 from the U. S. Naval Observatory [71–77], Table Mountain Observatory, and Nikolaev Observatory [78]. Figures 33–34 show residuals for transit observations from the La Palma Observatory [79] and the U. S. Naval Observatory in Washington, D.C.

E. Saturn

The orbit of Saturn is most accurately determined from radio range and VLBI measurements of the Cassini spacecraft. The period of the Cassini orbit about Saturn varies from 14 days to 28 days, which is much longer than the tracking passes and longer than the period of spacecraft orbits about the inner planets. For DE421, the process used to determine ranges to Saturn from Cassini data for the first three years after entering orbit about Saturn in 2004 showed systematic effects in range residuals. These were determined to be caused by use of the range measurements along with Doppler measurements to determine the spacecraft orbits relative to Saturn. For DE430, we have used spacecraft orbits that were fit without the range data, allowing the range measurements to be used to determine the orbit of Saturn. We have found that range measurements are strongly correlated for each orbit segment, where the ends of the orbit segments are defined by a Saturn pericenter or a major maneuver used to change the spacecraft orbit. We therefore use only one range measurement per orbit segment. Figure 35 shows the Cassini range measurement residuals. The range residuals are larger for the latter part of the mission, where the spacecraft orbit period is generally shortest, so there is less Doppler data in each orbit segment, leading to larger uncertainties in spacecraft orbit determination. The residuals for the VLBA observations of Cassini are shown in Figures 36–37.

Figure 38 shows residuals for the estimated position of Saturn from radio measurements of the Voyager spacecraft during their flybys. Astrometric observations of Saturn do not contribute much to the planetary ephemeris, but are included to assess them relative to the radio measurements. Figures 39–50 show residuals for CCD astrometric measurements of Saturn. Figure 51 shows residuals from relative astrometric measurements from Yerkes Observatory. Figures 52–54 show residuals for transit observations from Bordeaux Observatory, the La Palma Observatory, and the U. S. Naval Observatory in Washington, D.C.

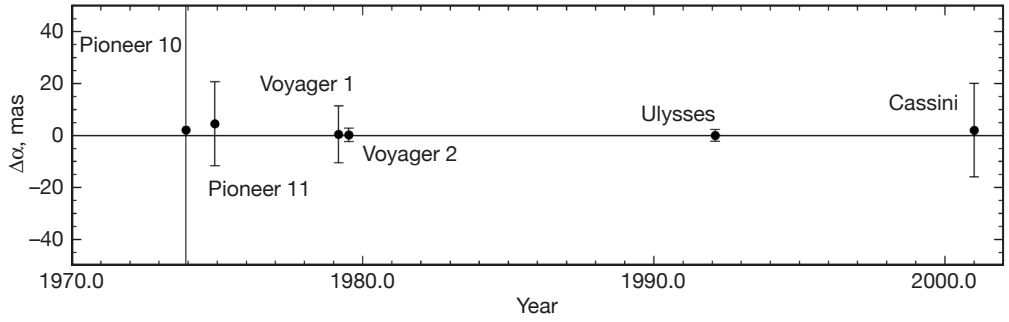

Figure 21. Right ascension residuals from spacecraft flybys of Jupiter.

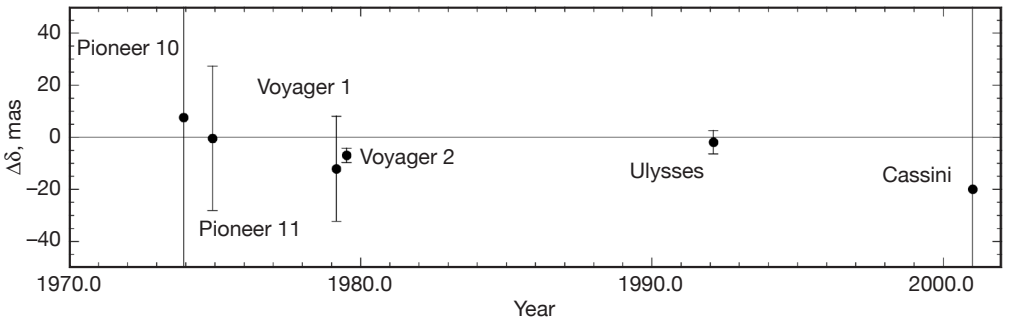

Figure 22. Declination residuals from spacecraft flybys of Jupiter.

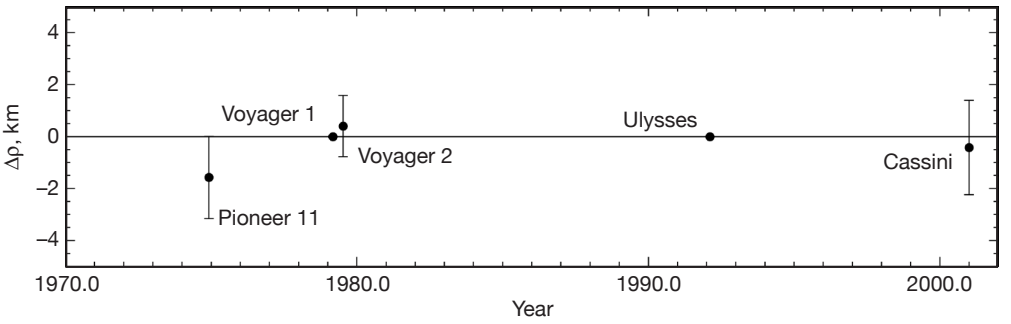

Figure 23. Range residuals from spacecraft flybys of Jupiter.

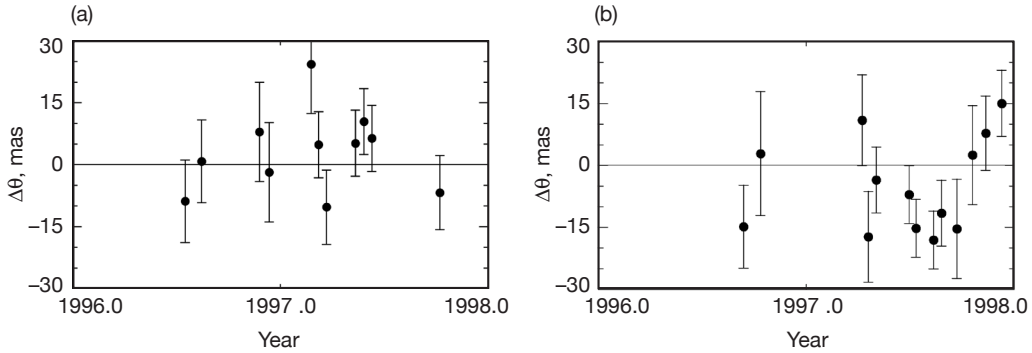

Figure 24. VLBI residuals for Galileo spacecraft in orbit about Jupiter. (a) Goldstone–Madrid baseline; (b) Goldstone–Canberra baseline.

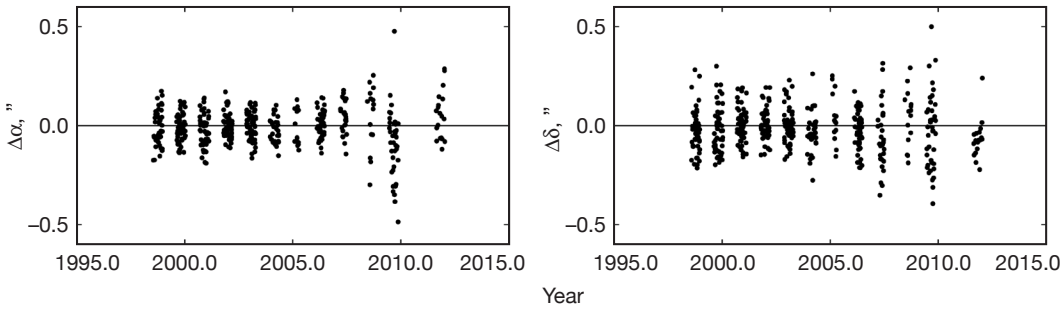

Figure 25. Residuals from astrometric observations of Io by U. S. Naval Observatory at Flagstaff.

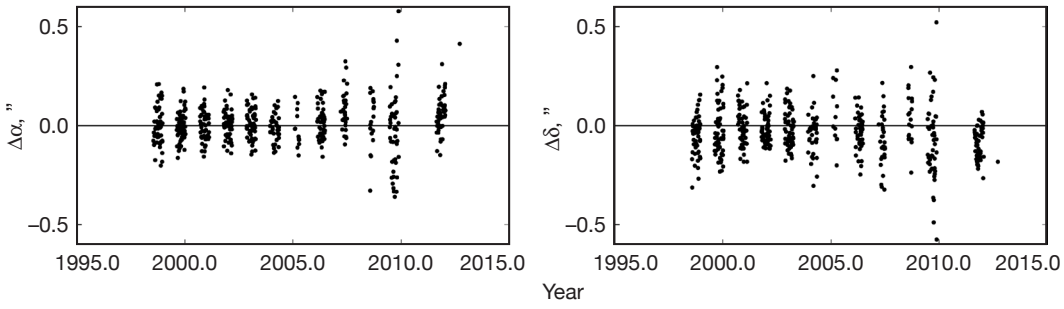

Figure 26. Residuals from astrometric observations of Europa by U. S. Naval Observatory at Flagstaff.

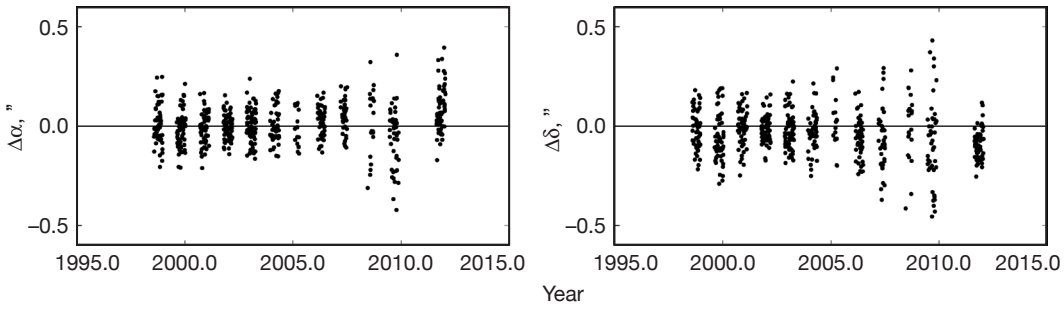

Figure 27. Residuals from astrometric observations of Ganymede by U. S. Naval Observatory at Flagstaff.

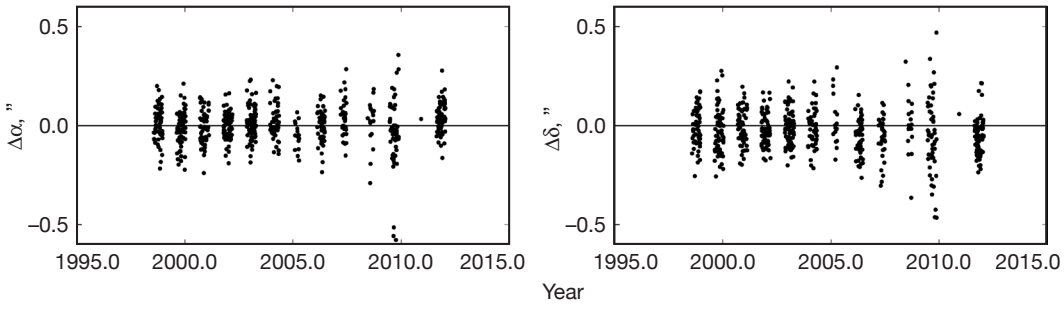

Figure 28. Residuals from astrometric observations of Callisto by U. S. Naval Observatory at Flagstaff.

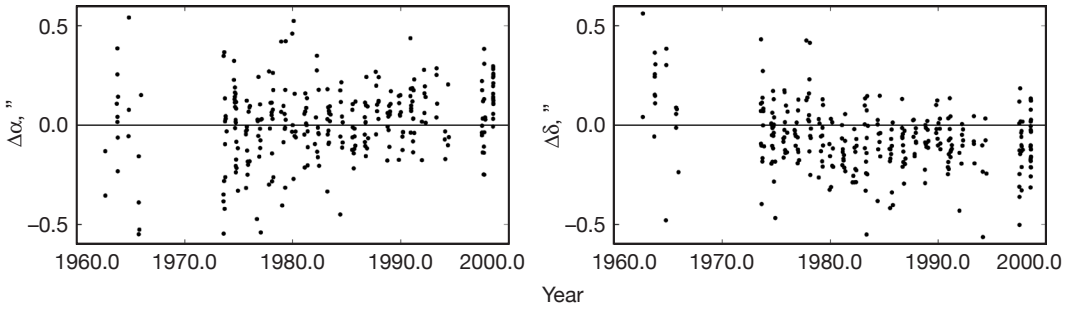

Figure 29. Residuals from astrometric observations of Io by Nikolaev Observatory.

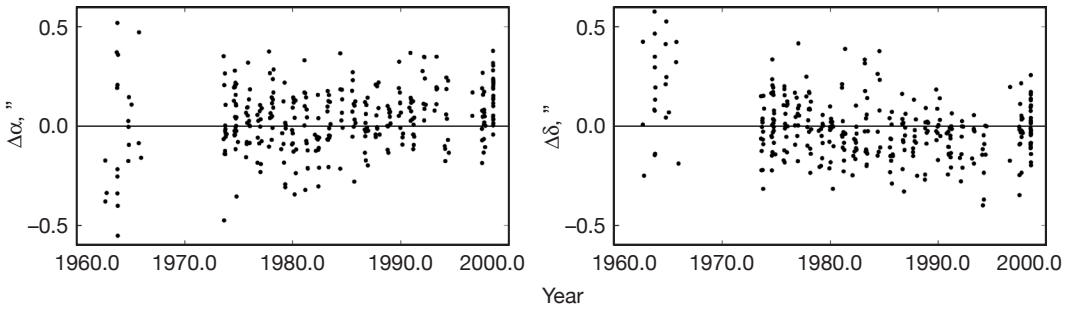

Figure 30. Residuals from astrometric observations of Europa by Nikolaev Observatory.

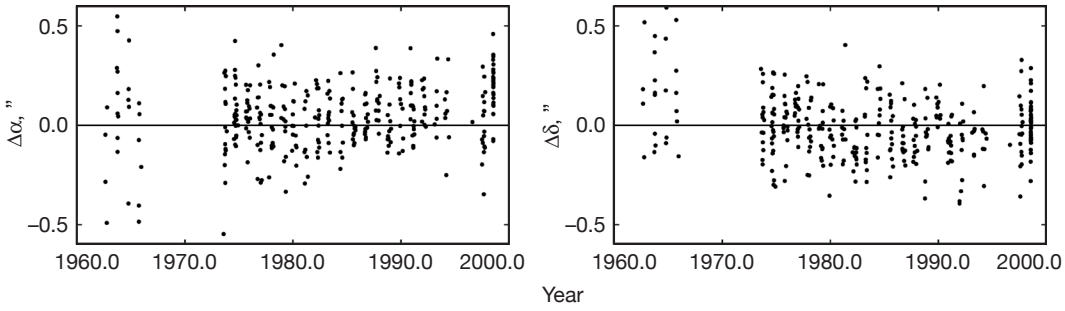

Figure 31. Residuals from astrometric observations of Ganymede by Nikolaev Observatory.

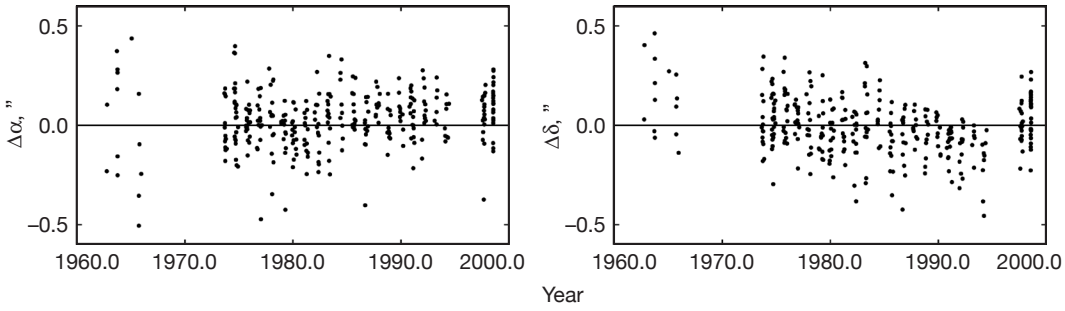

Figure 32. Residuals from astrometric observations of Callisto by Nikolaev Observatory.

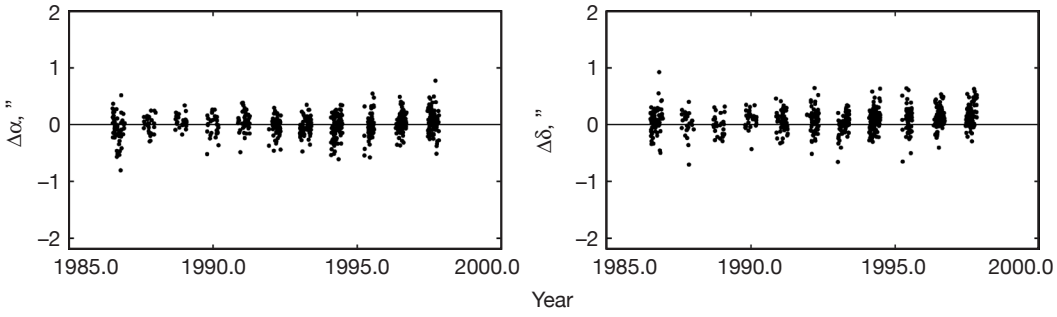

Figure 33. Residuals from astrometric observations of Jupiter by La Palma Observatory.

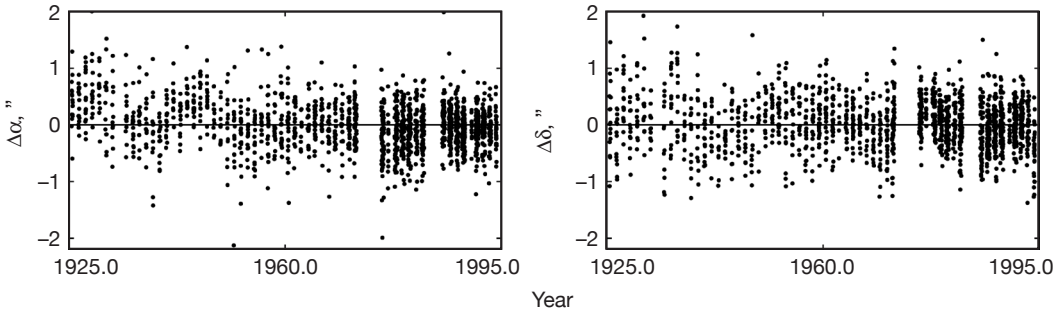

Figure 34. Residuals from transit observations of Jupiter by U. S. Naval Observatory in Washington.

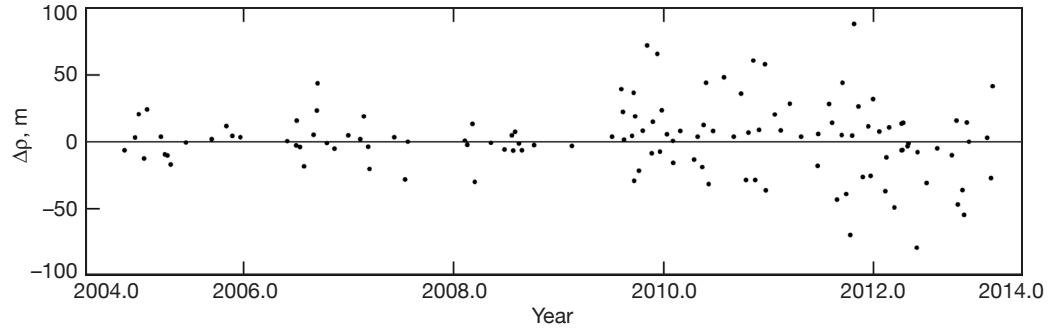

Figure 35. Range residuals from Cassini in orbit about Saturn.

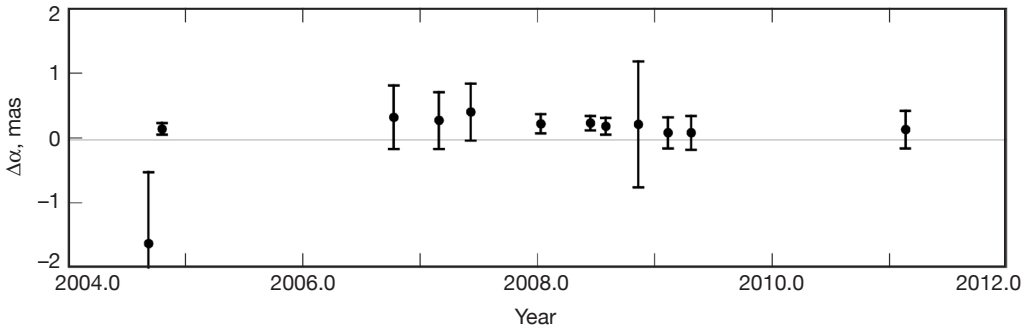

Figure 36. Right ascension residuals from VLBA observations of Cassini at Saturn.

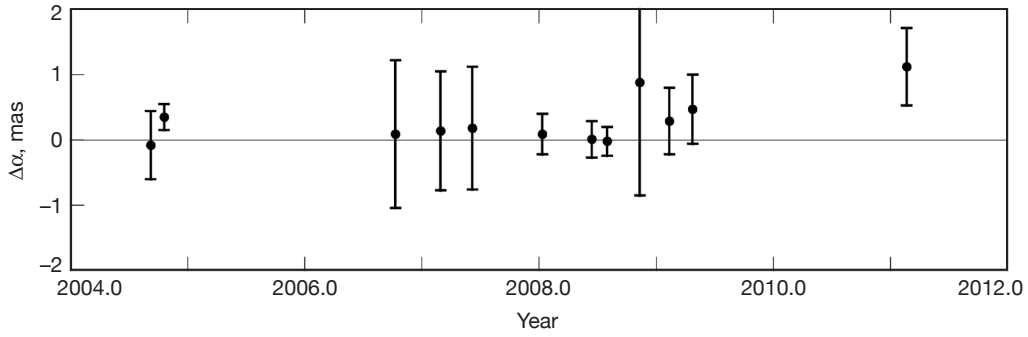

Figure 37. Declination residuals from VLBA observations of Cassini at Saturn.

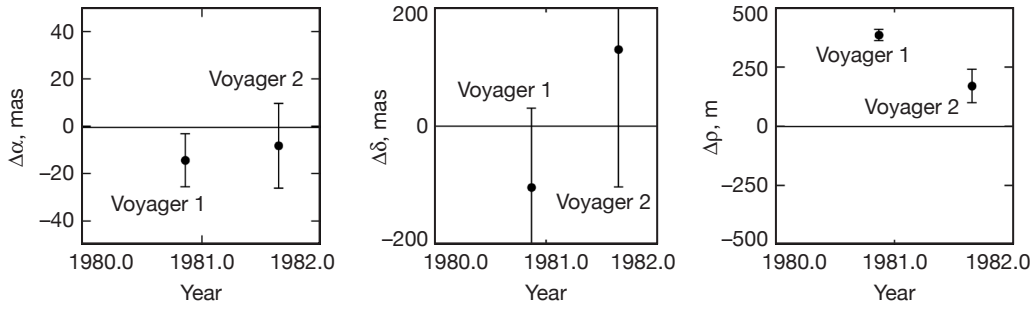

Figure 38. Residuals from Voyager 1 and 2 flybys of Saturn.

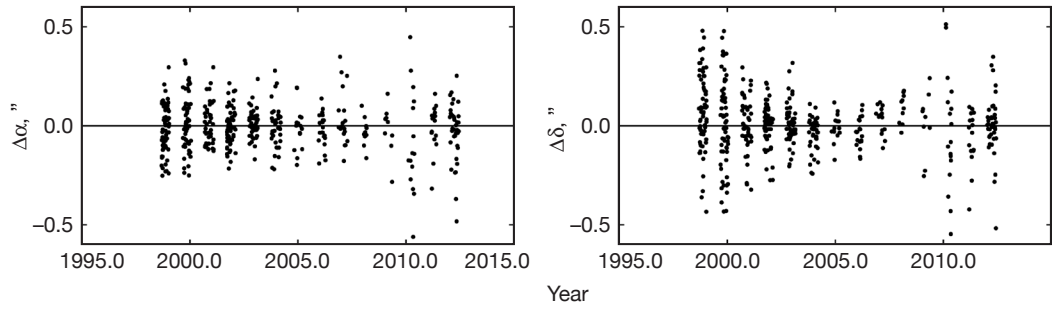

Figure 39. Residuals from astrometric observations of Dione by U. S. Naval Observatory at Flagstaff.

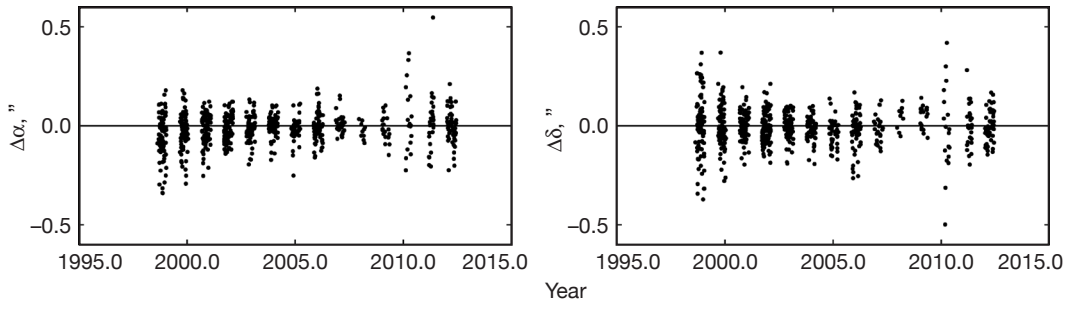

Figure 40. Residuals from astrometric observations of Rhea by U. S. Naval Observatory at Flagstaff.

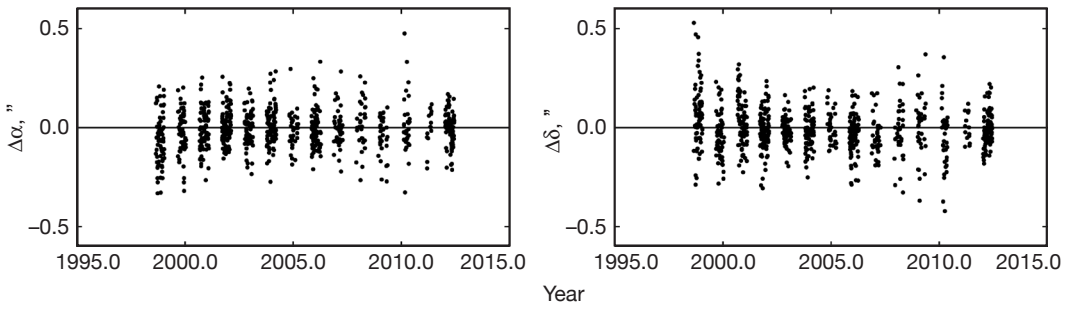

Figure 41. Residuals from astrometric observations of Titan by U. S. Naval Observatory at Flagstaff.

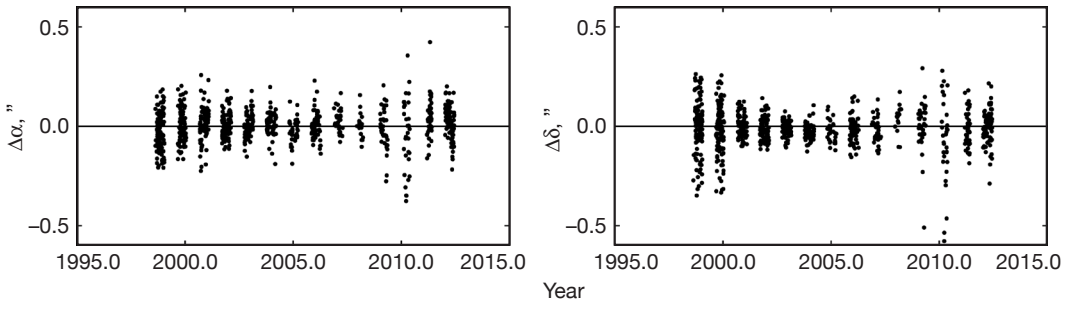

Figure 42. Residuals from astrometric observations of Iapetus by U. S. Naval Observatory at Flagstaff.

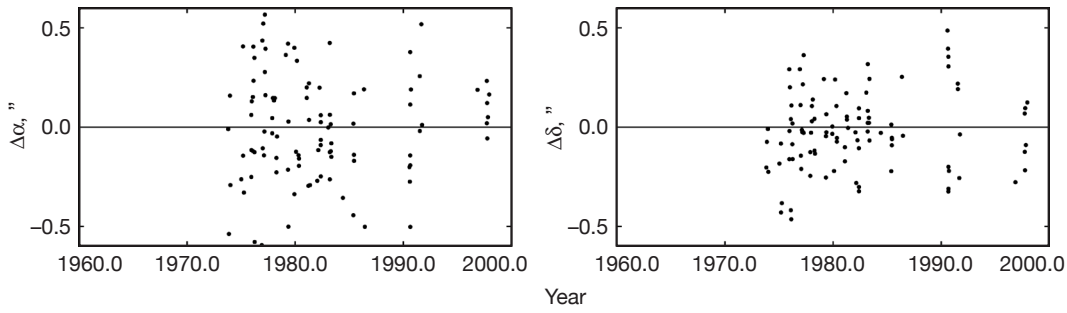

Figure 43. Residuals from astrometric observations of Tethys by Nikolaev Observatory.

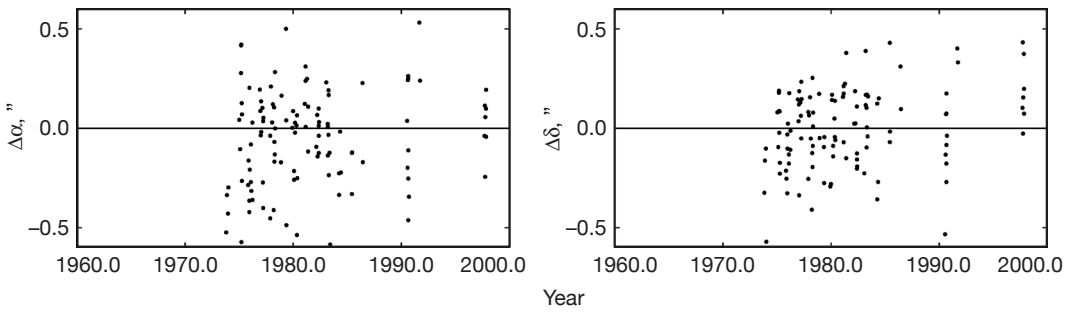

Figure 44. Residuals from astrometric observations of Dione by Nikolaev Observatory.

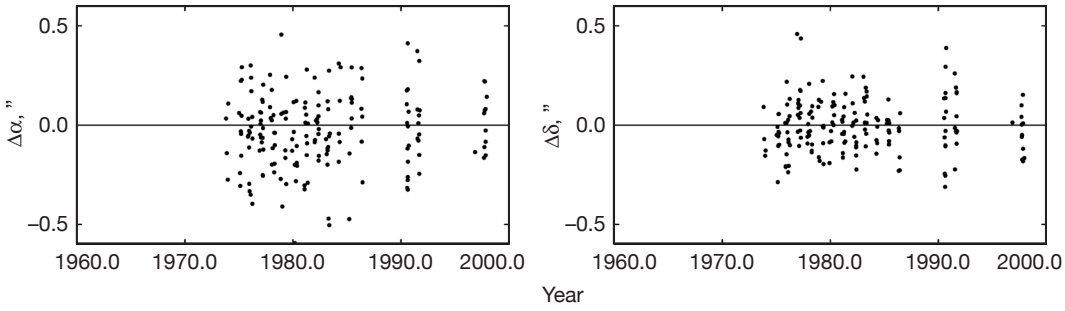

Figure 45. Residuals from astrometric observations of Rhea by Nikolaev Observatory.

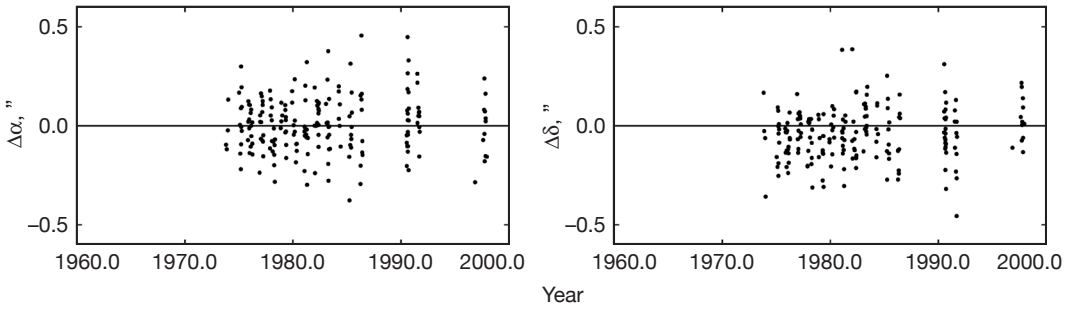

Figure 46. Residuals from astrometric observations of Titan by Nikolaev Observatory.

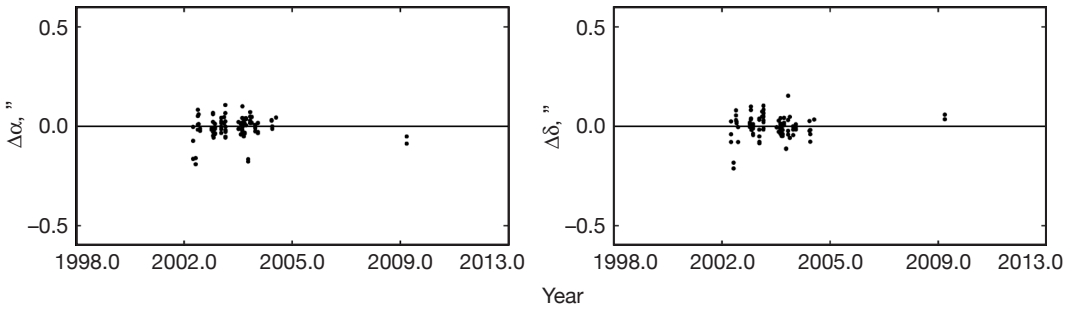

Figure 47. Residuals from astrometric observations of Rhea by Table Mountain Observatory.

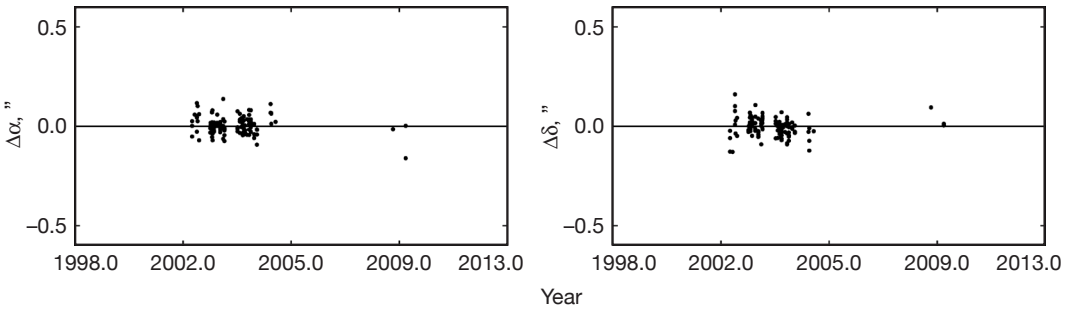

Figure 48. Residuals from astrometric observations of Titan by Table Mountain Observatory.

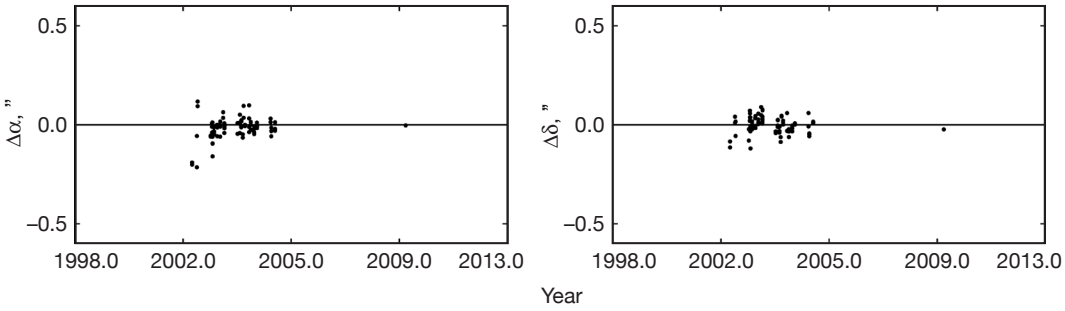

Figure 49. Residuals from astrometric observations of Hyperion by Table Mountain Observatory.

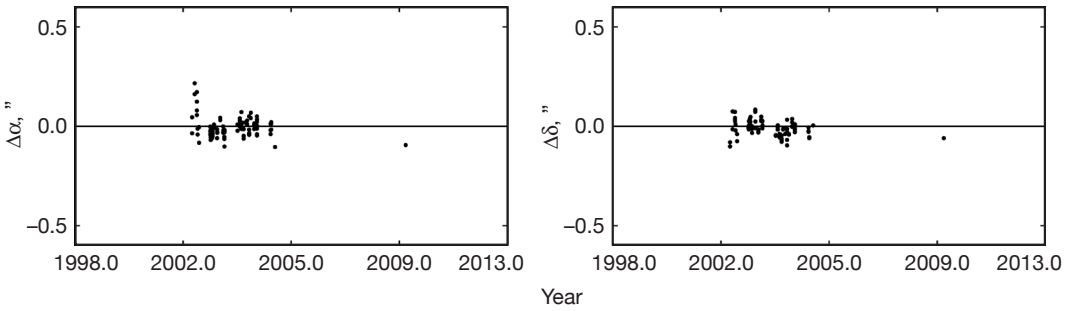

Figure 50. Residuals from astrometric observations of Iapetus by Table Mountain Observatory.

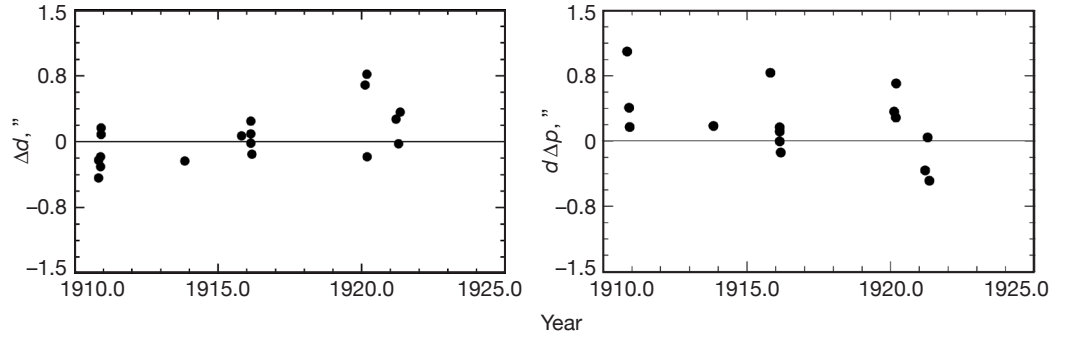

Figure 51. Residuals of angular distance *d* and distance times position angle *p* of Saturn from Yerkes Observatory.

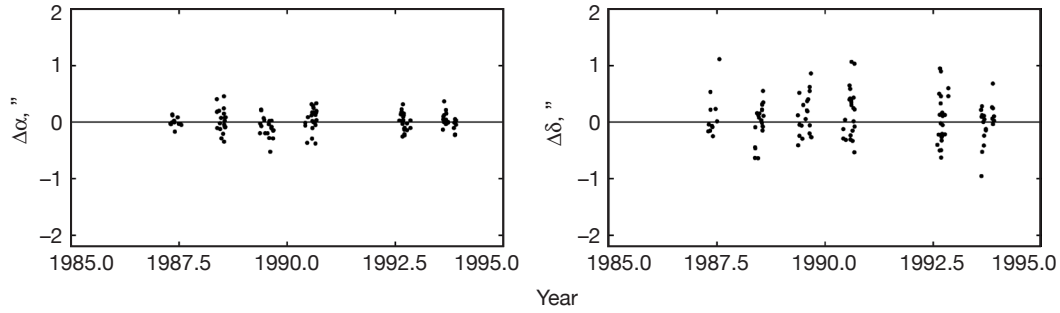

Figure 52. Residuals from transit observations of Saturn by Bordeaux Observatory.

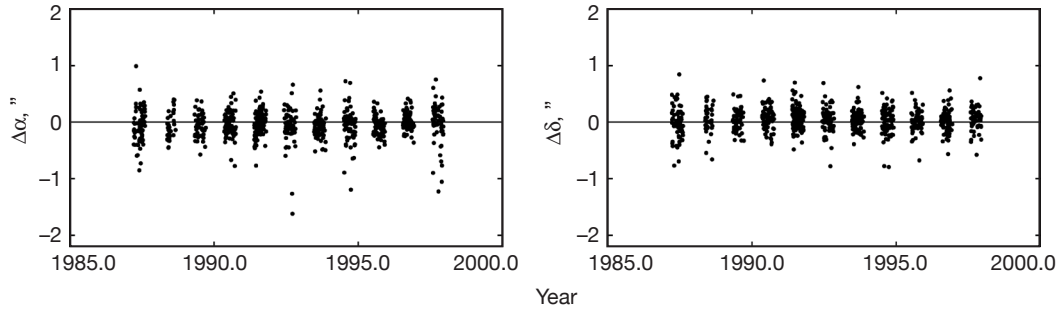

Figure 53. Residuals from astrometric observations of Saturn by La Palma Observatory.

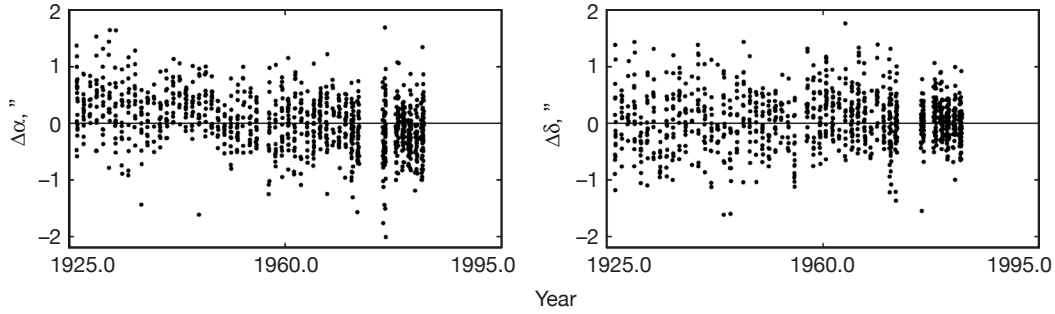

Figure 54. Residuals from transit observations of Saturn by U. S. Naval Observatory in Washington.

F. Uranus and Neptune

All measurements of Uranus and Neptune are astrometric except for flybys by the Voyager 2 spacecraft in 1986 and 1989, respectively, that give a three-dimensional radio-tracking position for one time for each planet. The astrometric data include measurements of the planets themselves and of their major satellites that have accurate enough orbits with respect to the planet: Titania and Oberon for Uranus and Triton for Neptune. The measurements for Uranus cover more than one orbit, giving a fairly well constrained orbit estimate. Measurements of Neptune cover less then one orbit, so the uncertainty in some orbital elements is more than one order of magnitude larger than for Uranus. The residuals of the Uranus measurements are shown in Figures 55–66 and for Neptune in Figures 67–76.

G. Pluto

Pluto's orbit has been determined from ground-based astrometric data only. Measurements from the Hubble Space Telescope (HST) are used to determine the relative orbits of Pluto and its satellites. Most HST observations of the Pluto system do not give positions relative to stars, and those that do are limited by the accuracy of star catalogs and are not much better than ground-based measurements. Like Neptune, measurements of Pluto cover less than one orbit, so several orbit elements, such as the semi-major axis, are relatively poorly known. The astrometric data used here are from the U. S. Naval Observatory [71–77], the Pulkovo Observatory [80], the Observatório do Pico dos Dias,[14] and Table Mountain Observatory. Other astrometric data for Pluto used for DE421 were not included here, since they were of limited time span and used star catalogs not easily corrected to the ICRF2 frame. In addition to the astrometric data, occultation timing measurements that determine the angular position of Pluto have been included [58]. Residuals for the astrometric data are given in Figures 77–80 and for the occultation measurements in Figure 81.

VI. Initial Conditions and Constants

The values of many of the constants used in the equations of motion are estimated along with the initial conditions for the Sun, Moon, and planets where alternative estimates are not sufficiently accurate. Values used for the integration of DE430 are given below. The values are given in double precision, which is sufficient to reproduce the integration. However, most values have uncertainties that are much larger than the number of digits indicate.

Table 4 lists the values of the speed of light and the astronomical unit that are defining constants for DE430 and DE431. The values of the PPN parameters β and γ were held fixed at their nominal values. The initial positions and velocities of the Moon and planets relative to the Sun were estimated as part of the ephemeris fit. The position and velocity of the Sun were adjusted to have the barycenter at the integration origin at the initial time, which is the TDB-compatible Julian day 2440400.5. The positions and velocities of the Earth and Moon with respect to the integration center were input using the Earth–Moon barycenter with respect to the solar system barycenter and the Moon with respect to the Earth. The initial conditions for the Sun and planets are given in Table 5, and for the Moon in Table 6.

[14] G. Benedetti-Rossi et al., *Astronomy and Astrophysics*, submitted, 2014.

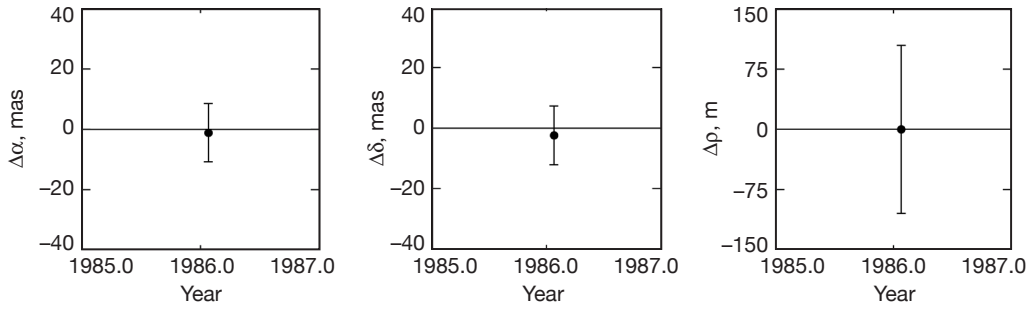

Figure 55. Residuals from Voyager 2 flyby of Uranus.

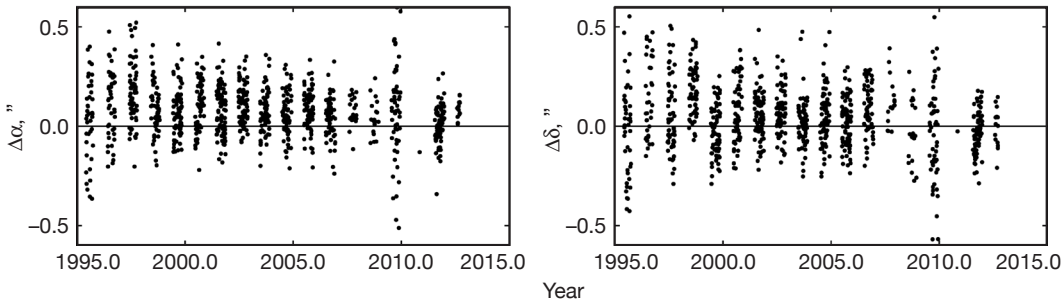

Figure 56. Residuals from astrometric observations of Uranus by U. S. Naval Observatory at Flagstaff.

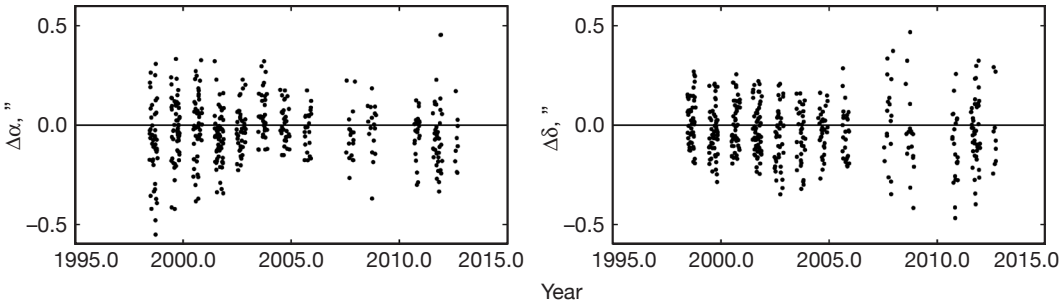

Figure 57. Residuals from astrometric observations of Titania by U. S. Naval Observatory at Flagstaff.

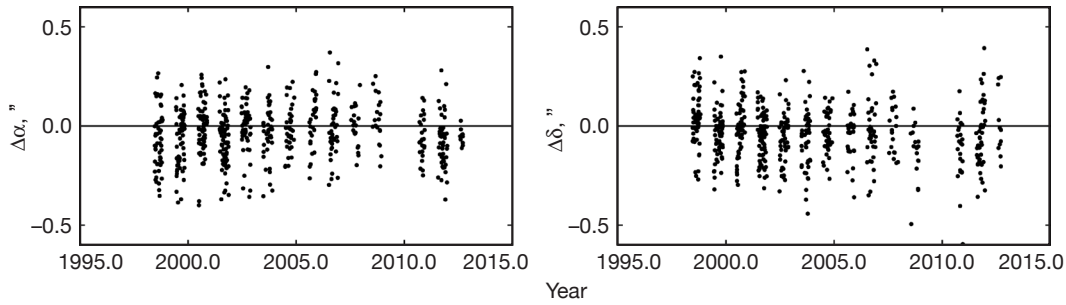

Figure 58. Residuals from astrometric observations of Oberon by U. S. Naval Observatory at Flagstaff.

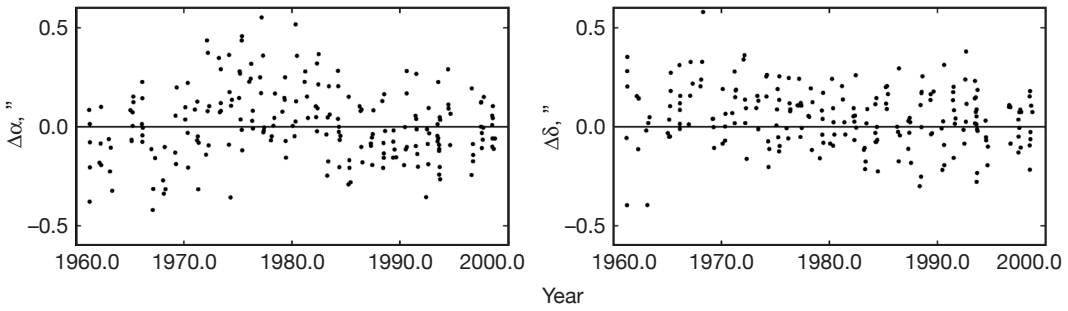

Figure 59. Residuals from astrometric observations of Uranus by Nikolaev Observatory.

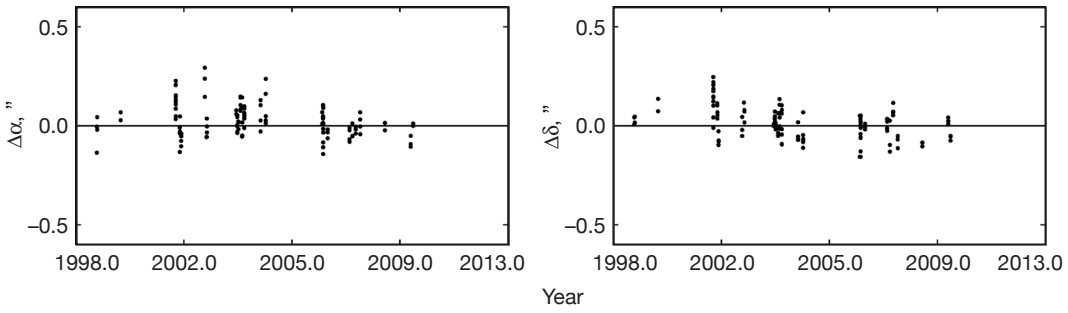

Figure 60. Residuals from astrometric observations of Uranus by Table Mountain Observatory.

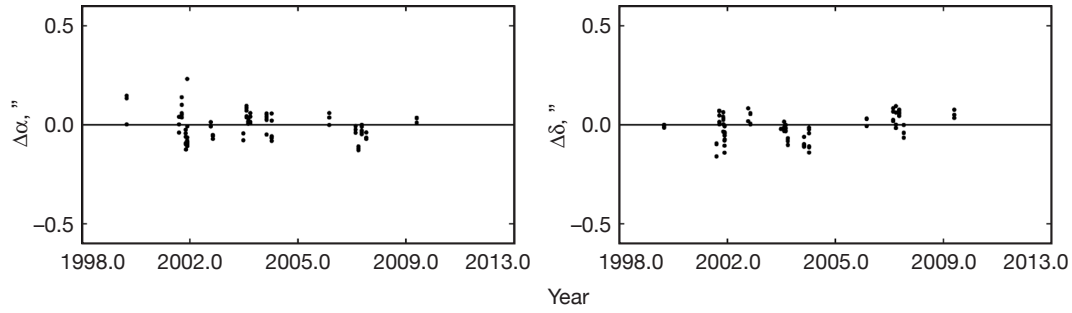

Figure 61. Residuals from astrometric observations of Titania by Table Mountain Observatory.

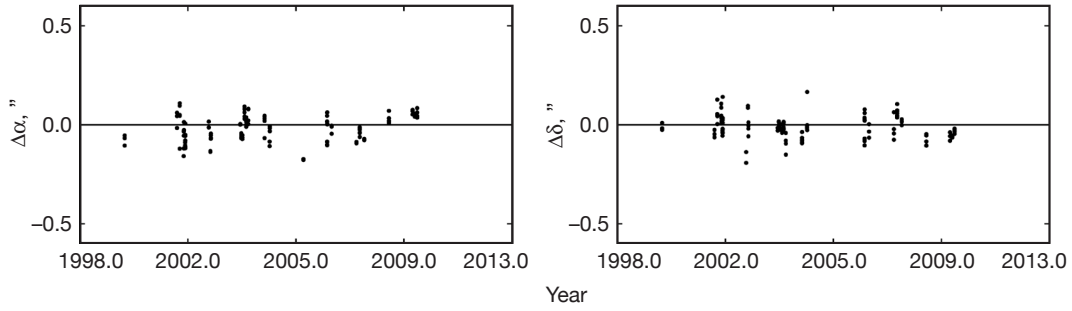

Figure 62. Residuals from astrometric observations of Oberon by Table Mountain Observatory.

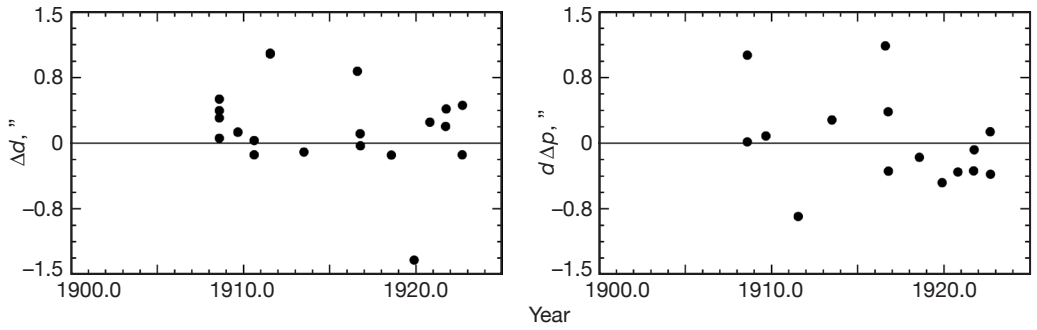

Figure 63. Residuals of angular distance *d* and distance times position angle *p* of Uranus from Yerkes Observatory.

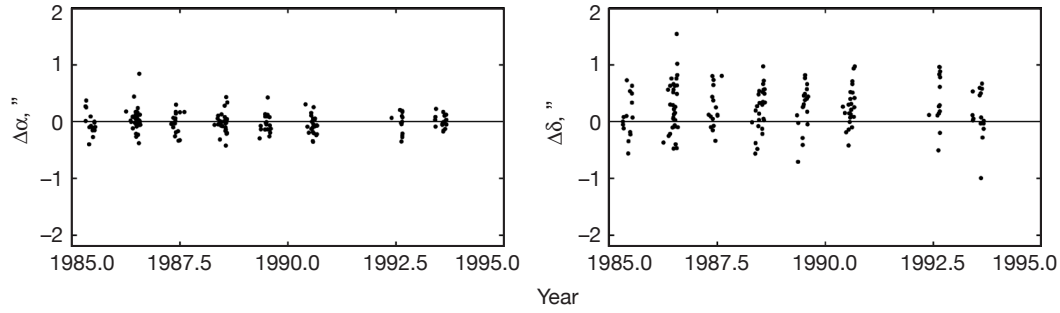

Figure 64. Residuals from transit observations of Uranus by Bordeaux Observatory.

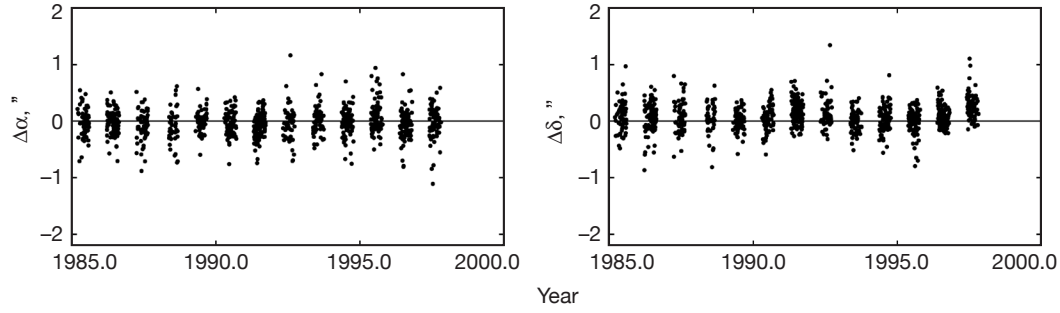

Figure 65. Residuals from astrometric observations of Uranus by La Palma Observatory.

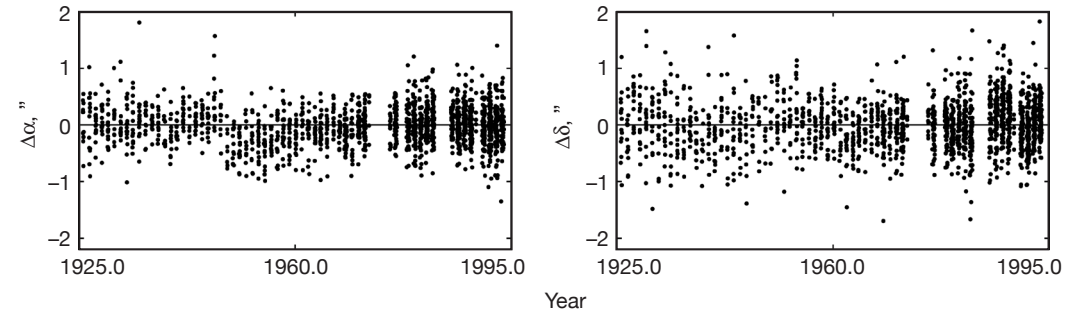

Figure 66. Residuals from transit observations of Uranus by U. S. Naval Observatory in Washington.

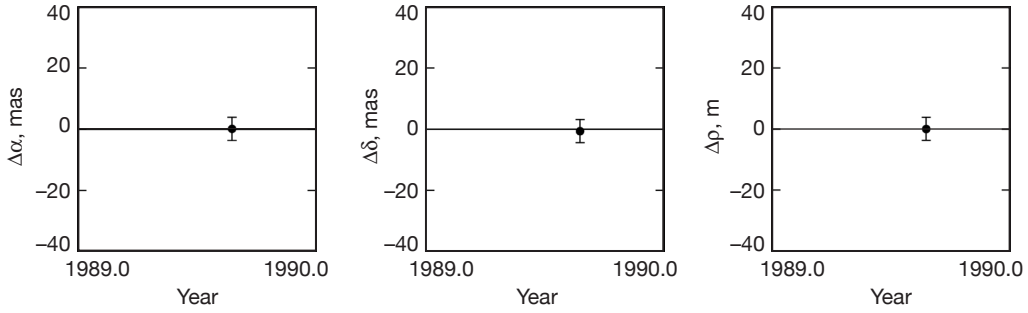

Figure 67. Residuals from Voyager 2 flyby of Neptune.

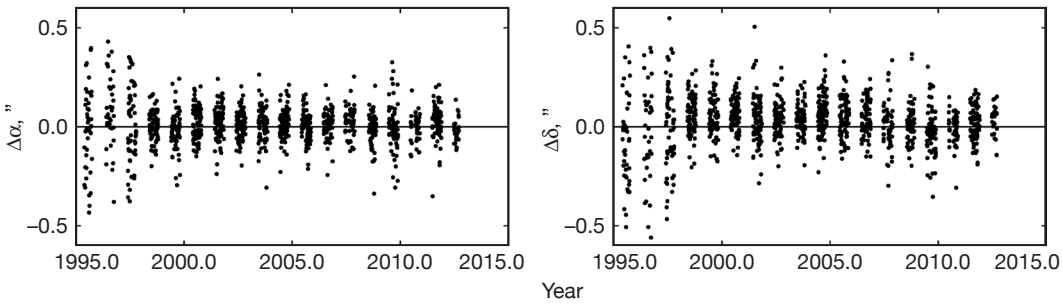

Figure 68. Residuals from astrometric observations of Neptune by U. S. Naval Observatory at Flagstaff.

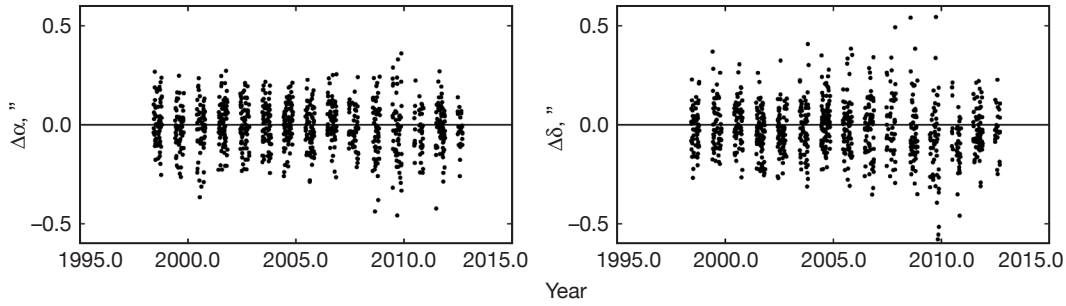

Figure 69. Residuals from astrometric observations of Triton by U. S. Naval Observatory at Flagstaff.

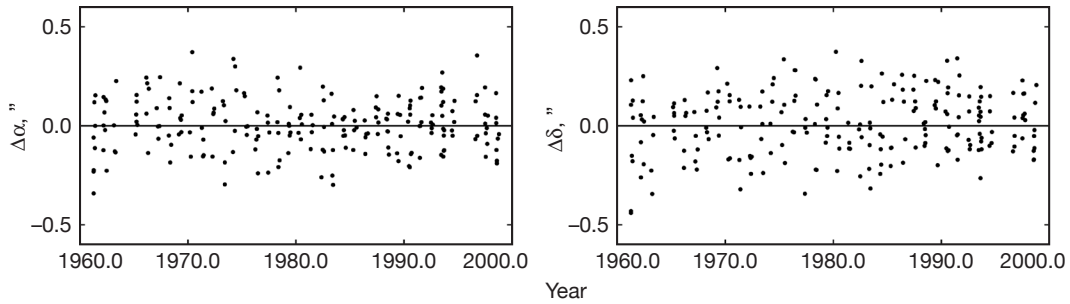

Figure 70. Residuals from astrometric observations of Neptune by Nikolaev Observatory.

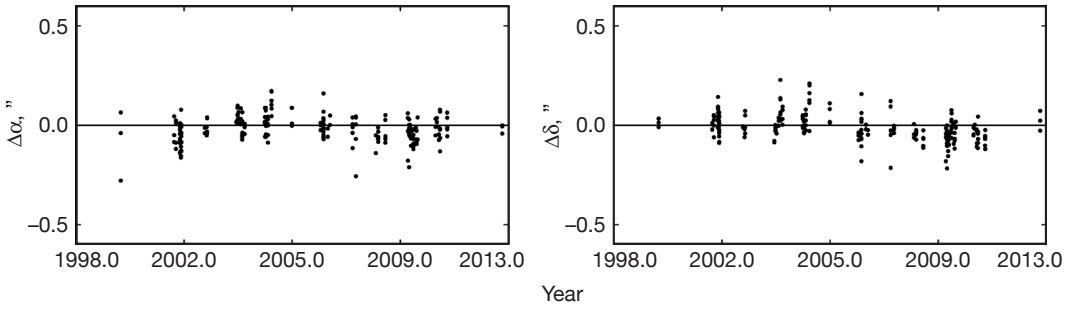

Figure 71. Residuals from astrometric observations of Neptune by Table Mountain Observatory.

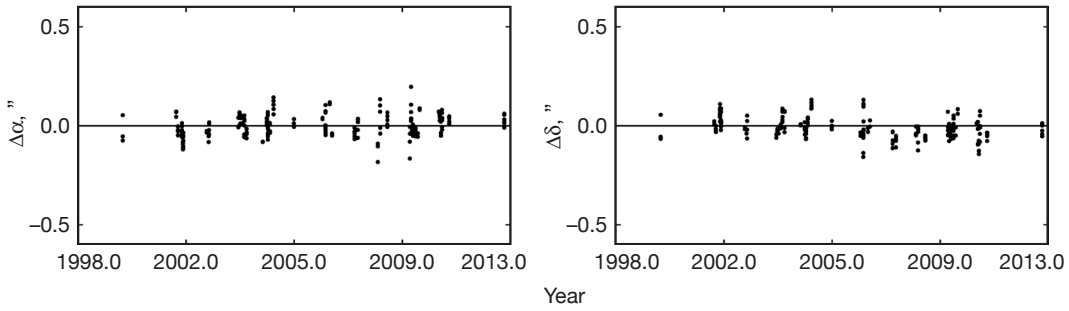

Figure 72. Residuals from astrometric observations of Triton by Table Mountain Observatory.

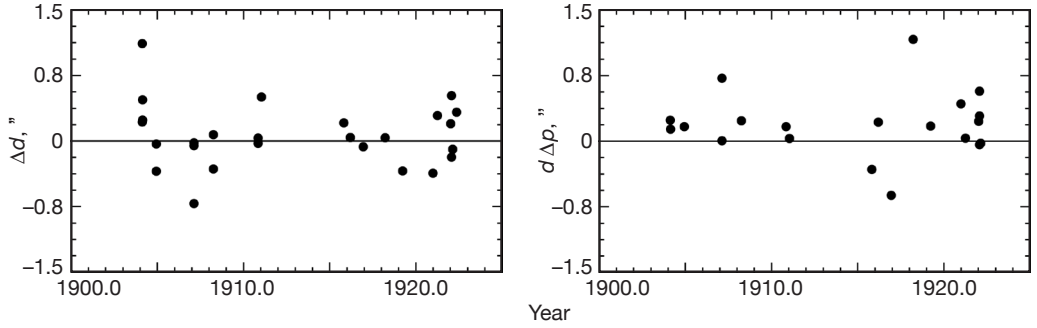

Figure 73. Residuals of angular distance *d* and distance times position angle *p* of Neptune from Yerkes Observatory.

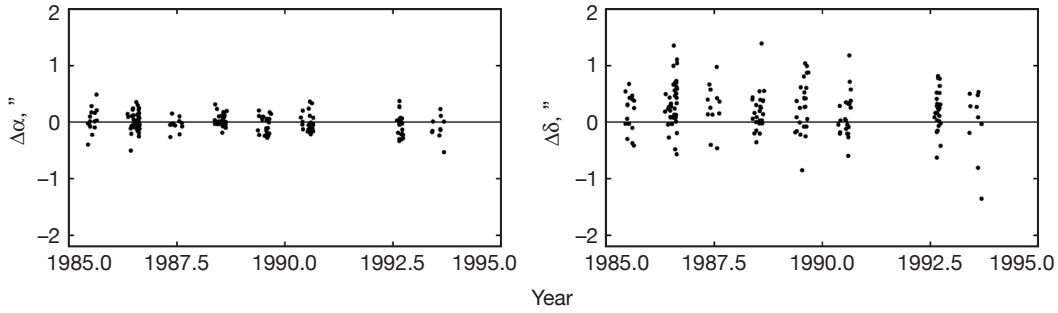

Figure 74. Residuals from transit observations of Neptune by Bordeaux Observatory.

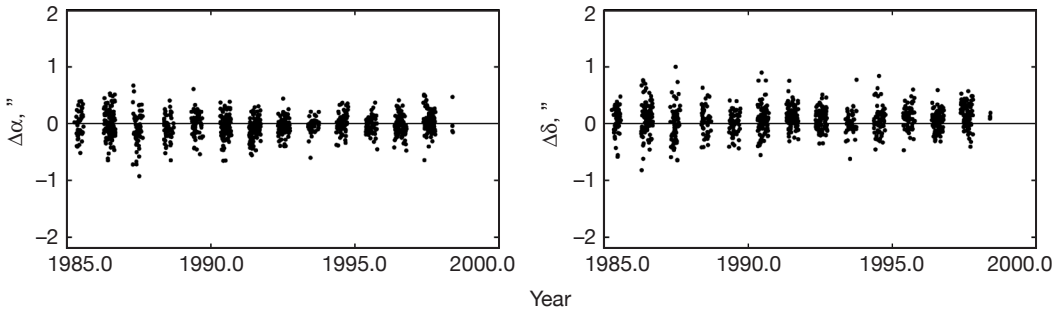

Figure 75. Residuals from astrometric observations of Neptune by La Palma Observatory.

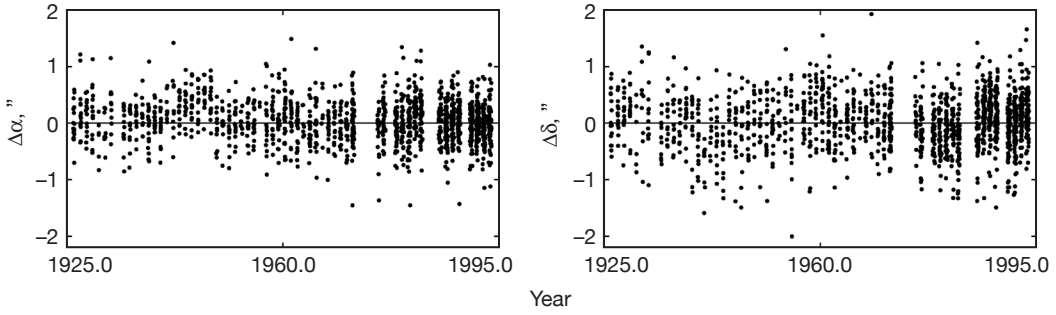

Figure 76. Residuals from transit observations of Neptune by U. S. Naval Observatory in Washington.

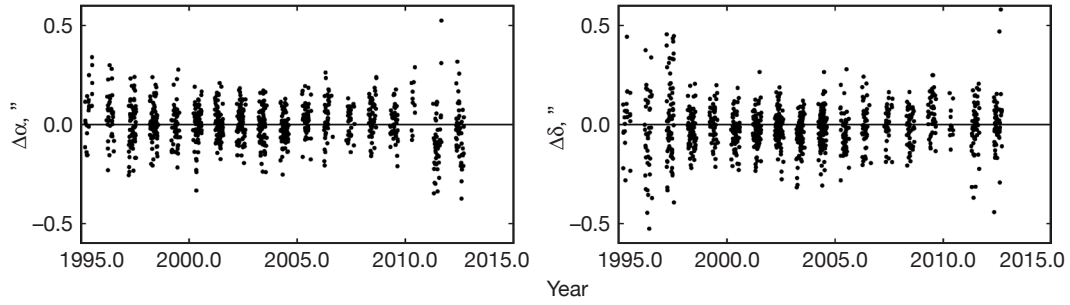

Figure 77. Residuals from astrometric observations of Pluto by U. S. Naval Observatory at Flagstaff.

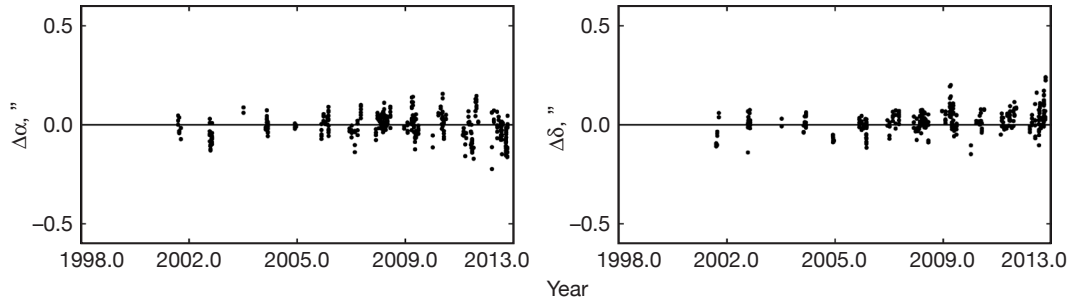

Figure 78. Residuals from astrometric observations of Pluto by Table Mountain Observatory.

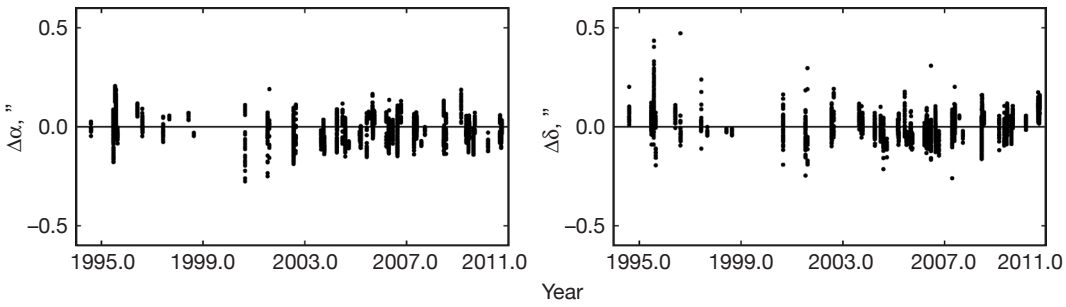

Figure 79. Residuals from astrometric observations of Pluto by Pico dos Dias Observatory.

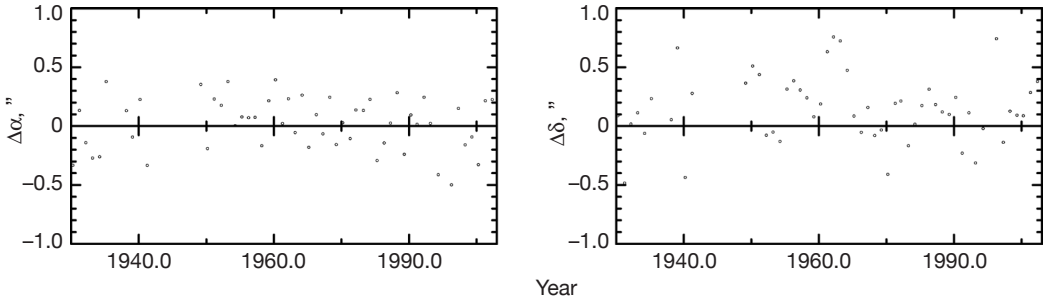

Figure 80. Residuals from astrometric observations of Pluto by Pulkovo Observatory.

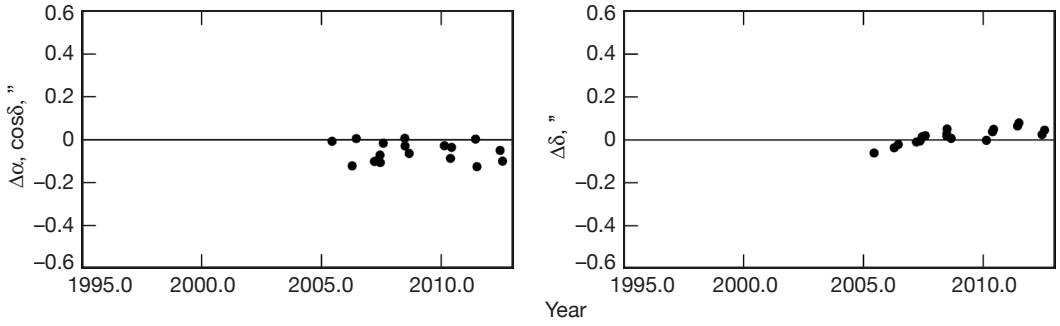

Figure 81. Residuals from occultation observations of Pluto.

Table 4. Defining constants.

c	299792.458 km/s	Speed of light
au	149597870.700 km	Astronomical unit
β	1.0	PPN parameter
γ	1.0	PPN parameter

Table 5. Initial positions (au) and velocities (au/day) of the Sun and planets at Julian day (TDB) 2440400.5 (June 28, 1969), given with respect to the integration origin in the ICRF2 frame.

Sun	x, y, z	0.00450250878464055477	0.00076707642709100705	0.00026605791776697764
	v_x, v_y, v_z	–0.00000035174953607552	0.00000517762640983341	0.00000222910217891203
Mercury	x, y, z	0.36176271656028195477	–0.09078197215676599295	–0.08571497256275117236
	v_x, v_y, v_z	0.00336749397200575848	0.02489452055768343341	0.01294630040970409203
Venus	x, y, z	0.61275194083507215477	–0.34836536903362219295	–0.19527828667594382236
	v_x, v_y, v_z	0.01095206842352823448	0.01561768426786768341	0.00633110570297786403
EM Bary	x, y, z	0.12051741410138465477	–0.92583847476914859295	–0.40154022645315222236
	v_x, v_y, v_z	0.01681126830978379448	0.00174830923073434441	0.00075820289738312913
Mars	x, y, z	–0.11018607714879824523	–1.32759945030298299295	–0.60588914048429142236
	v_x, v_y, v_z	0.01448165305704756448	0.00024246307683646861	–0.00028152072792433877
Jupiter	x, y, z	–5.37970676855393644523	–0.83048132656339789295	–0.22482887442656542236
	v_x, v_y, v_z	0.00109201259423733748	–0.00651811661280738459	–0.00282078276229867897
Saturn	x, y, z	7.89439068290953155477	4.59647805517127300705	1.55869584283189997764
	v_x, v_y, v_z	–0.00321755651650091552	0.00433581034174662541	0.00192864631686015503
Uranus	x, y, z	–18.26540225387235944523	–1.16195541867586999295	–0.25010605772133802236
	v_x, v_y, v_z	0.00022119039101561468	–0.00376247500810884459	–0.00165101502742994997
Neptune	x, y, z	–16.05503578023336944523	–23.94219155985470899295	–9.40015796880239402236
	v_x, v_y, v_z	0.00264276984798005548	–0.00149831255054097759	–0.00067904196080291327
Pluto	x, y, z	–30.48331376718383944523	–0.87240555684104999295	8.91157617249954997764
	v_x, v_y, v_z	0.00032220737349778078	–0.00314357639364532859	–0.00107794975959731297

Table 6. Initial position (au) and velocity (au/day) of the Moon at Julian day (TDB) 2440400.5 (June 28, 1969), given with respect to Earth in the ICRF2 frame.

Moon	x, y, z	–0.00080817735147818490	–0.00199462998549701300	–0.00108726268307068900
	v_x, v_y, v_z	0.00060108481561422370	–0.00016744546915764980	–0.00008556214140094871

The initial Euler angles and angular velocities for the lunar mantle and the initial angular velocities for the core were estimated as part of the ephemeris fit and are given in Table 7. The Euler angles rotate from the ICRF2 frame to the mantle or core frame, respectively. The angular velocities of the mantle and core are given in the mantle frame.

The mass parameters of the planetary systems are most accurately estimated from radio tracking data from spacecraft encounters, while the mass of the Pluto system is most accurately determined by observations of the Pluto system by the Hubble Space Telescope. The planetary system mass parameters that were used are listed in Table 8, and are consistent with the values adopted by the IAU [81]. The mass parameter of the Sun was held fixed as described in Section II.D. The mass parameters of the Earth and Moon were estimated. LLR data are sensitive to the sum of the Earth and Moon mass parameters, while ranging measurements to spacecraft are sensitive to the ratio of the mass of the Earth to the mass of the Moon. The estimated mass of the Earth agrees within uncertainties with estimates from satellite laser ranging [82–84]. The estimated mass parameter of the Moon agrees with independent estimates from the GRAIL mission within uncertainties [85,86].[15]

The extended body parameters of the Sun are given in Table 9. The solar radius is a nominal value [87] and the pole direction is from [88]. $J_{2\odot}$ was estimated. However, since the effect of Lense–Thirring precession due to the angular momentum of the Sun was not included in the dynamical model, the value estimated should be reduced by ~ 7 percent to represent the actual solar gravity field [89].

The extended body parameters of the Earth and Moon are given in Tables 10 and 11. These are described in more detail elsewhere.[16] The radius and zonal gravity coefficients for the Earth, including a rate of change in J_2, were taken from [18]. The Earth Love numbers $k_{20,E}$, $k_{21,E}$, and $k_{22,E}$ include a solid body contribution taken from [18] and a correction from an ocean model. Two time-lags for tidal deformation, the correction to the direction of the rotation axis direction at epoch J2000.0 and the linear rates in rotation axis direction, were estimated. Of the lunar extended body parameters, the quantities, β_L, γ_L, τ_m, f_c, and k_{vc} have been estimated from the LLR data fit. $\tilde{J}_{2,M}$, k_{2M}, and the higher degree and order lunar gravity harmonic coefficients are estimates from the GRAIL mission [85]. The time-dependent values of the degree-2 gravity harmonic coefficients, $J_{2,M}$, $C_{2,2M}$, $C_{2,1M}$, $S_{2,1M}$, and $S_{2,2M}$ were computed from the (time-varying) lunar moment of inertia tensor. The ratio of the core moment of inertia to the total moment of inertia of the undistorted Moon, α_c, was constrained to a previously determined value.

A set of 343 asteroids that have the largest perturbation on the orbit of Mars has been included in the integration. For DE430 and DE431, the positions of the asteroids were integrated iteratively with the positions of the Sun, Moon, and planets. The mass parameters of the 343 asteroids were estimated individually with a priori values and uncertainties. The majority of the constraints were based on radiometric measurements of asteroid diameters

[15] J. G. Williams, A. S. Konopliv, D. H. Boggs, R. S. Park, D.-N. Yuan, et al., "Lunar Interior Properties from the GRAIL Mission," *Journal of Geophysical Research*, submitted.

[16] J. G. Williams, D. H. Boggs, and W. M. Folkner, "DE430 Lunar Orbit, Physical Librations and Surface Coordinates," JPL Interoffice Memorandum 335-JW,DB,WF-20130722-016 (internal document), Jet Propulsion Laboratory, Pasadena, California, July 22, 2013.

Table 7. Lunar mantle and core initial Euler angles (radian) and angular velocities (radian/day) at Julian day (TDB) 2440400.5 (June 28, 1969). Note that the core angular velocity is expressed in the mantle frame.

ϕ_m, θ_m, ψ_m	0.00512830031411853500	0.38239278420173690000	1.29416700274878300000
$\omega_{m,x}, \omega_{m,y}, \omega_{m,z}$	0.00004573724185991433	–0.00000218986174567295	0.22994486018992250000
ϕ_c, θ_c, ψ_c	–0.00241990927040684100	0.41101946488652730000	–0.46309468558363680000
$\omega_{c,x}, \omega_{c,y}, \omega_{c,z}$	–0.00661836772247824400	–0.00107295445159005100	0.22964879652299730000

Table 8. Mass parameters of major bodies.

Body	GM, au^3/day^2	$GM_\odot / GM_{body}$	GM, km^3/s^2
Sun	0.29591220828559 1100E–03	1.000000	132712440041.939400
Mercury	0.49124804503647 6000E–10	6023682.155592	22031.780000
Venus	0.72434523326441 2000E–09	408523.718658	324858.592000
Earth	0.88876924451256 3400E–09	332946.048834	398600.435436
Mars	0.95495486955507 7000E–10	3098703.590291	42828.375214
Jupiter	0.28253458408338 7000E–06	1047.348625	126712764.800000
Saturn	0.84597060732450 3000E–07	3497.901768	37940585.200000
Uranus	0.12920248257829 6000E–07	22902.981613	5794548.600000
Neptune	0.15243573478851 1000E–07	19412.259776	6836527.100580
Pluto	0.21784410519741 8000E–11	135836683.768617	977.000000
Moon	0.10931894507423 7400E–10	27068703.241203	4902.800066

Table 9. Extended body parameters for the Sun.

$R_{\odot}$	696000.0	radius, km
$J_{2,\odot}$	2.1106088532726840E–07	Dynamical form–factor of the Sun
$\alpha_{p,\odot}$	268.13	Right ascension of spin axis direction, deg
$\delta_{p,\odot}$	63.87	Declination of spin axis direction, deg

Table 10. Extended body parameters for the Earth.

R_E	6378.1363	Radius, km
J_{2E}	0.00108262545	Zonal harmonics of the Earth
J_{3E}	–0.00000253241	
J_{4E}	–0.000001616	
$d(J_{2E})/dt$	–2.60E–11	Rate of change of J_{2E}, yr^{-1}
$k_{20,E}$	0.335	Potential Love number for long–period deformation
$k_{21,E}$	0.32	Potential Love number for diurnal deformation
$k_{22,E}$	0.32	Potential Love number for semi–diurnal deformation
τ'_0	0.0640	Orbital time–lag for long–period deformation, days
τ'_1	–0.0044	Orbital time–lag for diurnal deformation, days
τ'_2	–0.1000	Orbital time–lag for semi–diurnal deformation, days
τ_0	0.0	Rotational time–lag for long–period deformation, days
τ_1	7.3632190228041890E–03	Rotational time–lag for dirunal deformation, days
τ_2	2.5352978633388720E–03	Rotational time–lag for semi–diurnal deformation, days
Φ_{x_0}	5.6754203322893470E–03	X–axis rotation at J2000.0, ″
Φ_{y_0}	–1.7022656914989530E–02	Y–axis rotation at J2000.0, ″
$d\Phi_x/dt$	2.7689915574483550E–04	Negative obliquity rate correction, ″/yr
$d\Phi_y/dt$	–1.2118591216559240E–03	Precession rate correction times sine of obliquity, ″/yr

Table 11. Extended body parameters for the Moon.

R_M	1738.0	Radius, km
β_L	6.3102131934887270E–04	Lunar moment parameters
γ_L	2.2773171480091860E–04	
$k_{2,M}$	0.024059	Potential love number
τ_M	9.5830547273306690E–02	Time–lag for the solid–body tide, days
α_c	0.0007	Ratio of polar moment of inertia of core to mean total polar moment of inertia
f_c	2.4623904789198150E–04	Oblateness of core
k_v/C_T	1.6365616533709530E–08	Friction coefficient between core and mantle, radian/day
$\tilde{J}_{2,M}$	2.0321568464952570E–04	Undistorted 2nd zonal harmonic coefficient
$J_{3,M}$	8.4597026974594570E–06	Zonal harmonic coefficients
$J_{4,M}$	–9.7044138365700000E–06	
$J_{5,M}$	7.4221608384052890E–07	
$J_{6,M}$	–1.3767531350969900E–05	
$S_{3,1,M}$	5.8915551555318640E–06	Tesseral harmonic coefficients
$S_{3,2,M}$	1.6844743962783900E–06	
$S_{3,3,M}$	–2.4742714379805760E–07	
$S_{4,1,M}$	1.5789202789245720E–06	
$S_{4,2,M}$	–1.5153915796731720E–06	
$S_{4,3,M}$	–8.0349266627431070E–07	
$S_{4,4,M}$	8.2964257754075220E–08	
$S_{5,1,M}$	–3.5272289393243820E–06	
$S_{5,2,M}$	1.7107886673430380E–07	
$S_{5,3,M}$	2.8736257616334340E–07	
$S_{5,4,M}$	5.2652110720146800E–10	
$S_{5,5,M}$	–6.7824035473995330E–09	
$S_{6,1,M}$	–2.0453507141252220E–06	
$S_{6,2,M}$	–2.6966834353574270E–07	
$S_{6,3,M}$	–7.1063745295915780E–08	
$S_{6,4,M}$	–1.5361616966632300E–08	
$S_{6,5,M}$	–8.3465073195142520E–09	
$S_{6,6,M}$	1.6844213702632920E–09	
$C_{3,1,M}$	2.8480741195592860E–05	
$C_{3,2,M}$	4.8449420619770600E–06	
$C_{3,3,M}$	1.6756178134114570E–06	
$C_{4,1,M}$	–5.7048697319733210E–06	
$C_{4,2,M}$	–1.5912271792977430E–06	
$C_{4,3,M}$	–8.0678881596778210E–08	
$C_{4,4,M}$	–1.2692158612216040E–07	
$C_{5,1,M}$	–8.6629769308983560E–07	
$C_{5,2,M}$	7.1199537967353330E–07	
$C_{5,3,M}$	1.5399750424904520E–08	
$C_{5,4,M}$	2.1444704319218450E–08	
$C_{5,5,M}$	7.6596153884006140E–09	
$C_{6,1,M}$	1.2024363601545920E–06	
$C_{6,2,M}$	–5.4703897324156850E–07	
$C_{6,3,M}$	–6.8785612757292010E–08	
$C_{6,4,M}$	1.2915580402925160E–09	
$C_{6,5,M}$	1.1737698784460500E–09	
$C_{6,6,M}$	–1.0913395178881540E–09	

provided by the WISE and SIMPS surveys [9,10]. In a similar previous analysis [7], information on individual asteroid mass parameters was excluded, to allow independent estimates based on the range data to Martian spacecraft. For DE430 and DE431, asteroid mass parameter estimates from other techniques were included as a priori constraints. Estimates were included based on close encounters between asteroids [90,91], masses of binary asteroids [92–95], and masses determined from radio tracking of spacecraft directly affected by the gravity of individual asteroids [96–99]. The mass parameters used for DE430/DE431 are given in Table 12. The initial positions and velocities of the asteroids were taken from the Horizons online solar system data service [13] and are given in Table 13.

Acknowledgments

The planetary ephemeris accuracies are limited by the accuracy of measurements to which they are fit. These measurements are the results of the efforts of dozens of observers and hundreds of dedicated scientists and engineers operating the many spacecraft missions to the Moon and planets. We would like to thank especially the following for directly delivering measurements for inclusion in the ephemeris development: Tom Murphy, Peter Shelus, Randy Ricklefs, Jerry Wiant, Jean-Marie Torre, and colleagues for recent lunar laser ranging data; Tony Taylor, Maria Zuber, and Dave Smith for detailed information on the MESSENGER spacecraft dynamics; Alex Konopliv for producing range measurements adjusted to the central body for MESSENGER, Mars Global Surveyor, Mars Odyssey, and Mars Reconnaissance Orbiter; Jim Border for the Magellan and Mars spacecraft VLBI measurements; Trevor Morely, Frank Budnik, and colleagues for Venus Express and Mars Express range and Venus Express VLBI measurements; Bob Jacobson for reduction of Voyager, Pioneer, and Cassini spacecraft tracking data; Hugh Harris and Alice Monet for observations of the outer planets at the U. S. Naval Observatory in Flagstaff; Bill Owen for observations of the outer planets from Table Mountain Observatory; Julio Camargo, Gustavo Benedetti-Rossi, Felipe Braga Ribas, Marcelo Assafin, Alex Dias-Oliveira, and Roberto Vieira Martins for observations of Pluto from Observatório do Pico dos Dias; Bruno Sicardy and Marcelo Assafin for recent occultation measurements of the position of Pluto. This work is also greatly indebted to the earlier work by Myles Standish and Skip Newhall, who created much of the software for the development of the ephemerides.

Table 12. Mass parameters of asteroids (1 of 7).

Number	Name	GM, au^3/day^2	$GM_{ast}/GM_{\odot}$	GM, km^3/s^2
1	Ceres	0.140047655617234400E–12	4.73E–10	62.809393
2	Pallas	0.310444819893871300E–13	1.05E–10	13.923011
3	Juno	0.361753831714793700E–14	1.22E–11	1.622415
4	Vesta	0.385475018780881000E–13	1.30E–10	17.288009
5	Astraea	0.374873628455203200E–15	1.27E–12	0.168126
6	Hebe	0.831241921267337200E–15	2.81E–12	0.3728
7	Iris	0.216434444257140700E–14	7.22E–12	0.958161
8	Flora	0.589425652970690800E–15	1.99E–12	0.264349
9	Metis	0.107784100424073000E–14	3.64E–12	0.483396
10	Hygiea	0.123580078729412500E–13	4.18E–11	5.542392
11	Parthenope	0.133153625545997500E–14	4.50E–12	0.597175
12	Victoria	0.193177578518292000E–15	6.53E–13	0.086637
13	Egeria	0.179700489450744600E–14	6.07E–12	0.805931
14	Irene	0.110064567957506800E–14	3.72E–12	0.493624
15	Eunomia	0.467830741835090500E–14	1.58E–11	2.098155
16	Psyche	0.341158682619381200E–14	1.15E–11	1.530048
17	Thetis	0.208150639646973800E–15	7.03E–13	0.093353
18	Melpomene	0.200892773665113200E–15	6.79E–13	0.090098
19	Fortuna	0.103564484013119400E–14	3.50E–12	0.464472
20	Massalia	0.919980747763091100E–16	3.11E–13	0.04126
21	Lutetia	0.252944287204099900E–15	8.55E–13	0.113442
22	Kalliope	0.120262444348346000E–14	4.06E–12	0.53936
23	Thalia	0.189533176041978300E–15	6.41E–13	0.085003
24	Themis	0.189390166752538200E–14	6.40E–12	0.849388
25	Phocaea	0.723984152236621100E–16	2.45E–13	0.03247
26	Proserpina	0.163734395226108400E–15	5.53E–13	0.073433
27	Euterpe	0.388800389854578800E–15	1.31E–12	0.174371
28	Bellona	0.292627274429452800E–15	9.89E–13	0.131239
29	Amphitrite	0.197584236512452000E–14	6.68E–12	0.886137
30	Urania	0.148201901643752900E–15	5.01E–13	0.066466
31	Euphrosyne	0.634328047364860200E–14	2.14E–11	2.844872
32	Pomona	0.119958501623344000E–15	4.05E–13	0.0538
34	Circe	0.294454129152128600E–15	9.95E–13	0.132059
35	Leukothea	0.235225617324184100E–15	7.95E–13	0.105495
36	Atalante	0.169706001840970900E–15	5.74E–13	0.076111
37	Fides	0.218562057711305600E–15	7.39E–13	0.098022
38	Leda	0.132328596474676800E–15	4.47E–13	0.059348
39	Laetitia	0.149751968255670100E–14	5.06E–12	0.671616
40	Harmonia	0.295241408030842200E–15	9.98E–13	0.132412
41	Daphne	0.932422376219886900E–15	3.15E–12	0.418178
42	Isis	0.276531664347438100E–15	9.35E–13	0.124021
43	Ariadne	0.727539385334071200E–16	2.46E–13	0.032629
44	Nysa	0.468864072012922000E–16	1.58E–13	0.021028
45	Eugenia	0.842567801856793400E–15	2.85E–12	0.37788
46	Hestia	0.327280000000000000E–15	1.11E–12	0.14678
47	Aglaja	0.554352356159888900E–15	1.87E–12	0.248619
48	Doris	0.253109172601506800E–14	8.55E–12	1.135159
49	Pales	0.754948162931440200E–16	2.55E–13	0.033858
50	Virginia	0.163332639111751800E–15	5.52E–13	0.073252

Table 12. Mass parameters of asteroids. (Continued: 2 of 7)

Number	Name	GM, au^3/day^2	$GM_{ast}/GM_{\odot}$	GM, km^3/s^2
51	Nemausa	0.257054911335314500E–15	8.69E–13	0.115285
52	Europa	0.247678810125586700E–14	8.37E–12	1.110804
53	Kalypso	0.623924331077516500E–16	2.11E–13	0.027982
54	Alexandra	0.562417365019245900E–15	1.90E–12	0.252236
56	Melete	0.369928831270212600E–15	1.25E–12	0.165908
57	Mnemosyne	0.368060192063965100E–15	1.24E–12	0.16507
58	Concordia	0.848117391146600300E–16	2.87E–13	0.038037
59	Elpis	0.633944272758765100E–15	2.14E–12	0.284315
60	Echo	0.509113678301446400E–16	1.72E–13	0.022833
62	Erato	0.108904819196005700E–15	3.68E–13	0.048842
63	Ausonia	0.564040174397624300E–16	1.91E–13	0.025296
65	Cybele	0.318065928265254100E–14	1.07E–11	1.426481
68	Leto	0.343102659123796900E–15	1.16E–12	0.153877
69	Hesperia	0.514461002087673500E–15	1.74E–12	0.230728
70	Panopaea	0.276888884015784600E–15	9.36E–13	0.124181
71	Niobe	0.142449274635095600E–15	4.81E–13	0.063886
72	Feronia	0.799505104491654100E–16	2.70E–13	0.035857
74	Galatea	0.350737445129561400E–15	1.19E–12	0.157301
75	Eurydike	0.435737462507712700E–16	1.47E–13	0.019542
76	Freia	0.831220000000000100E–15	2.81E–12	0.37279
77	Frigga	0.493129550950072900E–16	1.67E–13	0.022116
78	Diana	0.840190625346388700E–16	2.84E–13	0.037681
79	Eurynome	0.835182433140794000E–16	2.82E–13	0.037457
80	Sappho	0.116144395411310800E–15	3.92E–13	0.052089
81	Terpsichore	0.102236755455613400E–15	3.45E–13	0.045852
82	Alkmene	0.660126076693077000E–16	2.23E–13	0.029606
83	Beatrix	0.109683489062603500E–15	3.71E–13	0.049191
84	Klio	0.125731265563188600E–15	4.25E–13	0.056389
85	Io	0.925408545301853800E–15	3.13E–12	0.415033
86	Semele	0.215239955702289100E–15	7.27E–13	0.096532
87	Sylvia	0.219929517357407300E–14	7.43E–12	0.986353
88	Thisbe	0.257711412731104700E–14	8.71E–12	1.155799
89	Julia	0.340203115743942900E–15	1.15E–12	0.152576
90	Antiope	0.123519636282849100E–15	4.17E–13	0.055397
91	Aegina	0.244046167770100600E–15	8.25E–13	0.109451
92	Undina	0.403694351768607300E–15	1.36E–12	0.181051
93	Minerva	0.564773071797647600E–15	1.91E–12	0.253293
94	Aurora	0.127923000000000000E–14	4.32E–12	0.573717
95	Arethusa	0.271661970839325900E–15	9.18E–13	0.121837
96	Aegle	0.154656769562432500E–14	5.23E–12	0.693614
97	Klotho	0.103149563583763100E–15	3.49E–13	0.046261
98	Ianthe	0.244283174173206900E–15	8.26E–13	0.109558
99	Dike	0.735266201384159100E–16	2.48E–13	0.032976
100	Hekate	0.136597719646869700E–15	4.62E–13	0.061262
102	Miriam	0.128126622566059800E–15	4.33E–13	0.057463
103	Hera	0.100111801685864600E–15	3.38E–13	0.044899
104	Klymene	0.481223966780187300E–15	1.63Ev12	0.215822
105	Artemis	0.371546679753414500E–15	1.26E–12	0.166633
106	Dione	0.539739999999999800E–15	1.82E–12	0.242066

Table 12. Mass parameters of asteroids. (Continued: 3 of 7)

Number	Name	GM, au^3/day^2	$GM_{ast}/GM_{\odot}$	GM, km^3/s^2
107	Camilla	0.167172099170064400E–14	5.65E–12	0.749743
109	Felicitas	0.108261858615819300E–15	3.66E–13	0.048554
110	Lydia	0.140769857221050400E–15	4.76E–13	0.063133
111	Ate	0.335191928112805600E–16	1.13E–13	0.015033
112	Iphigenia	0.579603970155323500E–16	1.96E–13	0.025994
113	Amalthea	0.255802139245781900E–16	8.64E–14	0.011472
114	Kassandra	0.170500000000000000E–15	5.76E–13	0.076467
115	Thyra	0.552582419038552700E–16	1.87E–13	0.024783
117	Lomia	0.447136801784178900E–15	1.51E–12	0.200535
118	Peitho	0.270007596259813500E–16	9.12E–14	0.012109
120	Lachesis	0.118898494995200800E–14	4.02E–12	0.533243
121	Hermione	0.700790692204134300E–15	2.37E–12	0.314295
124	Alkeste	0.887727082656233800E–16	3.00E–13	0.039813
127	Johanna	0.366116824306172300E–15	1.24E–12	0.164198
128	Nemesis	0.965012951054875100E–15	3.26E–12	0.432795
129	Antigone	0.465424524739797500E–15	1.57E–12	0.208736
130	Elektra	0.993662954590924800E–15	3.36E–12	0.445644
132	Aethra	0.131961412217015600E–16	4.46E–14	0.005918
134	Sophrosyne	0.336204654208871600E–15	1.14E–12	0.150783
135	Hertha	0.951560504184620700E–16	3.22E–13	0.042676
137	Meliboea	0.856126059955389200E–15	2.89E–12	0.38396
139	Juewa	0.422428821437744500E–15	1.43E–12	0.189453
140	Siwa	0.313167325322240600E–15	1.06E–12	0.140451
141	Lumen	0.376614060167083300E–15	1.27E–12	0.168906
143	Adria	0.112608611474888300E–15	3.81E–13	0.050503
144	Vibilia	0.699516335498308700E–15	2.36E–12	0.313723
145	Adeona	0.755823292622889200E–15	2.55E–12	0.338976
146	Lucina	0.394160000000000000E–15	1.33E–12	0.176775
147	Protogeneia	0.406817291771643100E–15	1.37E–12	0.182452
148	Gallia	0.165952595163453000E–15	5.61E–13	0.074427
150	Nuwa	0.453364684879681200E–15	1.53E–12	0.203328
154	Bertha	0.829838876716369400E–15	2.80E–12	0.372171
156	Xanthippe	0.263360000000000000E–15	8.90E–13	0.118113
159	Aemilia	0.288240661838050000E–15	9.74E–13	0.129272
160	Una	0.102484870587440500E–15	3.46E–13	0.045963
162	Laurentia	0.237290753793420100E–15	8.02E–13	0.106422
163	Erigone	0.865800000000000100E–16	2.93E–13	0.03883
164	Eva	0.418326020317249000E–15	1.41E–12	0.187613
165	Loreley	0.106845990270469300E–14	3.61E–12	0.479189
168	Sibylla	0.534709999999999800E–15	1.81E–12	0.23981
171	Ophelia	0.151098849092935500E–15	5.11E–13	0.067766
172	Baucis	0.431771576449205300E–16	1.46E–13	0.019364
173	Ino	0.391242854708310100E–15	1.32E–12	0.175467
175	Andromache	0.289909719621158200E–15	9.80E–13	0.13002
176	Iduna	0.167134755200936100E–15	5.65E–13	0.074958
177	Irma	0.453728862942509900E–16	1.53E–13	0.020349
181	Eucharis	0.167967668335482500E–15	5.68E–13	0.075331
185	Eunike	0.113558589448392200E–14	3.84E–12	0.509294
187	Lamberta	0.941936446359531100E–15	3.18E–12	0.422445

Table 12. Mass parameters of asteroids. (Continued: 4 of 7)

Number	Name	GM, au^3/day^2	$GM_{ast}/GM_{\odot}$	GM, km^3/s^2
191	Kolga	0.172525552363828900E–15	5.83E–13	0.077375
192	Nausikaa	0.251194126565783300E–15	8.49E–13	0.112657
194	Prokne	0.272305872890598200E–15	9.20E–13	0.122125
195	Eurykleia	0.835481985073780800E–16	2.82E–13	0.03747
196	Philomela	0.450141365611792800E–15	1.52E–12	0.201882
198	Ampella	0.205385768290833100E–16	6.94E–14	0.009211
200	Dynamene	0.175546167825261400E–15	5.93E–13	0.07873
201	Penelope	0.101472968957165600E–15	3.43E–13	0.045509
203	Pompeja	0.184924720803005400E–15	6.25E–13	0.082936
205	Martha	0.915149992259589400E–16	3.09E–13	0.041043
206	Hersilia	0.117896698493573100E–15	3.98E–13	0.052875
209	Dido	0.259310730988729300E–15	8.76E–13	0.116297
210	Isabella	0.131453781488021000E–15	4.44E–13	0.058955
211	Isolda	0.304651155649041000E–15	1.03E–12	0.136632
212	Medea	0.386749965775167900E–15	1.31E–12	0.173452
213	Lilaea	0.952238918721723900E–16	3.22E–13	0.042707
216	Kleopatra	0.690797124746742500E–15	2.33E–12	0.309813
221	Eos	0.181684062017330300E–15	6.14E–13	0.081483
223	Rosa	0.139060396851984600E–15	4.70E–13	0.062367
224	Oceana	0.395205903434527200E–16	1.34E–13	0.017724
225	Henrietta	0.414565717253527800E–15	1.40E–12	0.185927
227	Philosophia	0.120484595454650200E–15	4.07E–13	0.054036
230	Athamantis	0.176089871551513500E–15	5.95E–13	0.078974
233	Asterope	0.197159196662545500E–15	6.66E–13	0.088423
236	Honoria	0.113632939011338100E–15	3.84E–13	0.050963
238	Hypatia	0.529666935807391100E–15	1.79E–12	0.237548
240	Vanadis	0.110486225287326500E–15	3.73E–13	0.049552
241	Germania	0.300548362594600500E–15	1.02E–12	0.134792
247	Eukrate	0.270972707241621300E–15	9.16E–13	0.121527
250	Bettina	0.196885501859924200E–15	6.65E–13	0.0883
259	Aletheia	0.628085855393638300E–15	2.12E–12	0.281688
266	Aline	0.184133018752378200E–15	6.22E–13	0.082581
268	Adorea	0.526690110925434800E–15	1.78E–12	0.236213
275	Sapientia	0.186540000000000000E–15	6.30E–13	0.083661
276	Adelheid	0.224815504884368300E–15	7.60E–13	0.100827
283	Emma	0.205281017798695800E–15	6.94E–13	0.092066
287	Nephthys	0.480337378560961000E–16	1.62E–13	0.021542
303	Josephina	0.288486840395101100E–15	9.75E–13	0.129382
304	Olga	0.688327109660540100E–16	2.33E–13	0.03087
308	Polyxo	0.724054788525813900E–15	2.45E–12	0.324728
313	Chaldaea	0.115845913374079600E–15	3.91E–13	0.051955
322	Phaeo	0.827634952130435800E–16	2.80E–13	0.037118
324	Bamberga	0.138862658985619900E–14	4.69E–12	0.622779
326	Tamara	0.189152474665620900E–15	6.39E–13	0.084832
328	Gudrun	0.291270000000000000E–15	9.84E–13	0.13063
329	Svea	0.511430939429605700E–16	1.73E–13	0.022937
334	Chicago	0.326249337943456200E–15	1.10E–12	0.146318
335	Roberta	0.147567692588891100E–15	4.99E–13	0.066182
336	Lacadiera	0.564300000000000000E–16	1.91E–13	0.025308

Table 12. Mass parameters of asteroids. (Continued: 5 of 7)

Number	Name	GM, au^3/day^2	$GM_{ast}/GM_{\odot}$	GM, km^3/s^2
337	Devosa	0.345150745118659600E–16	1.17E–13	0.01548
338	Budrosa	0.514076834286322000E–16	1.74E–13	0.023056
344	Desiderata	0.536890970425833500E–15	1.81E–12	0.240788
345	Tercidina	0.123175211698841300E–15	4.16E–13	0.055242
346	Hermentaria	0.220991660771765600E–15	7.47E–13	0.099112
347	Pariana	0.219491221778173700E–16	7.42E–14	0.009844
349	Dembowska	0.700787392713029200E–15	2.37E–12	0.314293
350	Ornamenta	0.141000784057630900E–15	4.76E–13	0.063237
354	Eleonora	0.158509865715968900E–14	5.36E–12	0.710894
356	Liguria	0.268161319613518200E–15	9.06E–13	0.120267
357	Ninina	0.176195602610025700E–15	5.95E–13	0.079021
358	Apollonia	0.121780979958317900E–15	4.12E–13	0.054617
360	Carlova	0.336776057435300700E–15	1.14E–12	0.151039
362	Havnia	0.808707928810328300E–16	2.73E–13	0.036269
363	Padua	0.698419453021186600E–16	2.36E–13	0.031323
365	Corduba	0.776955520962180000E–16	2.63E–13	0.034845
366	Vincentina	0.115639547136458300E–15	3.91E–13	0.051863
369	Aeria	0.573458156633685800E–16	1.94E–13	0.025719
372	Palma	0.174595572627050000E–14	5.90E–12	0.783036
373	Melusina	0.137206175961377900E–15	4.64E–13	0.061535
375	Ursula	0.455859924880692500E–15	1.54E–12	0.204447
377	Campania	0.141442289208980800E–15	4.78E–13	0.063435
381	Myrrha	0.359349348076176100E–15	1.21E–12	0.161163
385	Ilmatar	0.110318518229682800E–15	3.73E–13	0.049476
386	Siegena	0.150793337119651900E–14	5.10E–12	0.676287
387	Aquitania	0.100446598396309400E–15	3.39E–13	0.045049
388	Charybdis	0.343334441285916900E–15	1.16E–12	0.153981
389	Industria	0.622510183873803300E–16	2.10E–13	0.027919
393	Lampetia	0.155860000000000000E–15	5.27E–13	0.069901
404	Arsinoe	0.145216789548421900E–15	4.91E–13	0.065128
405	Thia	0.557648047680853900E–15	1.88E–12	0.250097
407	Arachne	0.156785041404748300E–15	5.30E–13	0.070316
409	Aspasia	0.821449999999999900E–15	2.78E–12	0.368409
410	Chloris	0.361865469702973400E–15	1.22E–12	0.162292
412	Elisabetha	0.146557349756319100E–15	4.95E–13	0.065729
415	Palatia	0.540012140874342300E–16	1.82E–13	0.024219
416	Vaticana	0.148698562934496100E–15	5.03E–13	0.066689
419	Aurelia	0.367820000000000000E–15	1.24E–12	0.164962
420	Bertholda	0.483520000000000000E–15	1.63E–12	0.216852
423	Diotima	0.211243836059995200E–14	7.14E–12	0.947399
424	Gratia	0.737998534437522900E–16	2.49E–13	0.033098
426	Hippo	0.229797581279714500E–15	7.77E–13	0.103061
431	Nephele	0.634077834952169700E–16	2.14E–13	0.028437
432	Pythia	0.187801229589892800E–16	6.35E–14	0.008423
433	Eros	0.990000118979590300E–18	3.35E–15	0.000444
442	Eichsfeldia	0.555346562874691200E–16	1.88E–13	0.024907
444	Gyptis	0.907080484411450500E–15	3.07E–12	0.406813
445	Edna	0.115342108493158500E–15	3.90E–13	0.051729
449	Hamburga	0.135581713067348800E–15	4.58E–13	0.060806

Table 12. Mass parameters of asteroids. (Continued: 6 of 7)

Number	Name	GM, au^3/day^2	$GM_{ast}/GM_{\odot}$	GM, km^3/s^2
451	Patientia	0.229555939063746200E–14	7.76E–12	1.029526
454	Mathesis	0.768088477469999900E–16	2.60E–13	0.034448
455	Bruchsalia	0.228615933395781000E–15	7.73E–13	0.102531
464	Megaira	0.806351842900557800E–16	2.72E–13	0.036164
465	Alekto	0.653992577244023600E–16	2.21E–13	0.029331
466	Tisiphone	0.270714167365278100E–15	9.15E–13	0.121411
469	Argentina	0.322840000000000000E–15	1.09E–12	0.144789
471	Papagena	0.845943072895968300E–15	2.86E–12	0.379394
476	Hedwig	0.241931605646406600E–15	8.18E–13	0.108503
481	Emita	0.334070052970451900E–15	1.13E–12	0.149826
485	Genua	0.367379607992341800E–16	1.24E–13	0.016476
488	Kreusa	0.191515627988507800E–15	6.47E–13	0.085892
489	Comacina	0.548467242911317100E–15	1.85E–12	0.24598
490	Veritas	0.364149739778329100E–15	1.23E–12	0.163316
491	Carina	0.148589708382528900E–15	5.02E–13	0.06664
498	Tokio	0.129879292391702200E–15	4.39E–13	0.058249
503	Evelyn	0.111871833145007600E–15	3.78E–13	0.050173
505	Cava	0.341769850174723900E–15	1.15E–12	0.153279
506	Marion	0.197353139110484100E–15	6.67E–13	0.08851
508	Princetonia	0.341067697975348700E–15	1.15E–12	0.152964
511	Davida	0.519812697945749800E–14	1.76E–11	2.331286
514	Armida	0.293765207953148200E–15	9.93E–13	0.13175
516	Amherstia	0.696000000000000000E–16	2.35E–13	0.031215
517	Edith	0.108862665088002000E–15	3.68E–13	0.048823
521	Brixia	0.181244939644586100E–15	6.12E–13	0.081286
532	Herculina	0.931594859406562000E–15	3.15E–12	0.417807
535	Montague	0.725386164346611400E–16	2.45E–13	0.032533
536	Merapi	0.109756310328225100E–14	3.71E–12	0.492242
545	Messalina	0.194849861155712500E–15	6.58E–13	0.087387
547	Praxedis	0.281235774586576800E–16	9.50E–14	0.012613
554	Peraga	0.274856688034015000E–15	9.29E–13	0.123269
566	Stereoskopia	0.626740000000000000E–15	2.12E–12	0.281084
568	Cheruskia	0.859780218818313100E–16	2.91E–13	0.03856
569	Misa	0.611232197266831400E–16	2.07E–13	0.027413
584	Semiramis	0.217605956141594600E–16	7.35E–14	0.009759
585	Bilkis	0.117169915406794000E–16	3.96E–14	0.005255
591	Irmgard	0.200383935095216300E–16	6.77E–14	0.008987
593	Titania	0.501889934520749200E–16	1.70E–13	0.022509
595	Polyxena	0.222111336158284500E–15	7.51E–13	0.099614
596	Scheila	0.383508917087800200E–15	1.30E–12	0.171998
598	Octavia	0.615306415407552400E–16	2.08E–13	0.027596
599	Luisa	0.691187747327401000E–16	2.34E–13	0.030999
602	Marianna	0.215014674336122500E–15	7.27E–13	0.096431
604	Tekmessa	0.642603995331864300E–16	2.17E–13	0.02882
618	Elfriede	0.463868801607939000E–15	1.57E–12	0.208039
623	Chimaera	0.144979767976932900E–16	4.90E–14	0.006502
626	Notburga	0.166437787258821500E–15	5.62E–13	0.074645
635	Vundtia	0.169956695263313900E–15	5.74E–13	0.076223
654	Zelinda	0.359530000000000000E–15	1.21E–12	0.161244
449	Hamburga	0.135581713067348800E–15	4.58E–13	0.060806

Table 12. Mass parameters of asteroids. (Continued: 7 of 7)

Number	Name	GM, au^3/day^2	$GM_{ast}/GM_\odot$	GM, km^3/s^2
663	Gerlinde	0.120495494885781800E–15	4.07E–13	0.054041
667	Denise	0.909429441579076000E–16	3.07E–13	0.040787
674	Rachele	0.143837480044678900E–15	4.86E–13	0.064509
675	Ludmilla	0.159234708844922700E–15	5.38E–13	0.071415
680	Genoveva	0.995816201002551800E–16	3.37E–13	0.044661
683	Lanzia	0.104361036125065600E–15	3.53E–13	0.046804
690	Wratislavia	0.476375353165424700E–15	1.61E–12	0.213648
691	Lehigh	0.945370522582010200E–16	3.19E–13	0.042399
694	Ekard	0.149386680301335600E–15	5.05E–13	0.066998
696	Leonora	0.111777344239748500E–15	3.78E–13	0.050131
702	Alauda	0.889506728492704500E–15	3.01E–12	0.398931
704	Interamnia	0.525616867849366200E–14	1.78E–11	2.357317
705	Erminia	0.291750035064825000E–15	9.86E–13	0.130846
709	Fringilla	0.154560085386599100E–15	5.22E–13	0.069318
712	Boliviana	0.502042422129256500E–15	1.70E–12	0.225159
713	Luscinia	0.142681578483330100E–15	4.82E–13	0.063991
735	Marghanna	0.859762026371732300E–16	2.91E–13	0.038559
739	Mandeville	0.713824339752934800E–16	2.41E–13	0.032014
740	Cantabia	0.118928144393176900E–15	4.02E–13	0.053338
747	Winchester	0.621574606623668800E–15	2.10E–12	0.278767
751	Faina	0.179893748114765000E–15	6.08E–13	0.08068
752	Sulamitis	0.499820481258924800E–16	1.69E–13	0.022416
760	Massinga	0.581679210057327800E–16	1.97E–13	0.026087
762	Pulcova	0.208180128309056600E–15	7.04E–13	0.093366
769	Tatjana	0.197251539856937600E–15	6.67E–13	0.088465
772	Tanete	0.252061449253389500E–15	8.52E–13	0.113046
773	Irmintraud	0.195761609064233300E–15	6.62E–13	0.087796
776	Berbericia	0.305671194466365300E–15	1.03E–12	0.137089
778	Theobalda	0.477435477387998300E–16	1.61E–13	0.021412
780	Armenia	0.148574053476563100E–15	5.02E–13	0.066633
784	Pickeringia	0.163082309665980900E–15	5.51E–13	0.07314
786	Bredichina	0.158301988046999200E–15	5.35E–13	0.070996
788	Hohensteina	0.215815568176360100E–15	7.29E–13	0.09679
790	Pretoria	0.175589918332470000E–14	5.93E–12	0.787496
791	Ani	0.121964875174107500E–15	4.12E–13	0.0547
804	Hispania	0.226710334145990500E–15	7.66E–13	0.101676
814	Tauris	0.455595956637723700E–15	1.54E–12	0.204328
849	Ara	0.103549725015275900E–15	3.50E–13	0.046441
895	Helio	0.378647503308948400E–15	1.28E–12	0.169818
909	Ulla	0.336297549276103900E–15	1.14E–12	0.150825
914	Palisana	0.411726826839954200E–16	1.39E–13	0.018465
980	Anacostia	0.153529788855662000E–15	5.19E–13	0.068856
1015	Christa	0.125837659264500500E–15	4.25E–13	0.056436
1021	Flammario	0.761714098728426500E–16	2.57E–13	0.034162
1036	Ganymed	0.646776721323746100E–16	2.19E–13	0.029007
1093	Freda	0.287164048267019600E–15	9.70E–13	0.128789
1107	Lictoria	0.954912821588764700E–16	3.23E–13	0.042826
1171	Rusthawelia	0.624856870846376100E–16	2.11E–13	0.028024
1467	Mashona	0.111528013303481700E–15	3.77E–13	0.050019

Table 13. Initial positions (au) and velocities (au/day) of the asteroids with respect to the Sun at Julian day (TDB) 2440400.5 (June 28, 1969) in the ICRF2 frame (1 of 15).

1	Ceres	x,y,z	1.438681809676469747	–2.204373633189407045	–1.326397853361325874
		v_x,v_y,v_z	0.008465406136316316	0.004684247977335608	0.000466157738595739
2	Pallas	x,y,z	0.203832272462290465	–3.209619436062307152	0.623843179079393351
		v_x,v_y,v_z	0.008534313855651248	–0.000860659210123161	–0.000392901992572746
3	Juno	x,y,z	0.461207259670432135	–3.006098959780790114	–0.580164049296942208
		v_x,v_y,v_z	0.008395458298285176	0.003111908045571209	0.000273059675893248
4	Vesta	x,y,z	0.182371836377417107	2.386628211277654010	0.924596062836265498
		v_x,v_y,v_z	–0.010174496747119257	0.000041478190529952	0.001344157634155624
5	Astraea	x,y,z	2.489297359488491956	1.036395265106434982	0.210563198822894787
		v_x,v_y,v_z	–0.005569115604615741	0.007959732929200320	0.003113959705731406
6	Hebe	x,y,z	1.339049495814490065	1.442775542206668815	0.079273672077323748
		v_x,v_y,v_z	–0.008775983793258694	0.009426820472364830	0.003535716141864189
7	Iris	x,y,z	1.892475267790300286	–0.848414748075139946	–0.157159319044464590
		v_x,v_y,v_z	0.002786950314570632	0.011314057384917047	0.004975132577079665
8	Flora	x,y,z	–2.119655892430383659	0.808466233981220750	0.533397871779012545
		v_x,v_y,v_z	–0.005818098320155988	–0.008811943327809565	–0.002835330893491553
9	Metis	x,y,z	–2.424658333778681119	–0.125325594242630484	0.185966267773321953
		v_x,v_y,v_z	–0.001166914352512719	–0.009845348309999084	–0.004559667512580128
10	Hygiea	x,y,z	2.444257569754775261	2.180591649726027814	1.162855082530954043
		v_x,v_y,v_z	–0.005924505919570356	0.005979686441736038	0.002286438610925529
11	Parthenope	x,y,z	–1.231933494613708824	–1.941584219024864888	–0.648652135887457293
		v_x,v_y,v_z	0.010146729938442466	–0.004310578383941682	–0.002342316786027452
13	Egeria	x,y,z	1.110470035635196862	–1.956883630909689531	–1.669729176939996007
		v_x,v_y,v_z	0.008850484510873332	0.004168221460244788	0.000793489279402694
14	Irene	x,y,z	2.968959552750401354	0.179534605878148124	–0.441493212476667563
		v_x,v_y,v_z	0.000114431097969882	0.008313751393872647	0.003664818027075008
15	Eunomia	x,y,z	–1.438397661546355177	2.001287639171841271	0.767257269566094968
		v_x,v_y,v_z	–0.009735666014582665	–0.002981534818366074	–0.003694080871985814
16	Psyche	x,y,z	1.459069269212805553	–2.194286961057163143	–0.872045420720389042
		v_x,v_y,v_z	0.008193866970882068	0.006328897736618455	0.002167069206448382
18	Melpomene	x,y,z	–2.742133025533653790	–0.012766315168109336	0.239819478175997858
		v_x,v_y,v_z	–0.000996361773223022	–0.008953551423450837	–0.002237582813053089
19	Fortuna	x,y,z	–2.421846633153337702	–1.337431649320276250	–0.581397545560000673
		v_x,v_y,v_z	0.004769326689664416	–0.007520729608529603	–0.002981882787056496
20	Massalia	x,y,z	–0.446957693127368383	1.855382149831718674	0.778094121440758957
		v_x,v_y,v_z	–0.012511421939296488	–0.002534666129817137	–0.001141856361378328
21	Lutetia	x,y,z	–0.401500082512939060	–2.034737356634178429	–0.878857903014080954
		v_x,v_y,v_z	0.011859546440634965	–0.000138986487715931	–0.000750181020252093
22	Kalliope	x,y,z	–1.360169904369056937	–2.672544709790108275	–1.131055224812947957
		v_x,v_y,v_z	0.008015423798989894	–0.002573715371792212	–0.003469704484884123
23	Thalia	x,y,z	–1.381180931801666123	–2.177231877010123551	–0.869547456324116008
		v_x,v_y,v_z	0.007230267698506810	–0.005803206866356805	–0.004345034311979445
24	Themis	x,y,z	–1.986326887180129397	1.713080040332319420	0.782177241944561841
		v_x,v_y,v_z	–0.007376541658456220	–0.007515395858827745	–0.003291592430864249
25	Phocaea	x,y,z	1.862187339641438788	–0.320827452239953126	0.370298833532256677
		v_x,v_y,v_z	0.004047653066899725	0.012783082342996164	0.002077625994146512
27	Euterpe	x,y,z	–1.260198559466741086	1.418639340820153416	0.648923808375896249
		v_x,v_y,v_z	–0.010819473664968254	–0.006731978199858915	–0.002575089185167887

Table 13. Initial positions (au) and velocities (au/day) of the asteroids with respect to the Sun at Julian day (TDB) 2440400.5 (June 28, 1969) in the ICRF2 frame. (Continued: 2 of 15.)

28	Bellona	x,y,z	–1.473796460584195778	1.739643135937173790	0.633933941012944979
		v_x,v_y,v_z	–0.009328149750934787	–0.007427778551081034	–0.001181230605742862
29	Amphitrite	x,y,z	–0.146988273583742862	–2.362796893883333915	–1.340108464209891492
		v_x,v_y,v_z	0.010080728492092296	–0.000192196827316014	–0.000039573406685344
30	Urania	x,y,z	–2.606330961010526526	–0.080313889098223457	–0.119443301999580323
		v_x,v_y,v_z	–0.000271687607297601	–0.009151555703778012	–0.004227028420836736
31	Euphrosyne	x,y,z	–2.344572196151709420	–2.202248246583482949	–1.499371924448428484
		v_x,v_y,v_z	0.004929226633590931	–0.003894954486494073	–0.005777736992660197
41	Daphne	x,y,z	2.186522806828394838	2.716000834079776549	0.352083724354172178
		v_x,v_y,v_z	–0.006362487833486645	0.004588916254801226	0.000658460597293756
42	Isis	x,y,z	–2.311906318139493433	1.564709507254086418	1.081663757432244743
		v_x,v_y,v_z	–0.005375422471534914	–0.006572477821943680	–0.002070451318821641
45	Eugenia	x,y,z	–1.286740660767531352	–2.064333827345071093	–0.581533957673131763
		v_x,v_y,v_z	0.009624183869937625	–0.005447390675875109	–0.002359148283535982
51	Nemausa	x,y,z	2.325725710714735328	0.919631243406134669	0.195346323188101051
		v_x,v_y,v_z	–0.004226342069996713	0.009366245889668433	0.002292473770765156
52	Europa	x,y,z	1.630504392123616197	–2.807391275567590050	–1.120111554599330095
		v_x,v_y,v_z	0.007545901962567781	0.004385628274804682	0.000681057876133087
60	Echo	x,y,z	–2.053758095409557338	0.542618601186906857	0.167604428744862921
		v_x,v_y,v_z	–0.005053755262744046	–0.010634893001978403	–0.003929518991233821
63	Ausonia	x,y,z	–0.711507633861145239	–1.727049410575609123	–0.980245752936226511
		v_x,v_y,v_z	0.011957874480153950	–0.003468676332191662	–0.001404339015793962
65	Cybele	x,y,z	–2.818818186481110377	–1.452785968979383169	–0.459547659952798004
		v_x,v_y,v_z	0.005491212616137729	–0.007709765186399763	–0.002980907967655813
69	Hesperia	x,y,z	–2.731373586077875171	–0.173990396273168008	–0.091512829062557879
		v_x,v_y,v_z	–0.000835829539403114	–0.010410309605217057	–0.002792056931756292
78	Diana	x,y,z	–2.230308915264555658	–0.612004762065796459	–0.543275243058195634
		v_x,v_y,v_z	0.001875816436270626	–0.009912063988588916	–0.005874203423004298
94	Aurora	x,y,z	1.217204321473684070	2.230213797067274850	1.349204301622864088
		v_x,v_y,v_z	–0.009480919363038220	0.003964160607269546	0.002537794862740618
97	Klotho	x,y,z	–1.909756234729403035	–2.678800550963929439	–0.452067580136410296
		v_x,v_y,v_z	0.006291707122836601	–0.005039334023207890	–0.001538832193933371
98	Ianthe	x,y,z	–2.189380245469819020	0.226114692352493402	0.112525782901568755
		v_x,v_y,v_z	–0.002121664740945849	–0.009612549934188979	–0.007843089126949381
105	Artemis	x,y,z	–2.150697286825749899	0.541875356226059646	–0.099139411741416952
		v_x,v_y,v_z	–0.000933995664699450	–0.011865009015818844	–0.000510278917224607
111	Ate	x,y,z	–2.065235972301910916	–1.395192740371126838	–0.851171268109567225
		v_x,v_y,v_z	0.005618108019220444	–0.008131544741012933	–0.003600368200049119
135	Hertha	x,y,z	–1.852065839438821637	–1.414537091163847737	–0.701764695699997887
		v_x,v_y,v_z	0.008706738823410954	–0.006122907739411309	–0.002836580152272733
139	Juewa	x,y,z	–2.286169743218249728	0.129793402866451107	0.113110508166727894
		v_x,v_y,v_z	–0.001144921173599620	–0.010129177653436634	–0.006915213503334226
145	Adeona	x,y,z	1.101693094201525502	2.046278461562542006	0.733533233415469499
		v_x,v_y,v_z	–0.010477714288306773	0.002702890747395121	0.003883525044571004
187	Lamberta	x,y,z	1.552362680005133111	–1.667017286215509042	–1.224506107407864253
		v_x,v_y,v_z	0.010026916904808853	0.004083994537401527	0.001832035781453411
192	Nausikaa	x,y,z	–2.180257484088014674	–1.605283294502194646	–1.009730329227873646
		v_x,v_y,v_z	0.006837112554701223	–0.005228654546530322	–0.002756824225065406

Table 13. Initial positions (au) and velocities (au/day) of the asteroids with respect to the Sun at Julian day (TDB) 2440400.5 (June 28, 1969) in the ICRF2 frame. (Continued: 3 of 15.)

194	Prokne	x,y,z	1.495439006518376468	–1.277354772575368669	–0.299878060343942709
		v_x,v_y,v_z	0.008680667325646010	0.010437900139680028	0.000134167930615169
216	Kleopatra	x,y,z	–2.623737352933921407	–2.141208444909570296	–0.848460319932531903
		v_x,v_y,v_z	0.005369324233200630	–0.005867957040039504	–0.000585039109819107
230	Athamantis	x,y,z	–2.280008375035697199	–0.880463965508790358	–0.645752311103840460
		v_x,v_y,v_z	0.004331702501765179	–0.009223170407939286	–0.002470255504286102
324	Bamberga	x,y,z	1.398759064223541682	–1.287476729008325105	–0.669098428660833799
		v_x,v_y,v_z	0.007164363244556328	0.009219958777618218	0.006857861727407507
337	Devosa	x,y,z	2.057440180433961707	–1.322162885949879740	–0.780976069801601058
		v_x,v_y,v_z	0.005188028188451134	0.007591643038099468	0.004670779035477783
344	Desiderata	x,y,z	–1.436281403678767443	2.243805682206950092	2.055782461490350155
		v_x,v_y,v_z	–0.006473875571808206	–0.004308997045040672	–0.001132197443002879
354	Eleonora	x,y,z	0.400598302733801259	–2.845496057705452220	–0.363223167203308106
		v_x,v_y,v_z	0.009411661670619676	–0.002169498446596223	–0.002270974488656075
372	Palma	x,y,z	–2.501245479525921134	–1.473356596063249313	–2.186348442117559632
		v_x,v_y,v_z	0.004414109643858683	–0.005694498088384558	–0.004127573934799787
405	Thia	x,y,z	–1.680813989369112971	–0.720962772281693809	–0.636265292808031457
		v_x,v_y,v_z	0.006053497060520836	–0.012004513735606900	–0.003193078939729851
409	Aspasia	x,y,z	2.627942640819607600	0.032856722306475961	0.499378874814495721
		v_x,v_y,v_z	–0.000121147420399894	0.009800913286716541	0.003214451046459611
419	Aurelia	x,y,z	–0.832205073692585229	2.925043505666568677	1.070613454084370586
		v_x,v_y,v_z	–0.007845381994993020	–0.002434064039560803	–0.001376245101202946
451	Patientia	x,y,z	1.259008304010221346	2.454041267595273634	0.690482754870751503
		v_x,v_y,v_z	–0.009063543500060710	0.003448045666261337	0.004183420491116245
488	Kreusa	x,y,z	–2.067224538805315426	–1.883392328874813781	–0.393159264399483011
		v_x,v_y,v_z	0.005745445324864604	–0.007721753293565463	–0.004781672638324677
511	Davida	x,y,z	–2.160191561573574504	1.486363108760649254	1.096959097247329984
		v_x,v_y,v_z	–0.007390695920479255	–0.007779023504823501	–0.000485540781565076
532	Herculina	x,y,z	–0.293159404090669762	–2.481691048455131110	–0.725934583722743554
		v_x,v_y,v_z	0.010153432932361773	–0.002073902764508174	–0.003634391919195946
554	Peraga	x,y,z	1.567515331928776900	–1.756839671087627286	–0.730145653545691942
		v_x,v_y,v_z	0.007168202681128191	0.007126474516266886	0.003646321528209388
654	Zelinda	x,y,z	2.454317123300634673	–1.156415934845627769	0.311816838296415377
		v_x,v_y,v_z	0.001774157409192030	0.007979676971587255	0.004592146292516224
704	Interamnia	x,y,z	2.462835232264114715	–0.115048121589235539	0.784219288788080227
		v_x,v_y,v_z	–0.001309568805636822	0.010348987192429257	0.004812522889055394
747	Winchester	x,y,z	–0.834902081339142454	2.059697173467183617	0.613292775285328884
		v_x,v_y,v_z	–0.012134738848543374	–0.002004140070559451	0.002575815432470426
12	Victoria	x,y,z	–0.507844534173903961	2.607456081000619541	0.819717059989116925
		v_x,v_y,v_z	–0.009185378920496397	–0.000281429685500620	–0.001275015521881669
17	Thetis	x,y,z	–0.224334228105830036	–1.994047200796976282	–0.713424849893356972
		v_x,v_y,v_z	0.012457106084712540	–0.000945089974559068	–0.001398683846484221
26	Proserpina	x,y,z	–2.278602546659383776	1.125007532904078289	0.661062309969335460
		v_x,v_y,v_z	–0.004431095916543229	–0.008819825820419791	–0.004062402214390301
32	Pomona	x,y,z	–0.901728147437201644	–2.125115524966149305	–0.803811944165582326
		v_x,v_y,v_z	0.010194219116656746	–0.004774494291409794	–0.000989390504731257
34	Circe	x,y,z	–2.391157252691995083	0.282992268249411760	0.070390275547792716
		v_x,v_y,v_z	–0.001758506796666345	–0.010942908417041593	–0.003566166537380931

Table 13. Initial positions (au) and velocities (au/day) of the asteroids with respect to the Sun at Julian day (TDB) 2440400.5 (June 28, 1969) in the ICRF2 frame. (Continued: 4 of 15.)

35	Leukothea	x,y,z	–2.185818508920677861	–0.647312389706184987	–0.427069919068639725
		v_x,v_y,v_z	0.004403906713249404	–0.010009270813997396	–0.006061965347001481
36	Atalante	x,y,z	2.077067513068779459	–0.589147154522667860	–0.516882702948444517
		v_x,v_y,v_z	0.001483717270391386	0.009307317089508693	0.008367140895652419
37	Fides	x,y,z	–2.571178583038596699	–1.322068718023980072	–0.637055179528812743
		v_x,v_y,v_z	0.003566522119529630	–0.007751964656304541	–0.003895555791525518
38	Leda	x,y,z	–1.235289907955999134	1.834720116439384707	0.766832361464905965
		v_x,v_y,v_z	–0.010386680301307009	–0.004838101200633434	–0.003684794791298678
39	Laetitia	x,y,z	2.336193952026537790	0.759000796514275100	0.022176605809523606
		v_x,v_y,v_z	–0.003257699513685890	0.010731650305157095	0.002872519477197957
40	Harmonia	x,y,z	–0.690601749410825527	–2.038615544126432422	–0.813975363544205632
		v_x,v_y,v_z	0.010841792489889901	–0.002359683762911624	–0.001881496483239468
43	Ariadne	x,y,z	2.009602895794647015	–0.308045882132810533	0.000115161076006508
		v_x,v_y,v_z	0.003565080131794708	0.010950285369215265	0.004918573106272521
44	Nysa	x,y,z	–1.180941766350430466	1.554866402256739777	0.656611442582409666
		v_x,v_y,v_z	–0.010685573544758461	–0.006831046309965641	–0.002065889635700970
46	Hestia	x,y,z	–0.474973466355436691	–2.296851721557127579	–0.887903017375627823
		v_x,v_y,v_z	0.010895877228602094	–0.000193379625778825	–0.000061860987657291
47	Aglaja	x,y,z	1.067741941627274427	–2.006425563476340379	–1.093089277938812831
		v_x,v_y,v_z	0.010164990750471822	0.004729454222497436	0.002493051086595212
48	Doris	x,y,z	–1.620193164505671524	2.388346628469387944	0.711322099748724956
		v_x,v_y,v_z	–0.008761794768022678	–0.004974889431640200	–0.001595006590297288
49	Pales	x,y,z	–3.160577305628162748	–1.841530354628577504	–1.017849520123809803
		v_x,v_y,v_z	0.004122755888684796	–0.006077379179740559	–0.002511188490367351
50	Virginia	x,y,z	1.333238507267154427	–1.602799470048592578	–0.610763870330498060
		v_x,v_y,v_z	0.007993780997143859	0.009223622006417765	0.003430026595662231
53	Kalypso	x,y,z	–0.624015677324980311	–2.887904714321112287	–0.973890349097378372
		v_x,v_y,v_z	0.008425652319494320	–0.002165971738316451	–0.001225638323642568
54	Alexandra	x,y,z	–1.135653934893979367	–1.669000255199023952	–1.229167471346461094
		v_x,v_y,v_z	0.011014262220981971	–0.004397975120144764	–0.000793087156657538
56	Melete	x,y,z	–2.509110608187361979	–0.599826488136790070	–0.256184765903608447
		v_x,v_y,v_z	0.005001190631127405	–0.009156744414684281	–0.002380258455330665
57	Mnemosyne	x,y,z	–2.391692801502097954	–2.476663754241630322	–0.613024391539033098
		v_x,v_y,v_z	0.006142650670634989	–0.006122207358406149	–0.000426188587336327
58	Concordia	x,y,z	1.970644363722096504	1.898617820025757519	0.583347727462360521
		v_x,v_y,v_z	–0.007322186137912932	0.006519792084242099	0.002412465398938618
59	Elpis	x,y,z	–2.174043173151056330	1.754505167862759452	0.521206662638497353
		v_x,v_y,v_z	–0.007194625470952607	–0.006696283399313014	–0.001604669222795236
62	Erato	x,y,z	–0.974153514232837803	–3.190444885566684707	–1.264820437591952285
		v_x,v_y,v_z	0.008304485139178936	–0.001176603633891707	–0.000760024384788282
68	Leto	x,y,z	2.150832185782553196	–0.472704842227096689	–0.504675337037531091
		v_x,v_y,v_z	0.003447895159962464	0.010633207649093934	0.005531722529065961
70	Panopaea	x,y,z	–0.512732908153528344	2.523947930349827118	1.619878869724124648
		v_x,v_y,v_z	–0.008876233401680499	–0.001390534286671486	0.000743421116570644
71	Niobe	x,y,z	–2.102963729152515615	1.401034628378233560	0.430525013472648932
		v_x,v_y,v_z	–0.004028656274637795	–0.007045329097739382	–0.007586343532703573
72	Feronia	x,y,z	–0.698145332366829519	2.293578863469888596	0.742562228176233741
		v_x,v_y,v_z	–0.009984751110793636	–0.002036674761053411	–0.001163542296488656

Table 13. Initial positions (au) and velocities (au/day) of the asteroids with respect to the Sun at Julian day (TDB) 2440400.5 (June 28, 1969) in the ICRF2 frame. (Continued: 5 of 15.)

74	Galatea	x,y,z	2.002901140763306831	0.640809773926249604	0.274754411294356571
		v_x,v_y,v_z	–0.003966716076468380	0.011826725481734445	0.004119277914981450
75	Eurydike	x,y,z	–3.200842305137657107	1.220975490656682982	0.662752781812484315
		v_x,v_y,v_z	–0.003148422634162045	–0.006154368263463862	–0.003334345423877219
76	Freia	x,y,z	2.635360768423828937	1.437884630898934590	0.615131758192210332
		v_x,v_y,v_z	–0.006649269126403664	0.007319514417658025	0.002778582333891908
77	Frigga	x,y,z	–2.690246721423859899	–1.025385948689222948	–0.492898536579899738
		v_x,v_y,v_z	0.002901323944706134	–0.008214417661668621	–0.003990796639863591
79	Eurynome	x,y,z	–0.855375263619381876	–2.558706256410499424	–0.931566610102818493
		v_x,v_y,v_z	0.009085151348455443	–0.001894651404025254	–0.000307424335130962
80	Sappho	x,y,z	1.608537185631021771	–0.946571596217173794	–0.123702344488760718
		v_x,v_y,v_z	0.005907288892718746	0.011656883717961289	0.004089724891808015
81	Terpsichore	x,y,z	–0.299527408394068329	–2.820136290562028858	–1.711616630966411812
		v_x,v_y,v_z	0.008642357666503482	0.000392975155467740	0.000185079802975043
82	Alkmene	x,y,z	3.160151220673873329	–0.517688310655634809	–0.330346049201625136
		v_x,v_y,v_z	0.000372867010599650	0.007874899115079248	0.003828789513816485
83	Beatrix	x,y,z	2.537243040037000963	0.677406600928586178	0.239904468813102290
		v_x,v_y,v_z	–0.002746008298400088	0.008573152131379970	0.004656090987115207
84	Klio	x,y,z	–2.867387466643116500	0.123974227957666397	–0.213371959277415285
		v_x,v_y,v_z	0.000843918676535950	–0.007659425932435818	–0.004589100376152419
85	Io	x,y,z	2.196277362267318622	0.413880157287253858	0.281126843760316159
		v_x,v_y,v_z	–0.001029040843236626	0.011980721214998944	0.002569598620931192
86	Semele	x,y,z	2.434775829626800281	–0.701653670472491275	–0.530519782084361902
		v_x,v_y,v_z	0.002147727796190763	0.010457520401758034	0.004381939368423997
87	Sylvia	x,y,z	–3.660362899261072389	–0.885526882959144834	0.312168187323252744
		v_x,v_y,v_z	0.001817747464846094	–0.007261471114931983	–0.003982770842554424
88	Thisbe	x,y,z	0.351034977545771065	2.726034310628392632	1.255821730738119202
		v_x,v_y,v_z	–0.009085998946397741	0.002504365492940864	0.000217136735120159
89	Julia	x,y,z	0.668287897791156604	1.784401165953789503	1.391068013944257720
		v_x,v_y,v_z	–0.010183706148394674	0.005465198051083607	0.001141423763308724
90	Antiope	x,y,z	–2.527596410164981489	2.393097637265075850	1.176158237649570948
		v_x,v_y,v_z	–0.005785028160541267	–0.005353734747955876	–0.002166792449198574
91	Aegina	x,y,z	–0.087297607412163220	–2.585707806328295000	–1.234058824506656826
		v_x,v_y,v_z	0.009596957524554405	–0.000169138133959666	–0.000157156795888277
92	Undina	x,y,z	–1.042907269635494405	–2.875324060333224629	–0.930751854561716052
		v_x,v_y,v_z	0.009168658604880101	–0.001743405265776949	–0.002351877046242883
93	Minerva	x,y,z	0.585579552533172509	2.601997108680597304	1.615157088233035720
		v_x,v_y,v_z	–0.008803902414859047	0.001797983571727375	0.001256003779502425
95	Arethusa	x,y,z	2.542078873825008856	0.235650434494874467	0.625470306990500435
		v_x,v_y,v_z	–0.002373003952808578	0.010704165151006678	0.002903697708982936
96	Aegle	x,y,z	–2.188255307668921734	1.381773051127626495	0.553799995799386546
		v_x,v_y,v_z	–0.005576550150666639	–0.007277112779745350	–0.006521139973971324
99	Dike	x,y,z	2.444770853104723862	–0.615836362049607455	–0.892420122928066495
		v_x,v_y,v_z	0.005698847921220206	0.007805584032288921	0.004109108981978736
100	Hekate	x,y,z	–2.808466634462525313	1.998234760159137258	0.967652214689530998
		v_x,v_y,v_z	–0.004808839856292163	–0.006555049055444871	–0.001867365486725437
102	Miriam	x,y,z	–0.802979209614599232	2.471520362371176116	0.813851431023047911
		v_x,v_y,v_z	–0.010278712148820868	–0.000277333514340038	–0.000609446487533852

Table 13. Initial positions (au) and velocities (au/day) of the asteroids with respect to the Sun at Julian day (TDB) 2440400.5 (June 28, 1969) in the ICRF2 frame. (Continued: 6 of 15.)

103	Hera	x,y,z	–1.624169502869726278	–2.061934384710811141	–0.618220991356126959
		v_x,v_y,v_z	0.008815595236548105	–0.005135987476149960	–0.002424171731408047
104	Klymene	x,y,z	2.604625804466561778	0.829861198407666256	0.297592323238799750
		v_x,v_y,v_z	–0.004595135750289872	0.008958088103164813	0.004449410220144689
106	Dione	x,y,z	1.186951890089662287	–2.641679471918139566	–1.357909134882829605
		v_x,v_y,v_z	0.008062335558122698	0.004854178905816693	0.001679190825653463
107	Camilla	x,y,z	–2.814482356149371256	–2.125615900337749942	–0.466315209535505482
		v_x,v_y,v_z	0.005016321991106533	–0.007283280755178675	–0.001833852210438387
109	Felicitas	x,y,z	–2.272223718831077210	–2.256013715954339638	–1.348118693877923713
		v_x,v_y,v_z	0.005498298783944774	–0.004679670760771524	–0.002914631877323399
110	Lydia	x,y,z	–2.913671600037018194	0.137720105704674162	0.356482845934635972
		v_x,v_y,v_z	–0.000701525427796519	–0.008631983066179964	–0.004265106303010358
112	Iphigenia	x,y,z	2.101268187945320776	0.423210543438176212	0.263994487858637827
		v_x,v_y,v_z	–0.002085691485880794	0.011003103680878389	0.005201699139327664
113	Amalthea	x,y,z	–0.845649935641415329	2.041704300606039801	0.834445540016974907
		v_x,v_y,v_z	–0.010061995082559373	–0.004862835207405551	–0.001044300650685426
114	Kassandra	x,y,z	1.003458535932775675	2.302229181420444970	0.755029808593063345
		v_x,v_y,v_z	–0.010372485650250500	0.002522166795368615	0.001098397718920128
115	Thyra	x,y,z	–2.132402872023013263	–1.407030770831705802	–1.230888073340032474
		v_x,v_y,v_z	0.005718496513543697	–0.006581478727881280	–0.002888515609029340
117	Lomia	x,y,z	2.270382224122074355	–1.589433030843294015	–1.113929084766832167
		v_x,v_y,v_z	0.006230326658274393	0.005926784306392254	0.005024462275567959
118	Peitho	x,y,z	2.285956748706956976	–0.605001706866287292	–0.594092775417243146
		v_x,v_y,v_z	0.001960243453552381	0.009608024580505914	0.005023973278452842
120	Lachesis	x,y,z	1.349895569447842503	2.571965525676553455	1.547065365110619428
		v_x,v_y,v_z	–0.008469966093690717	0.003282200584511912	0.001536525822077163
121	Hermione	x,y,z	1.334266785923234888	–2.574571237468854079	–1.410921022512830580
		v_x,v_y,v_z	0.008404347099665236	0.005070569717777809	0.001205938930940049
124	Alkeste	x,y,z	–2.030985757945451553	–1.291015452637479966	–0.500252551887808372
		v_x,v_y,v_z	0.006742453819955392	–0.008540992687351152	–0.003142188428784029
127	Johanna	x,y,z	0.258596371131005198	2.254521103975096530	1.302780291910047072
		v_x,v_y,v_z	–0.010847729029494223	0.000155121847092949	0.001051653942880798
128	Nemesis	x,y,z	–1.950614158630362915	1.800692994261967828	1.063538206084451820
		v_x,v_y,v_z	–0.007974900712854933	–0.005725400853334638	–0.001714798269305732
129	Antigone	x,y,z	0.173250908378126567	3.306268588514498230	0.822759553307659597
		v_x,v_y,v_zz	–0.008289119212281256	–0.000667809291620081	0.001070909483343232
130	Elektra	x,y,z	0.808865897608793016	–2.931039369795729321	–0.391590456276819932
		v_x,v_y,v_z	0.008508223312724572	0.004812568858903731	–0.001548417459331940
132	Aethra	x,y,z	–0.480193840132689453	1.653722981508809253	0.319743825909667823
		v_x,v_y,v_z	–0.011837731432955296	–0.005329218981514342	–0.007488534336320045
134	Sophrosyne	x,y,z	–2.011298631478445564	1.214628009571321776	0.731179432571293253
		v_x,v_y,v_z	–0.007359702096515807	–0.006723867635909852	–0.005074877395244866
137	Meliboea	x,y,z	2.185732502051722648	–1.145086389525992177	–0.022766323557119300
		v_x,v_y,v_z	0.006166935083607356	0.010027540696906241	0.002522495066251339
140	Siwa	x,y,z	2.349717450635818938	0.565740387115059251	0.098983118555951627
		v_x,v_y,v_z	–0.000542241084460003	0.010767145886680794	0.004484878043585674
141	Lumen	x,y,z	2.001263396461105071	0.319678076806489797	0.526316075837815478
		v_x,v_y,v_z	–0.003483509074753528	0.010893891066401524	0.006389004515172658

Table 13. Initial positions (au) and velocities (au/day) of the asteroids with respect to the Sun at Julian day (TDB) 2440400.5 (June 28, 1969) in the ICRF2 frame. (Continued: 7 of 15.)

143	Adria	x,y,z	2.882421698483517147	0.042452435493852865	0.333727709970750852
		v_x,v_y,v_z	–0.000265760440917905	0.008189549513733274	0.005447974152432384
144	Vibilia	x,y,z	–3.202644502264647475	–0.708133625995427840	–0.034778692392227049
		v_x,v_y,v_z	0.001746328337486271	–0.007334586431819497	–0.003503786791915789
146	Lucina	x,y,z	–0.811168586625490406	–2.275206201114596816	–0.838736864314022 01
		v_x,v_y,v_z	0.010109426082854705	–0.002536990665401319	–0.003737855276866437
147	Protogeneia	x,y,z	–0.135653717885019648	–2.925539832035890520	–1.233404347151997538
		v_x,v_y,v_z	0.009577394154474565	–0.000281048647997959	0.000208962558114589
148	Gallia	x,y,z	–2.002954304100418081	1.803600909370170813	0.562676288618840337
		v_x,v_y,v_z	–0.007969397030290469	–0.006450526750365626	0.001741973397159357
150	Nuwa	x,y,z	–0.513703300992534251	2.766574982586356590	1.080652555085234834
		v_x,v_y,v_z	–0.009840605686461229	–0.000320540289433122	–0.000310864131154414
154	Bertha	x,y,z	–2.074683900631499434	–1.800589925977038375	–0.921944736183594959
		v_x,v_y,v_z	0.006609578012061634	–0.005176399972958075	–0.006376303490757747
156	Xanthippe	x,y,z	2.923916135163274088	–0.729762768653841376	0.218492453225095001
		v_x,v_y,v_z	0.003649642497220172	0.007950919425059762	0.003317878320056731
159	Aemilia	x,y,z	–0.410767564198755042	2.618954330535652186	0.940439073970279371
		v_x,v_y,v_z	–0.010553589480557164	–0.001942707083642232	0.000168561775632459
160	Una	x,y,z	1.905452096025585851	1.518779824511213183	0.757828350346318791
		v_x,v_y,v_z	–0.007533973461247138	0.007222883364505983	0.003809404100424659
162	Laurentia	x,y,z	0.262514031180226981	2.400281690284028269	1.275022530741664051
		v_x,v_y,v_z	–0.010860656605817488	–0.000837744879289118	0.000338095109459147
163	Erigone	x,y,z	1.974914535093617252	0.857554972320634268	0.236073131153163474
		v_x,v_y,v_z	–0.006815687100308090	0.009482254283590926	0.003447148757209308
164	Eva	x,y,z	–3.040157320355995285	–1.519642316497472834	0.691762796895534549
		v_x,v_y,v_z	0.002976277102337891	–0.005406627734211578	–0.004499142864886430
165	Loreley	x,y,z	–1.922737034954617341	–1.819614502509028009	–1.400331048398380185
		v_x,v_y,v_z	0.007959370240945991	–0.006004630422629679	–0.001928143622055610
168	Sibylla	x,y,z	3.116554420775199397	–0.994993474666817534	–0.224327412952326943
		v_x,v_y,v_z	0.002733580426163316	0.008691053371313727	0.003163655969657688
171	Ophelia	x,y,z	3.452516715258505897	–0.216190515721613213	–0.255374648951711414
		v_x,v_y,v_z	0.000240618327164227	0.008055044745482545	0.003396706876313383
172	Baucis	x,y,z	–2.385328686094084105	–0.620107743369059716	–0.620470933066101904
		v_x,v_y,v_z	0.004378392174801965	–0.008170672938126655	–0.004757814902613166
173	Ino	x,y,z	0.171242886080394535	2.394184022514683097	0.451640900560661918
		v_x,v_y,v_z	–0.011142161189368808	0.002538588490091165	0.001950356324201864
175	Andromache	x,y,z	–0.474252178163027949	–2.648333222299060541	–1.305222351194791353
		v_x,v_y,v_z	0.010262122260410241	0.000548159272351288	0.000029475418796883
176	Iduna	x,y,z	–1.387628365703582611	2.833854776034395506	–0.091557754074181458
		v_x,v_y,v_z	–0.009225262571539295	–0.002671178335674209	–0.001428340199372592
177	Irma	x,y,z	2.007796292614895339	–1.022926044579357097	–0.462360572116189250
		v_x,v_y,v_z	0.004104738603731208	0.010480904746312239	0.004870438746756638
181	Eucharis	x,y,z	2.120681612712470798	–2.907144330458012238	–0.813722768281753606
		v_x,v_y,v_z	0.005865675784688143	0.005572377170526862	–0.000342831237219019
185	Eunike	x,y,z	–2.747368952622216920	–1.338746669764243169	0.422267924686840546
		v_x,v_y,v_z	0.003978039639761641	–0.008185576126933353	–0.001011821450492685
191	Kolga	x,y,z	–2.879887570364938920	0.953404430384273138	0.413481905229524382
		v_x,v_y,v_z	–0.003754265666355869	–0.008618960919399883	–0.001665556221000780

Table 13. Initial positions (au) and velocities (au/day) of the asteroids with respect to the Sun at Julian day (TDB) 2440400.5 (June 28, 1969) in the ICRF2 frame. (Continued: 8 of 15.)

195	Eurykleia	x,y,z	2.922594899011714986	0.199160094596518983	0.060339478431695619
		v_x,v_y,v_z	–0.001056479499979637	0.008538247223234249	0.005019069716262851
196	Philomela	x,y,z	2.870866810351882403	–0.754636097994081934	–0.748530242754146369
		v_x,v_y,v_z	0.003302144455379505	0.008603231629111158	0.003663627801932320
198	Ampella	x,y,z	0.543891836565843279	1.941671690331441047	0.932327670839411482
		v_x,v_y,v_z	–0.010661276142588431	0.005661564198512067	0.000542576864013208
200	Dynamene	x,y,z	–0.109999438475556419	–2.621860198978502865	–1.470414945946262097
		v_x,v_y,v_z	0.009376565385604106	0.000133656901059443	0.000810938484734692
201	Penelope	x,y,z	–2.800980089172922849	1.352246370925753505	0.554783862366244662
		v_x,v_y,v_z	–0.004186345686485028	–0.007367963765518988	–0.002243604557722191
203	Pompeja	x,y,z	1.500547182112841327	–2.086139267712977308	–1.025020464889739635
		v_x,v_y,v_z	0.008286480532474490	0.005407135390513565	0.002806033412514854
205	Martha	x,y,z	–2.770579982860186696	0.663732478579504792	–0.116643403811919136
		v_x,v_y,v_z	–0.002353576283912810	–0.009404587572302536	–0.002658971716332037
206	Hersilia	x,y,z	1.238747961716257118	–2.376780403456169921	–0.929349158559885868
		v_x,v_y,v_z	0.008918338308673593	0.004410268226602005	0.001280757530674212
209	Dido	x,y,z	2.268898815817652626	2.057453499016182352	1.209244033679382824
		v_x,v_y,v_z	–0.006436569904961379	0.005714772045042667	0.003406952267267044
210	Isabella	x,y,z	2.231740920050496513	0.842042304704040623	0.316984455862986181
		v_x,v_y,v_z	–0.004831339830972945	0.009318806983407490	0.005200751457433266
211	Isolda	x,y,z	2.711875240815070143	0.430216506380016683	0.382482385748132425
		v_x,v_y,v_z	–0.003510234716571616	0.009467947330119904	0.003781089466930833
212	Medea	x,y,z	–1.966750173220412679	–2.504391441888097258	–1.362061306592617482
		v_x,v_y,v_z	0.007097449121202490	–0.004667784575521242	–0.001897190061895615
213	Lilaea	x,y,z	2.419306968138564606	1.377064626174480333	0.236934520281399275
		v_x,v_y,v_z	–0.003663586080577670	0.008842945171148394	0.003566597801239553
221	Eos	x,y,z	1.777939852260157272	2.264787669587976726	0.385115431224176685
		v_x,v_y,v_z	–0.007376964281696770	0.006641442036154265	0.002628969249503958
223	Rosa	x,y,z	–2.914424443137129561	–0.575564316487753080	–0.183166473580308381
		v_x,v_y,v_z	0.000831640269428134	–0.009184748787445272	–0.004253682939508904
224	Oceana	x,y,z	1.306840552514852316	–1.909320111535164788	–1.052599637885983652
		v_x,v_y,v_z	0.009528257077708791	0.004737845515644764	0.002779620693421142
225	Henrietta	x,y,z	–2.528098762364009211	–1.638702365555180007	–0.383411150052558269
		v_x,v_y,v_z	0.007735421152555965	–0.006833347198704122	0.000439444841229691
227	Philosophia	x,y,z	–1.687868923923265596	2.423841903625734151	1.306304444440689938
		v_x,v_y,v_z	–0.006774671779471052	–0.005284654892018608	–0.003871706711383315
233	Asterope	x,y,z	–2.905158595265389554	0.237101371710457365	–0.201153100576835192
		v_x,v_y,v_z	–0.000352351008013982	–0.009087108811730400	–0.002949940598791083
236	Honoria	x,y,z	–0.748198375227333456	–2.637125772058928508	–0.758761586278685618
		v_x,v_y,v_z	0.010085435669044992	–0.000778370444183047	–0.000057970932084369
238	Hypatia	x,y,z	2.410309982055119260	1.056479210705921545	0.250822081348433867
		v_x,v_y,v_z	–0.004638599803102487	0.009855687835584624	0.001848375937922427
240	Vanadis	x,y,z	–2.921723067002446772	–0.802623949197874942	–0.228455192343604230
		v_x,v_y,v_z	0.001119414849423201	–0.008380246775381286	–0.003517310270921982
241	Germania	x,y,z	2.157026156705858178	–1.650363596987127091	–0.494242367750019174
		v_x,v_y,v_z	0.006296839602484864	0.007812769885222028	0.004076824994372825
247	Eukrate	x,y,z	2.169125903092219421	–0.866225171773255864	–0.996634072113313341
		v_x,v_y,v_z	0.003425982013346110	0.007075076118810717	0.007955063682203814

Table 13. Initial positions (au) and velocities (au/day) of the asteroids with respect to the Sun at Julian day (TDB) 2440400.5 (June 28, 1969) in the ICRF2 frame. (Continued: 9 of 15.)

250	Bettina	x,y,z	3.111197416227221346	–0.213218630746829368	–0.517813104094458687
		v_x,v_y,v_z	0.000132313329422579	0.007905211075541855	0.005535308622116215
259	Aletheia	x,y,z	–1.627318570822305688	–2.150337559305796731	–0.609408552011190818
		v_x,v_y,v_z	0.008749058066660119	–0.005149978486112262	–0.004087199673172721
266	Aline	x,y,z	0.229960468787527295	2.407979990359146338	0.736809718189577856
		v_x,v_y,v_z	–0.010856512774706088	0.002950023549757955	–0.001382815037831516
268	Adorea	x,y,z	0.639749669712347591	–2.794617398822625276	–1.162862315045730011
		v_x,v_y,v_z	0.009746292661459431	0.000795802448212805	–0.000055548373269038
275	Sapientia	x,y,z	2.660106410012033074	1.524565090452046245	0.389849845901316994
		v_x,v_y,v_z	–0.005534317791085139	0.006792087695683437	0.002829793913036671
276	Adelheid	x,y,z	–1.240280742637663192	2.649029697867973265	–0.023688532806399230
		v_x,v_y,v_z	–0.009129755737320335	–0.004387217468802240	–0.002182311342655559
283	Emma	x,y,z	–3.467100975427897414	0.326845469549111034	–0.273921918861556368
		v_x,v_y,v_z	–0.000408626057531563	–0.007480204767684386	–0.004047747264448866
287	Nephthys	x,y,z	2.272270153229304146	0.682382283976578408	–0.060915050989619822
		v_x,v_y,v_z	–0.002758331417138625	0.010301650913710764	0.003144420571901631
303	Josephina	x,y,z	–2.714456487118279693	–1.569383554448778861	–1.007607012785439293
		v_x,v_y,v_z	0.004977413077900846	–0.006790226956868332	–0.003754626824227870
304	Olga	x,y,z	–2.768985967086891264	0.841743117969856125	0.394982651347284053
		v_x,v_y,v_z	–0.002248382084316066	–0.008561565126572737	–0.001074438237890270
308	Polyxo	x,y,z	–1.042886921098909125	–2.332650336151194548	–0.811036990846228489
		v_x,v_y,v_z	0.009903231347078257	–0.003677357201775901	–0.001239523162032258
313	Chaldaea	x,y,z	0.771884768362409268	1.939556783718940913	0.398378002792229235
		v_x,v_y,v_z	–0.012098689536781022	0.002656162671110900	0.000678852180394095
322	Phaeo	x,y,z	–0.002682348362129571	–2.507699408031491384	–0.970531169598375820
		v_x,v_y,v_z	0.010244749836147331	0.001937251500163253	0.002228295777838911
326	Tamara	x,y,z	–2.071626956515489226	0.579660636027930942	1.193463031425092469
		v_x,v_y,v_z	–0.003544442645081844	–0.007757868782935538	–0.006335496904282256
328	Gudrun	x,y,z	–2.573274034716255709	–1.465047934437442967	–1.316844023039191125
		v_x,v_y,v_z	0.004832558218741573	–0.006280166157985758	–0.004956463301670980
329	Svea	x,y,z	–1.442616581613682669	2.004856633119884712	0.272499885424718813
		v_x,v_y,v_z	–0.008719664332914103	–0.006477652467348243	–0.000805394135272350
334	Chicago	x,y,z	3.443962847809292072	–1.324275053387580003	–0.714472534127118086
		v_x,v_y,v_z	0.003929882068712210	0.007676913891350206	0.002591553586693644
335	Roberta	x,y,z	–1.377939389741577925	–1.619477614777314223	–0.493517119258204406
		v_x,v_y,v_z	0.010492320292650055	–0.005901393082463712	–0.002553933297352890
336	Lacadiera	x,y,z	–0.658098578079305607	–1.795601132283736634	–0.719216342800300446
		v_x,v_y,v_z	0.011950088864493176	–0.003907291040290498	–0.000403494815576562
338	Budrosa	x,y,z	–2.903591948167865588	0.470290381099696342	–0.099200302996376888
		v_x,v_y,v_z	–0.001425800173495607	–0.008860750970051479	–0.004359767689390367
345	Tercidina	x,y,z	–0.007889583388479199	–2.379738144165251423	–0.650011796314688195
		v_x,v_y,v_z	0.010566766359888404	–0.000201418715010861	0.000963910315785457
346	Hermentaria	x,y,z	–2.982837107945091493	–0.700289625004069438	0.200506563052633757
		v_x,v_y,v_z	0.001487506028262646	–0.008384396621244858	–0.003812447082362887
347	Pariana	x,y,z	–0.865269383843656370	1.912864525007107019	1.057420519699953543
		v_x,v_y,v_z	–0.010024705149477772	–0.006143851860785796	–0.000494836214563871
349	Dembowska	x,y,z	–3.156748018124499122	–0.130959673144165373	0.211799005012422992
		v_x,v_y,v_z	–0.000235136952592180	–0.008001539901820919	–0.004667985924570656

Table 13. Initial positions (au) and velocities (au/day) of the asteroids with respect to the Sun at Julian day (TDB) 2440400.5 (June 28, 1969) in the ICRF2 frame. (Continued: 10 of 15.)

350	Ornamenta	x,y,z	1.897492886578636018	1.853115584753373568	–0.168626022505561857
		v_x,v_y,v_z	–0.006802174405994125	0.006550715887629770	0.006201849595058421
356	Liguria	x,y,z	2.403925905531135054	–1.080394157528443255	–0.637740553547901712
		v_x,v_y,v_z	0.002474022842116686	0.008698179268340399	0.005392308524943403
357	Ninina	x,y,z	2.550147267653644079	1.285776955010184519	–0.179678885435631430
		v_x,v_y,v_z	–0.004469547804037060	0.009229935506104934	0.002753264074857219
358	Apollonia	x,y,z	2.637397004060416439	–0.033680969059450810	–0.033009209749240563
		v_x,v_y,v_z	–0.001238942541646334	0.010294117142742979	0.003742764415514056
360	Carlova	x,y,z	2.365965905770136768	0.946364028961979908	–0.104711173321544837
		v_x,v_y,v_z	–0.005043923473529931	0.009797484839798252	0.003463941512246718
362	Havnia	x,y,z	2.006016399583006038	–1.335233497908418832	–0.941832432474522863
		v_x,v_y,v_z	0.006316106482288478	0.007613525568562483	0.004015883178030646
363	Padua	x,y,z	0.447395563619500725	2.418709764219945324	1.128484276493210148
		v_x,v_y,v_z	–0.010190467851460631	0.001811104511745787	0.001955672995458056
365	Corduba	x,y,z	–0.946605401455762441	–2.952167141736141698	–0.579774951531645599
		v_x,v_y,v_z	0.008854160018258806	–0.001893748322970214	–0.000150172926506452
366	Vincentina	x,y,z	0.181803553220394987	2.727350474248680712	1.834488045213377383
		v_x,v_y,v_z	–0.009184575428991438	0.001029954077974214	0.000256959389362181
369	Aeria	x,y,z	–2.461889264933398547	1.041415912802037491	1.026022247881923644
		v_x,v_y,v_z	–0.004941491515371925	–0.008124405678199062	–0.002138953770784814
373	Melusina	x,y,z	–0.690418739044735830	–2.379811252254516063	–1.898265743321774224
		v_x,v_y,v_z	0.009694322965289898	–0.000476657325627097	–0.000644192905393674
375	Ursula	x,y,z	–1.436446171450740827	–2.028484833217823802	–1.788540836866821859
		v_x,v_y,v_z	0.009100906971536040	–0.003641283355002899	–0.001642880584566145
377	Campania	x,y,z	0.269537079909927590	2.385864264311093219	0.778604188267153829
		v_x,v_y,v_z	–0.011005666135096655	0.001823320353539882	–0.000108001402849965
381	Myrrha	x,y,z	–2.995154522909969863	–0.463362473245098105	0.425103778189245829
		v_x,v_y,v_z	0.002132868519734355	–0.009335695766624439	–0.003072148504579520
385	Ilmatar	x,y,z	2.204123556353274616	1.619262542204616961	1.359899523537142940
		v_x,v_y,v_z	–0.007197099139091408	0.005191410685294344	0.003343985294701643
386	Siegena	x,y,z	–1.541442636926875664	–2.888691935130070387	–0.066078605278559938
		v_x,v_y,v_z	0.008201852800212111	–0.003247965605600923	–0.000826380013421358
387	Aquitania	x,y,z	1.673856039456203204	2.530440646483403278	0.105238509303274774
		v_x,v_y,v_z	–0.006165312103874345	0.006354675190666645	0.002907264021179044
388	Charybdis	x,y,z	2.320935330770025118	–1.396656836528137102	–0.777937804577914949
		v_x,v_y,v_z	0.005967878297330536	0.007526833190292071	0.004390084907098427
389	Industria	x,y,z	–0.690870585159074957	2.285976832122341484	0.972909194639388297
		v_x,v_y,v_z	–0.010061709744287462	–0.002641850906012974	–0.002795471716741464
393	Lampetia	x,y,z	0.425228759538625878	3.223104999989440334	0.691457827571683836
		v_x,v_y,v_z	–0.007669952102573410	0.003507362513697180	–0.000448442801262118
404	Arsinoe	x,y,z	–1.528713317148434614	1.538431701390180706	1.056814160805905178
		v_x,v_y,v_z	–0.006833201218737411	–0.008984287880902874	–0.001895810188518365
407	Arachne	x,y,z	–2.404168202561030032	1.294823426614003070	0.330302008894303445
		v_x,v_y,v_z	–0.005206693346373313	–0.007456531256292877	–0.004441540417027833
410	Chloris	x,y,z	–1.920013803213842740	–1.236776042431182887	–0.102806516019325112
		v_x,v_y,v_z	0.007955416951132228	–0.007973149544052796	–0.004854681062882307
412	Elisabetha	x,y,z	–0.660465882532509707	2.488779742331803213	1.036836462101317080
		v_x,v_y,v_z	–0.009611438891560443	–0.003517675356754544	0.001146633004327251

Table 13. Initial positions (au) and velocities (au/day) of the asteroids with respect to the Sun at Julian day (TDB) 2440400.5 (June 28, 1969) in the ICRF2 frame. (Continued: 11 of 15.)

415	Palatia	x,y,z	2.248246074358777769	–0.101981217325653323	–0.299618390748721652
		v_x,v_y,v_z	–0.002060353514605755	0.011553860188848762	0.004093646216743197
416	Vaticana	x,y,z	–0.968717353915249380	2.586243865176183654	1.726458358232957346
		v_x,v_y,v_z	–0.007646026045771258	–0.004063877953498320	–0.000635412624451350
420	Bertholda	x,y,z	–3.434992155705478112	0.152957066714952405	–0.330353631186631247
		v_x,v_y,v_z	–0.000402294197824229	–0.008601469926580190	–0.003283044092787496
423	Diotima	x,y,z	–1.836130012842030368	–2.232281627979681993	–0.765829327150786887
		v_x,v_y,v_z	0.007840938442101581	–0.004797111494305463	–0.004122385161061739
424	Gratia	x,y,z	2.554859642210790316	–0.721209544624070054	–0.683662530131363688
		v_x,v_y,v_z	0.002391618765227667	0.009552423334085201	0.003497050935833218
426	Hippo	x,y,z	–2.022547942292763690	–1.005817143532471203	–1.399553685672040970
		v_x,v_y,v_z	0.005977729090057320	–0.008172230606490322	–0.004212443868015491
431	Nephele	x,y,z	2.126339087775298786	1.733215636283283123	0.656190187417207027
		v_x,v_y,v_z	–0.005642781181932892	0.008360067976273988	0.003651458241242074
432	Pythia	x,y,z	1.351686874096238222	–1.350586724406483530	–0.907107472146849059
		v_x,v_y,v_z	0.009952768047903163	0.007416635165718826	0.000909632185035547
433	Eros	x,y,z	1.052635242977920882	0.652108246501082123	0.560644019635677004
		v_x,v_y,v_z	–0.011649113662952394	0.009302582981661403	0.003194192782337934
442	Eichsfeldia	x,y,z	2.438069471682043687	0.500402393682477853	–0.018372380659463668
		v_x,v_y,v_z	–0.001598988743082291	0.009827743844217883	0.003532527264151718
444	Gyptis	x,y,z	–0.122162596591544409	–2.551357499130834761	–0.622759399088688381
		v_x,v_y,v_z	0.010779467918873202	0.001166454438831065	0.000838720795358274
445	Edna	x,y,z	–2.638867450404819515	2.337072213589934222	0.386737481707201902
		v_x,v_y,v_z	–0.005987522043549823	–0.003764390073667395	–0.004911559441873959
449	Hamburga	x,y,z	1.415715061146446185	1.814956624851498335	0.711298139664957252
		v_x,v_y,v_z	–0.010126512689018213	0.004544417521285093	0.002585888565144427
454	Mathesis	x,y,z	1.286986769213538828	–1.948908329703617 32	–1.156799971769590929
		v_x,v_y,v_z	0.009804719465114024	0.003999746415627610	0.001524892144668299
455	Bruchsalia	x,y,z	–2.056825944515058957	–2.004397979321892453	–0.509262841989271742
		v_x,v_y,v_z	0.008122040874298211	–0.003536097158237312	–0.003611496524712439
464	Megaira	x,y,z	0.667444028746538631	–2.252197234941088144	–0.993641094169664063
		v_x,v_y,v_z	0.009943729528332137	0.005243255029627681	0.000165611503527442
465	Alekto	x,y,z	3.485008134627705534	0.426960893387227702	0.475918006579878372
		v_x,v_y,v_z	–0.000224571561215830	0.007624192788766146	0.003685169590851310
466	Tisiphone	x,y,z	–2.667676861175595882	1.739553822505467640	0.048087007997351904
		v_x,v_y,v_z	–0.004238745317538407	–0.006912875729415020	–0.005683670800648313
469	Argentina	x,y,z	–2.277066624323161648	–0.948290331570841527	–0.878659731572872693
		v_x,v_y,v_z	0.004890309880280551	–0.008845224571058706	–0.005480291439275048
471	Papagena	x,y,z	–2.365805692852444686	–2.593457491934213266	–0.508479129862948076
		v_x,v_y,v_z	0.005830421752087237	–0.004151641950916174	–0.003631216999264367
476	Hedwig	x,y,z	–1.681308000287230264	–1.540816635314435912	–1.120990466424186094
		v_x,v_y,v_z	0.008429343749817427	–0.006873524681428616	–0.001716598086040729
481	Emita	x,y,z	0.974450886978483366	1.931290124495535832	0.819035276347056418
		v_x,v_y,v_z	–0.010731270482033605	0.004061820639447179	0.004026303026251832
485	Genua	x,y,z	–0.684382743244631553	2.097786304663209034	0.329093928144473968
		v_x,v_y,v_z	–0.011962823721801429	–0.003569573771336420	–0.001358782018689436
489	Comacina	x,y,z	2.506508082475853438	–2.066222307541637271	–0.511544638179387667
		v_x,v_y,v_z	0.006047076129268948	0.006964815651859941	0.001033759739079085

Table 13. Initial positions (au) and velocities (au/day) of the asteroids with respect to the Sun at Julian day (TDB) 2440400.5 (June 28, 1969) in the ICRF2 frame. (Continued: 12 of 15.)

490	Veritas	x,y,z	0.036248932914226248	–3.171478757627256950	–0.801007823894895110
		v_x,v_y,v_z	0.009313455279943360	0.000902292183295022	0.000202399971558074
491	Carina	x,y,z	–1.361895485427903063	–3.165505741951435414	–0.225387122172941129
		v_x,v_y,v_z	0.008172836509484513	–0.003408744893633426	–0.000454450885764238
498	Tokio	x,y,z	–3.141633394765953380	–0.147256452035157803	0.502336236774096112
		v_x,v_y,v_z	0.000707169938473929	–0.007915881021043106	–0.003339475619994648
503	Evelyn	x,y,z	2.469457681649797731	0.897054685380899164	0.196502828408131963
		v_x,v_y,v_z	–0.005320146486079764	0.008280168851000714	0.004381003781921793
505	Cava	x,y,z	2.051381744115417849	0.715819257149662769	–0.079692452727947352
		v_x,v_y,v_z	–0.005500358097765526	0.010138687983931836	0.005377869001808236
506	Marion	x,y,z	2.338637506038451885	–2.236463709683592427	–0.970896012702498035
		v_x,v_y,v_z	0.005454153770407211	0.004892127964045382	0.004916880315758551
508	Princetonia	x,y,z	–1.834398047688895250	2.033726007866053731	1.680737578756668515
		v_x,v_y,v_z	–0.007530022629651348	–0.005443148627532285	–0.002038851357460140
514	Armida	x,y,z	–1.795059498387787666	2.342984019721451094	0.883644880995315685
		v_x,v_y,v_z	–0.008098171175524310	–0.004726881362335257	–0.002646867999807014
516	Amherstia	x,y,z	3.099051382763043705	0.296225047046435153	0.633503755281144221
		v_x,v_y,v_z	0.000113246728749009	0.007155674865686408	0.004973978514489579
517	Edith	x,y,z	0.558320524452791234	–3.192588255468263636	–1.370798827031080469
		v_x,v_y,v_z	0.008142074640245637	0.002287166228260473	0.001503486262573605
521	Brixia	x,y,z	–2.549496878032234903	–2.363059656332096470	–0.504053344408389448
		v_x,v_y,v_z	0.005060051620143621	–0.004986735600834600	–0.003179245956564224
535	Montague	x,y,z	–2.316646842841627585	0.712595568810880153	0.617355942561913063
		v_x,v_y,v_z	–0.003949779425587768	–0.009578278138314685	–0.003755534201261866
536	Merapi	x,y,z	–2.750766666063489296	–2.439053500410161668	–0.616255994545442776
		v_x,v_y,v_z	0.005689626184352026	–0.004264313174264865	–0.004857657183703378
545	Messalina	x,y,z	–3.088249528284030543	1.764074066249742057	0.869124506509039163
		v_x,v_y,v_z	–0.003538173057074548	–0.006065837986010540	–0.004381735842294599
547	Praxedis	x,y,z	1.676299422983591914	1.266883169004290322	0.274076519007798947
		v_x,v_y,v_z	–0.007644163901651690	0.010654276917228497	0.000771636508649015
566	Stereoskopia	x,y,z	3.108217299055801242	–0.038924752084866489	–0.306684557850228134
		v_x,v_y,v_z	0.000163401251640635	0.009232636979490162	0.004135544106424715
568	Cheruskia	x,y,z	2.499292317070373137	–0.704732562382201388	0.596817158342859422
		v_x,v_y,v_z	0.000384461732460371	0.010401955137544539	0.003335461022407042
569	Misa	x,y,z	–0.314868951447094259	–2.848132605531735528	–1.283448671165868582
		v_x,v_y,v_z	0.008734805915040946	–0.000862116582237407	–0.000205188117724297
584	Semiramis	x,y,z	–2.503710281861984743	–0.998160106756301402	–0.996565071101295330
		v_x,v_y,v_z	0.004900032034025778	–0.007159666424074737	–0.002463187315737590
585	Bilkis	x,y,z	1.912791286329316831	1.539478930510618904	0.440912149264970965
		v_x,v_y,v_z	–0.007907529478716448	0.006999464858132820	0.001976597919510323
591	Irmgard	x,y,z	3.001474010271674153	–0.872392399734546298	–0.271674947450289361
		v_x,v_y,v_z	0.003412279465211854	0.006515819416529907	0.004916384720291039
593	Titania	x,y,z	–0.426142954823842124	–2.875072915506421189	–1.351850274140791841
		v_x,v_y,v_z	0.008043320855626214	–0.000800619582345174	–0.003093655045037652
595	Polyxena	x,y,z	–2.275279297558304492	–1.787230083745405596	–1.091452381026450702
		v_x,v_y,v_z	0.006946976359411234	–0.004847860891067480	–0.005228807026657581
596	Scheila	x,y,z	2.068249321573481403	2.559630685610615686	0.793577660766494164
		v_x,v_y,v_z	–0.006190047319295022	0.004343781071425732	0.004070640552158299

Table 13. Initial positions (au) and velocities (au/day) of the asteroids with respect to the Sun at Julian day (TDB) 2440400.5 (June 28, 1969) in the ICRF2 frame. (Continued: 13 of 15.)

598	Octavia	x,y,z	–1.508523042247438273	1.946258357215855606	1.174114109004084749
		v_x,v_y,v_z	–0.009625203890116693	–0.004100840847587676	0.000525696328445862
599	Luisa	x,y,z	–2.896166748961349846	1.273195801188978793	1.640818403618105270
		v_x,v_y,v_z	–0.004659866001601793	–0.005499407621023489	–0.002708296082629357
602	Marianna	x,y,z	2.236421484533403614	0.256457028560368117	0.531502491866831517
		v_x,v_y,v_z	–0.002987755039934792	0.010015170339145833	0.007115827480249712
604	Tekmessa	x,y,z	–2.443492364975899278	–2.553672554973274167	–1.297289046740899066
		v_x,v_y,v_z	0.006146762368787255	–0.004416770321035214	–0.002442816546685167
618	Elfriede	x,y,z	2.516097127945998935	1.510176140872574457	–0.283377085143805829
		v_x,v_y,v_z	–0.004157210144504098	0.008684469448787927	0.003885209090645422
623	Chimaera	x,y,z	–2.409466239800548415	–0.465525463994251487	–0.851563289724215688
		v_x,v_y,v_z	0.002342861813000729	–0.008762166195659019	–0.005029967766286956
626	Notburga	x,y,z	–3.035450076806275543	0.421864008988716566	–0.127583860826996742
		v_x,v_y,v_z	–0.001866697145881276	–0.005612944658928348	–0.006561241265170950
635	Vundtia	x,y,z	2.006725589468375315	–2.376415931764492395	–0.496002046851244771
		v_x,v_y,v_z	0.006841157951777630	0.006652586659241708	0.001565035661244263
663	Gerlinde	x,y,z	2.983897565601330903	1.397628190931970993	1.091574612026383173
		v_x,v_y,v_z	–0.004331655563956410	0.007414701609598470	0.000530966741235238
667	Denise	x,y,z	–2.421777915332062658	–2.295475988992165650	0.452580813773379109
		v_x,v_y,v_z	0.004815408543036114	–0.007668419938770380	–0.000993922465387279
674	Rachele	x,y,z	–0.235827957791626630	2.008846377619600609	1.239571728159498454
		v_x,v_y,v_z	–0.011860879067687655	–0.002375626722544034	0.001425555621865033
675	Ludmilla	x,y,z	0.001979483768247084	2.107337311005498925	0.870011327043579530
		v_x,v_y,v_z	–0.012117274959326541	0.001965172863672976	–0.001430686736150516
680	Genoveva	x,y,z	–2.483498644334699357	1.961237812146513715	2.122017516184655506
		v_x,v_y,v_z	–0.004535242841718457	–0.005563771866247991	–0.003051609814162152
683	Lanzia	x,y,z	–0.038757248577513628	–2.929038122705282188	–1.100369444712229416
		v_x,v_y,v_z	0.009189739037992875	–0.001698156106930829	0.002602487296413445
690	Wratislavia	x,y,z	–1.572098580880649132	–2.754041913568673561	–1.335506562200244884
		v_x,v_y,v_z	0.008204336231111772	–0.003237602143731363	0.000474631125854728
691	Lehigh	x,y,z	–2.600679234384931426	–2.131333554500724148	–0.280098141039464121
		v_x,v_y,v_z	0.005534054469881479	–0.005798095800458341	–0.003891386736724764
694	Ekard	x,y,z	–2.073828833200439092	–1.723446996059183167	–0.871272150977313808
		v_x,v_y,v_z	0.008389896606921710	–0.005221711697173815	0.000631908650981562
696	Leonora	x,y,z	–2.528679514939249806	–2.344092579990681102	–1.934926268906861813
		v_x,v_y,v_z	0.005658575767356208	–0.004750757197783061	–0.001445326359372374
702	Alauda	x,y,z	0.731086409189228292	2.576019002727282015	1.840680315316418403
		v_x,v_y,v_z	–0.008610612355498393	0.003701586218457099	–0.001273396941220973
705	Erminia	x,y,z	1.527810127063314871	–1.738330529507490452	–2.020057855746948849
		v_x,v_y,v_z	0.008204195294184936	0.003409657750114686	0.003528767177190933
709	Fringilla	x,y,z	1.932009598635754166	1.322621695446154488	1.386519279952832973
		v_x,v_y,v_z	–0.006619431762339829	0.007378506450047627	0.004203577713780057
712	Boliviana	x,y,z	–2.181214001606280206	1.349361062281813073	–0.026299365363868094
		v_x,v_y,v_z	–0.006970304527136179	–0.007493618475270048	–0.003330760378138190
713	Luscinia	x,y,z	0.602542358281345058	–2.935328109946095054	–0.752927362734930772
		v_x,v_y,v_z	0.009618230119085674	0.002849533330894416	0.001959410111945836
735	Marghanna	x,y,z	–2.970874542187170952	–1.503348928425136677	–0.336696621923833705
		v_x,v_y,v_z	0.005083914736085787	–0.004623872868731655	–0.004610217116933856

Table 13. Initial positions (au) and velocities (au/day) of the asteroids with respect to the Sun at Julian day (TDB) 2440400.5 (June 28, 1969) in the ICRF2 frame. (Continued: 14 of 15.)

739	Mandeville	x,y,z	2.506148925696726870	–1.504824362532233950	–0.834400633180084061
		v_x,v_y,v_z	0.005428727641429763	0.007553927772582291	–0.000302902354564315
740	Cantabia	x,y,z	3.314248241247279569	–0.064714374102698397	–0.617044240710776459
		v_x,v_y,v_z	0.000448233529388049	0.008426445083442220	0.002733213589088293
751	Faina	x,y,z	–2.301643137177721954	0.965649183773619191	1.182110401173152026
		v_x,v_y,v_z	–0.005854981025964248	–0.007733688166168566	–0.002054122576185711
752	Sulamitis	x,y,z	2.048812749653873055	1.241773705314024756	0.317962157290045455
		v_x,v_y,v_z	–0.006453759688972923	0.008038950160103676	0.004297655236858543
760	Massinga	x,y,z	3.670126642304055498	–1.151050350627846441	–0.367902633175755500
		v_x,v_y,v_z	0.002369603147829039	0.005888743311020824	0.004396658729641872
762	Pulcova	x,y,z	3.175342326316428654	–1.199205892203630830	–0.047622057373297624
		v_x,v_y,v_z	0.002109743357951093	0.007234201884231036	0.004880661946113063
769	Tatjana	x,y,z	0.509160148400431334	–2.303342379809931284	–1.333719406992519119
		v_x,v_y,v_z	0.010933982442492730	0.002495895480057548	0.000346838301451201
772	Tanete	x,y,z	2.906025830739782823	0.647310471297706802	–1.267907728397291933
		v_x,v_y,v_z	0.001010921533345003	0.007595842568837846	0.005064697781475233
773	Irmintraud	x,y,z	–1.324784143882017373	–1.754236649382118429	–1.608060869413702854
		v_x,v_y,v_z	0.009439627055445330	–0.004735182301384725	–0.001496436978411633
776	Berbericia	x,y,z	–2.430375861485484013	1.244119991480070464	1.499556777478691094
		v_x,v_y,v_z	–0.006193479474740193	–0.007012659876802435	–0.001255056722427736
778	Theobalda	x,y,z	2.578770540715112691	0.484679459667908874	0.746658068287141652
		v_x,v_y,v_z	–0.005606680738267385	0.008333234968279164	0.004809669391709696
780	Armenia	x,y,z	–2.947260333629879270	1.443734931655717313	0.745070083337502465
		v_x,v_y,v_z	–0.004292145745643914	–0.007903853241575533	–0.000226820581777773
784	Pickeringia	x,y,z	–1.216179274985955239	–1.725991913871303796	–1.130983048638923849
		v_x,v_y,v_z	0.010795481346361395	–0.004416936010313539	–0.003972330176354399
786	Bredichina	x,y,z	–0.640973967234059860	3.011946086754773155	1.482664510763615384
		v_x,v_y,v_z	–0.008114458019644099	–0.003635735760200800	0.000726237470920756
788	Hohensteina	x,y,z	–2.065161763450813925	–1.731735607044430303	–0.269841031252473607
		v_x,v_y,v_z	0.007166218568798618	–0.008400928402379429	–0.001362268879167860
790	Pretoria	x,y,z	–3.312660708096480278	0.159833898455113310	–1.180393653213523963
		v_x,v_y,v_z	0.001800283505532356	–0.008606461983801833	–0.001971983915071157
791	Ani	x,y,z	–0.693006042192073846	–2.790965988787078800	–0.471075353887803139
		v_x,v_y,v_z	0.010149322918663708	–0.000178409023167429	–0.002316736158141167
804	Hispania	x,y,z	1.180236347016857978	–1.755994298920930508	–1.316225480612562171
		v_x,v_y,v_z	0.009748138526187236	0.004495021926921983	0.004245447086389762
814	Tauris	x,y,z	–2.643337763228612580	–3.043511779699754172	–0.187636072682489108
		v_x,v_y,v_z	0.005375474685596784	–0.003186610433694088	–0.003752983540055900
849	Ara	x,y,z	–2.400436417716211412	–1.377376257048356312	–0.903371236042467940
		v_x,v_y,v_z	0.006630709229090170	–0.008101548494299364	0.000290406058693144
895	Helio	x,y,z	–1.153864786573528756	–2.970641315024131757	–1.742880474756495213
		v_x,v_y,v_z	0.006903078729138242	–0.004383767421712856	0.001915953866110696
909	Ulla	x,y,z	2.643585779564476823	–1.912997619870260957	–0.715076842818698211
		v_x,v_y,v_z	0.005129680510801807	0.008209415548612537	0.000169376652986247
914	Palisana	x,y,z	0.598245936709027260	–1.827975513352569470	–0.273954790847752927
		v_x,v_y,v_z	0.011446713245858879	0.003314424689681761	0.006488303174133064
980	Anacostia	x,y,z	–3.175758333328849048	0.485972795063543628	–0.719059100789527061
		v_x,v_y,v_z	–0.000142109533888624	–0.007460640782612650	–0.004030038096555623

Table 13. Initial positions (au) and velocities (au/day) of the asteroids with respect to the Sun at Julian day (TDB) 2440400.5 (June 28, 1969) in the ICRF2 frame. (Continued: 15 of 15.)

1015	Christa	x,y,z	–1.566656583058677832	2.568332206936112527	1.085692881000842158
		v_x,v_y,v_z	–0.008675523560380710	–0.004175198720726467	–0.000110280407398696
1021	Flammario	x,y,z	–2.936407649398657060	0.239975615662415959	0.837347923291067331
		v_x,v_y,v_z	–0.003624193796013200	–0.008360760098837189	–0.001485430871488255
1036	Ganymed	x,y,z	–2.506653200603659926	2.486748461463569093	–0.616157838784046952
		v_x,v_y,v_z	–0.006637194622358507	–0.002518711399848999	–0.001898585862499638
1093	Freda	x,y,z	–2.277804058924099539	–1.843336426423987318	–0.338410936166434473
		v_x,v_y,v_z	0.007229516437050462	–0.003691334503305957	–0.006389991099609126
1107	Lictoria	x,y,z	–2.569057933925188664	–1.937453059103700248	–0.421229684865389586
		v_x,v_y,v_z	0.004720513971195381	–0.007449150358726622	–0.003422150642625780
1171	Rusthawelia	x,y,z	2.560542567362555477	–1.071816228353758005	–0.550580177371690072
		v_x,v_y,v_z	0.002594814272586507	0.009717147787535695	0.003755086238400567
1467	Mashona	x,y,z	0.966768996929490920	–2.152669618944333507	–1.688772902845859569
		v_x,v_y,v_z	0.009795683288059361	0.001634297002254343	0.004184325487804071

References

[1] W. M. Folkner, J. G. Williams, and D. H. Boggs, "The Planetary and Lunar Ephemeris DE421," *The Interplanetary Network Progress Report*, vol. 42-178, Jet Propulsion Laboratory, Pasadena, California, pp. 1–34, August 15, 2009. http://ipnpr.jpl.nasa.gov/progress_report/42-178/178C.pdf

[2] E. M. Standish, X X Newhall, J. G. Williams, and W. M. Folkner, *JPL Planetary and Lunar Ephemerides*, Richmond, Virginia: Willmann-Bell, Inc., 1997.

[3] X X Newhall, "Numerical Representation of Planetary Ephemerides," *Celestial Mechanics*, vol. 45, pp. 305–310, 1989.

[4] E. M. Standish and J. G. Williams, "Orbital Ephemerides of the Sun, Moon, and Planets," *The Explanatory Supplement to the Astronomical Almanac, Third Edition*, eds. S. Urban and P. K. Seidelmann, Mill Valley, California: University Science Books, pp. 305–345, 2012.

[5] J. G. Williams, D. H. Boggs, C. F. Yoder, J. T. Ratcliff, and J. O. Dickey, "Lunar Rotational Dissipation in Solid Body and Molten Core," *Journal of Geophysical Research*, vol. 106, pp. 27933–27968, 2001.

[6] J. G. Williams and D. H. Boggs, "Lunar Core and Mantle: What Does LLR See?", *Proceedings of the 16th International Workshop on Laser Ranging, SLR — the Next Generation*, ed. Stanislaw Schillak, October 2008, Poznan, Poland, pp. 101–120, 2009. http://www.astro.amu.edu.pl/ILRS_Workshop_2008/index.php

[7] P. Kuchynka and W. M. Folkner, "A New Approach to Determining Asteroid Masses from Planetary Range Measurements," *Icarus*, vol. 222, pp. 243–253, 2013.

[8] D. L. Matson, G. J. Veeder, E. F. Tedesco, L. A. Lebofsky, and R. G. Walker, "IRAS Survey of Asteroids," *Advances in Space Research*, vol. 6, pp. 47–56, 1986.

[9] J. R. Masiero, A. K. Mainzer, T. Grav, J. M. Bauer, R. M. Cutri, et al., "Main Belt Asteroids with WISE/NEOWISE: I. Preliminary Albedos and Diameters," *Astrophysical Journal*, vol. 741, article 68, 20 pages, 2011.

[10] E. F. Tedesco, P. V. Noah, M. Noah, and S. D. Price, "The Supplemental IRAS Minor Planet Survey," *Astronomical Journal*, vol. 123, pp. 1056–1085, 2002.

[11] C. Ma, E. F. Arias, G. Bianco, D. A. Boboltz, S. L. Bolotin, et al., "The Second Realization of the International Celestial Reference Frame by Very Long Baseline Interferometry," *IERS Technical Note No. 35*, International Earth Rotation and Reference Systems Service, Verlag des Bundesamts für Kartographie und Geodäsie, Frankfurt, Germany, 2009.

[12] O. Titov, S. B. Lambert and A.-M. Gontier, "VLBI Measurement of the Secular Aberration Drift," *Astronomy and Astrophysics*, vol. 529, pp. A91–A97, 2011.

[13] J. D. Giorgini, D. K. Yeomans, A. B. Chamberlin, P. W. Chodas, R. A. Jacobson, et al., "JPL's On-Line Solar System Data Service," *Bulletin of the American Astronomical Society*, vol. 28, p. 1158, 1996.

[14] A. Fienga, H. Manche, J. Laskar, and M. Gastineau, "INPOP06: A New Numerical Planetary Ephemeris," *Astronomy and Astrophysics*, vol. 477, pp. 315–327, 2008.

[15] E. V. Pitjeva, "Influence of Asteroids and Trans-Neptunian Objects on the Motion of Major Planets and Masses of the Asteroid Main Belt and the TNO Ring," *Proceedings of the International Conference on Asteroid–Comet Hazard — 2009*, eds. A. M. Finkelstein, W. F. Huebner, and V. A. Shor, St. Petersburg, Russia, pp. 237–241, 2010.

[16] M. Soffel, S. A. Klioner, G. Petit, P. Wolf, S. M. Kopeikin, et al., "The IAU 2000 Resolutions for Astrometry, Celestial Mechanics, and Metrology in the Relativistic Framework: Explanatory Supplement," *Astronomical Journal*, vol. 126, pp. 2687–2706, 2003.

[17] A. Fienga, J. Laskar, T. Morley, H. Manche, P. Kuchynka, et al., "INPOP08, A 4-D Planetary Ephemeris: From Asteroid and Time-Scale Computations to ESA Mars Express and Venus Express Contributions," *Astronomy and Astrophysics*, vol. 507, pp. 1675–1686. 2009.

[18] G. Petit and B. Luzum, "IERS Conventions (2010)," *IERS Technical Note No. 36*, International Earth Rotation and Reference Systems Service, Verlag des Bundesamts für Kartographie und Geodäsie, Frankfurt, Germany, 2009.

[19] A. W. Irwin and T. Fukushima, "A Numerical Time Ephemeris of the Earth," *Astronomy and Astrophysics*, vol. 348, pp. 642–652, 1999.

[20] A. S. Konopliv, S. W. Asmar, W. M. Folkner, O. Karatekin, D. C. Nunes, et al., "Mars High-Resolution Gravity fields from MRO, Mars Seasonal Gravity and Other Dynamical Parameters," *Icarus*, vol. 211, pp. 401–428, 2011.

[21] J. H. Lieske, T. Lederle, W. Fricke, and B. Morando, "Expression for the Precession Quantities Based on the IAU (1976) System of Astronomical Constants," *Astronomy and Astrophysics*, vol. 58,pp. 1–16, 1977.

[22] J. H. Lieske, "Precession Matrix Based on IAU (1976) System of Astronomical Constants," *Astronomy and Astrophysics*, vol. 73, pp. 282–284, 1979.

[23] P. K. Seidelmann, "1980 IAU Theory of Nutation: The Final Report of the IAU Working Group on Nutation," *Celestial Mechanics*, vol. 27, pp. 79–106, 1982.

[24] A. Einstein, L. Infeld and B. Hoffmann, "The Gravitational Equations and the Problem of Motion," *Annals of Mathematics,* vol. 39, pp. 65–100,1938.

[25] C. M. Will and K. Nordtvedt, "Conservation Laws and Preferred Frames in Relativistic Gravity: I. Preferred Frame Theories and an Extended PPN Formalism," *Astrophysical Journal*, vol. 177, pp. 757–774, 1972.

[26] T. D. Moyer, *Formulation for Observed and Computed Values of Deep Space Network Data Types for Navigation*, Monograph 2, Deep-Space Communications and Navigation Systems Center of Excellence (DESCANSO), Deep-Space Communications and Navigation Series, Jet Propulsion Laboratory, Pasadena, California, October 2000. http://descanso.jpl.nasa.gov/Monograph/series2/Descanso2_all.pdf

[27] C. F. Yoder, "Effects of the Spin-Interaction and the Inelastic Tidal Deformation on the Lunar Physical Librations," *Natural and Artificial Satellite Motion,* ed. P. E. Nacozy and S. Ferraz-Mello, Austin, Texas: University of Texas Press, pp. 211–221, 1979.

[28] D. H. Eckhardt, "Theory of the Libration of the Moon," *Moon and Planets*, vol. 25, pp. 3–49, 1981.

[29] P. L. Bender, D. G. Currie, R. H. Dicke, D. H. Eckhardt, J. E. Faller, et al., "The Lunar Laser Ranging Experiment," *Science*, vol. 182, pp. 229–238, 1973.

[30] J. O. Dickey, P. L. Bender, J. E. Faller, X X Newhall, R. L. Ricklefs, et al., "Lunar Laser Ranging: a Continuing Legacy of the Apollo Program," *Science*, vol. 265, pp. 482–490, 1994.

[31] J. B. R. Battat, T. W. Murphy, Jr., E. G. Adelberger, B. Gillespie, C. D. Hoyle, et al., "The Apache Point Observatory Lunar Laser-Ranging Operation (APOLLO): Two Years of Millimeter-Precision Measurements of the Earth–Moon Range," *Publications of the Astronomical Society of the Pacific*, vol. 121, pp. 29–40, 2009.

[32] P. J. Shelus, "MLRS: A Lunar/Artificial Satellite Laser Ranging Facility at the McDonald Observatory," *IEEE Transactions on Geoscience and Remote Sensing*, Ge-23, pp. 385–390, 1985.

[33] M. R. Pearlman, J. J. Degnan, and J. M. Bosworth, "The International Laser Ranging Service," *Advances in Space Research*, vol. 30, pp. 135–143, 2002.

[34] E. Samain, J. F. Mangin, C. Veillet, J. M. Torre, P. Fridelance, et al., "Millimetric Lunar Laser Ranging at OCA (Observatoire de la Côte d'Azur)," *Astronomy and Astrophysics Supplement*, vol. 130, pp. 235–244, 1998.

[35] T. W. Murphy, Jr., E. G. Adelberger, J. B. R. Battat, L. N. Carey, C. D. Hoyle, et al., "The Apache Point Observatory Lunar Laser-Ranging Operation: Instrument Description and First Detections," *Publications of the Astronomical Society of the Pacific*, vol. 120, pp. 20–37, 2008.

[36] P. Kuchynka and W. M. Folkner, "Station-Specific Errors in Mars Ranging Measurements," *The Interplanetary Network Progress Report*, vol. 42–190, Jet Propulsion Laboratory, Pasadena, California, pp. 1–11, August 15, 2012.
http://ipnpr.jpl.nasa.gov/progress_report/42-190/190C.pdf

[37] D. W. Curkendall and J. S. Border, "Delta-DOR: The One-Nanoradian Navigation Measurement System of the Deep Space Network — History, Architecture and Componentry," *The Interplanetary Network Progress Report*, vol. 42–193, Jet Propulsion Laboratory, Pasadena, California, pp. 1–46, May 15, 2013.
http://ipnpr.jpl.nasa.gov/progress_report/42-193/193D.pdf

[38] D. L. Jones, E. Fomalont, V. Dhawan, J. Romney, W. M. Folkner, et al., "Very Long Baseline Array Astrometric Observations of the Cassini Spacecraft at Saturn," *Astronomical Journal*, vol. 141, no. 29, 10 pages, 2011.

[39] M. A. C. Perryman, L. Lindegren, J. Kovalevsky, E. Høg, U. Bastian, et al., "The Hipparcos Catalogue," *Astronomy and Astrophysics*, vol. 323, pp. L49–L52, 1997.

[40] J.-F. Lestrade, D. L. Jones, R. A. Preston, R. B. Phillips, M. A. Titus, et al., "Preliminary Link of the HIPPARCOS and VLBI Reference Frames," *Astronomy and Astrophysics*, vol. 304, pp. 182–188, 1995.

[41] E. E. Barnard, "Micrometer Observations of the Satellite of Neptune at the Oppositions of 1903–1904," *Astronomical Journal*, vol. 25, pp. 41–42, 1906.

[42] E. E. Barnard, "Observations of the Satellite of Neptune at the Opposition of 1906–7," *Astronomical Journal*, vol. 25, p. 164, 1907.

[43] E. E. Barnard, "Observations of the Satellite of Neptune at the Oppositions 1907–8 and 1908–9, Made with the 40-inch Telescope," *Astronomische Nachrichten*, vol. 181, pp. 321–326, 1909.

[44] E. E. Barnard, "Observations of the Satellites of Uranus," *Astronomical Journal*, vol. 26, pp. 47–50, 1909.

[45] E. E. Barnard, "Micrometer Measures of the Satellites of Saturn in the Years 1910, 1911, and 1912," *Astronomical Journal*, vol. 27, pp. 116–129, 1912.

[46] E. E. Barnard, "Observations of the Satellite of Neptune, 1910–1912," *Astronomical Journal*, vol. 27, pp. 111–112, 1912.

[47] E. E. Barnard, "Observations of the Satellites of Uranus," *Astronomical Journal*, vol. 27, pp. 104–106, 1912.

[48] E. E. Barnard, "Observations of the Satellites of Saturn," *Astronomical Journal*, vol. 29, pp. 33–37, 1915.

[49] E. E. Barnard, "Observations of the Satellites of Uranus," *Astronomical Journal*, vol. 29, pp. 39–40, 1915.

[50] E. E. Barnard, "Observations of the Satellite of Neptune," *Astronomical Journal*, vol. 30, pp. 2–4, 1916.

[51] E. E. Barnard, "Observations of the Satellites of Saturn at the Opposition of 1915–16," *Astronomical Journal*, vol. 30, pp. 33–40, 1916.

[52] E. E. Barnard, "Observations of the Satellite of Neptune," *Astronomical Journal*, vol. 30, pp. 214–216, 1917.

[53] E. E. Barnard, "Observations of the Satellite of Neptune," *Astronomical Journal*, vol. 32, pp. 103–104, 1919.

[54] E. E. Barnard, "Observations of the Satellites of Uranus," *Astronomical Journal*, vol. 32, pp. 105–107, 1919.

[55] E. E. Barnard, "Measures of the Satellites of Saturn and Position-Angles of the Ring," *Astronomical Journal*, vol. 37, pp. 157–172, 1927.

[56] E. E. Barnard, "Micrometer Observations of Neptune," *Astronomical Journal*, vol. 37, pp. 130–132, 1927.

[57] E. E. Barnard, "Observations of the Satellites of Uranus," *Astronomical Journal*, vol. 37, pp. 125–127, 1927.

[58] M. Assafin, J. I. B. Camargo, R. Vieira Martins, A. H. Andrei, B. Sicardy, et al., "Precise Predictions of Stellar Occultations by Pluto, Charon, Nix, and Hydra for 2008–2015," *Astronomy and Astrophysics,* vol. 515, pp. A32, 2010.

[59] D. K. Srinivasan, M. E. Perry, K. B. Fielhauer, D. E. Smith, and M. T. Zuber, "The Radio Frequency Subsystem and Radio Science on the MESSENGER Mission," *Space Science Reviews*, vol. 131, pp. 557–571, 2007.

[60] J. D. Anderson, G. Colombo, P. B. Esposito, E. L. Lau, and G. B. Trager, "The Mass, Gravity Field, and Ephemeris of Mercury," *Icarus*, vol. 71, pp. 337–349, 1987.

[61] Yu. N. Aleksandrov, A. S. Vyshlov, V. M. Dubrovin, A. L. Zaitsev, S. P. Ignatov, et al., "Radar Observations of Mars, Venus, and Mercury at a Wavelength of 39 cm in 1980," *Soviet Physics Doklady*, vol. 25, pp. 945–947, 1981.

[62] J. K. Harmon, D. B. Campbell, D. L. Bindschadler, J. W. Head, and I. I. Shapiro, "Radar Altimetry of Mercury: A Preliminary Analysis," *Journal of Geophysical Research*, vol. 91, pp. 385–401 ,1986.

[63] R. F. Jurgens, F. Rojas, M. Slade, E. M. Standish, and J. F. Chandler, "Mercury Radar Ranging Data from 1987 to 1997," *Astronomical Journal*, vol. 116, pp. 486–488, 1998.

[64] J. D. Anderson, R. F. Jurgens, E. L. Lau, and M. A. Slade, "Shape and Orientation of Mercury from Radar Ranging Data," *Icarus*, vol. 124, pp. 690–697, 1996.

[65] D. B. Campbell, R. B. Dyce, R. P. Ingalls, G. H. Pettengill, and I. I. Shapiro, "Venus Topography Revealed by Radar Data," *Science*, vol. 175, pp. 514–516, 1972.

[66] Yu. N. Aleksandrov, V. K. Golovkov, V. M. Dubrovin, A. L. Zaitsev, V. I. Kaevitser, et al., "The Reflection Properties and Surface Relief of Venus; Radar Surveys at 39-cm Wavelength," *Soviet Astronomy*, vol. 24, pp. 139–146, 1980.

[67] D. B. Campbell and B. A. Burns, "Earth-Based Radar Imagery of Venus," *Journal of Geophysical Research*, vol. 85, pp. 8271–8281, 1980.

[68] E. M. Standish and R. W. Hellings, "A Determination of the Masses of Ceres, Pallas and Vesta from Their Perturbations Upon the Orbit of Mars," *Icarus*, vol. 80, pp. 326–333, 1989.

[69] A. S. Konopliv, C. F. Yoder, E. M. Standish, D.-N. Yuan, and W. L. Sjogren, "A Global Solution for the Mars Static and Seasonal Gravity, Mars Orientation, Phobos and Deimos Masses, and Mars Ephemeris," *Icarus*, vol. 182, pp. 23–50, 2006.

[70] A. Fienga, J. Laskar, P. Kuchynka, H. Manche, G. Desvignes, M. Gastineau, I. Cognard, and G. Theureau, "The INPOP10a Planetary Ephemeris and Its Applications in Fundamental Physics," *Celestial Mechanics and Dynamical Astronomy,* vol. 111, pp. 363–385, 2011.

[71] R. C. Stone, D. G. Monet, A. K. B. Monet, R. L. Walker, H. D. Ables, A. R. Bird, and F. H. Harris, "The Flagstaff Astrometric Scanning Transit Telescope (FASTT) and Star Positions Determined in the Extragalactic Reference Frame," *Astronomical Journal*, vol. 111, pp. 1721–1742, 1996.

[72] R. C. Stone, "CCD Positions for the Outer Planets in 1995 Determined in the Extragalactic Reference Frame," *Astronomical Journal*, vol. 112, pp. 781–787, 1996.

[73] R. C. Stone, "CCD Positions for the Outer Planets in 1996–1997 Determined in the Extragalactic Reference Frame," *Astronomical Journal*, vol. 116, pp. 1461–1469,1998.

[74] R. C. Stone and F. H. Harris, "CCD Positions Determined in the International Celestial Reference Frame for the Outer Planets and Many of Their Satellites in 1995–1999," *Astronomical Journal*, vol. 119, pp. 1985–1998, 2000.

[75] R. C. Stone, "Positions for the Outer Planets and Many of their Satellites: IV. FASTT Observations Taken in 1999–2000," *Astronomical Journal*, vol. 120, pp. 2124–2130, 2000.

[76] R. C. Stone, "Positions for The Outer Planets and Many of Their Satellites: V. FASTT Observations Taken in 2000–2001," *Astronomical Journal*, vol. 122, pp. 2723–2733, 2001.

[77] R. C. Stone, D. G. Monet, A. K. B. Monet, F. H. Harris, H. D. Ables, et al., "Upgrades to the Flagstaff Astrometric Scanning Transit Telescope: A Fully Automated Telescope for Astrometry," *Astronomical Journal,* vol. 126, pp. 2060–2080, 2003.

[78] M. Vasilyev, G. Krasinsky, M. Sveshnikov, G. Gorel, and L. Gudkova, "Improving of Ephemerides of Jupiter Using Observations of Galilean Satellites Made in Nikolaev in 1962–1997," *Trudy IPA RAN (Proceedings of Institute of Applied Astronomy),* vol. 5, pp. 176–189, 2000.

[79] L. Helmer and L. V. Morrison, "Carlsberg Automatic Meridian Circle," *Vistas in Astronomy*, vol. 28, pp. 505–518, 1985.

[80] V. P. Rylkov, V. V. Vityazev, and A. A. Dementieva, "Pluto: An Analysis of Photographic Positions Obtained with the Pulkovo Normal Astrograph in 1930–1992," *Astronomical and Astrophysical Transactions*, vol. 6, pp. 251–281, 1995.

[81] B. Luzum, N. Capitaine, A. Fienga, W. Folkner, T. Fukushima, et al., "The IAU 2009 System of Astronomical Constants: The Report of the IAU Working Group on Numerical Standards for Fundamental Astronomy," *Celestial Mechanics and Dynamical Astronomy*, vol. 110, pp. 293–304, 2011.

[82] J. C. Ries, R. J. Eanes, C. K. Shum, and M. M. Watkins, "Progress in the Determination of the Gravitational Coefficient of the Earth," *Geophysical Research Letters*, vol. 19, pp. 529–531, 1992.

[83] P. Dunn, M. Torrence, R. Kolenkiewicz, and D. Smith, "Earth Scale Defined by Modern Satellite Ranging Observations," *Geophysical Research Letters*, vol. 26, pp. 1489–1492, 1999.

[84] J. C. Ries, "Satellite Laser Ranging and the Terrestrial Reference Frame: Principal Sources of Uncertainty in the Determination of the Scale," *Geophysical Research Abstracts*, vol. 9, no. 10809, EGU General Assembly, Vienna, Austria, April 15–20, 2007.

[85] A. S. Konopliv, R. S. Park, D.-N. Yuan, S. W. Asmar, M. M. Watkins, et al., "The JPL Lunar Gravity Field to Spherical Harmonic Degree 660 from the GRAIL Primary Mission," *Journal of Geophysical Research*, vol. 118, pp. 1415–1434, 2013.

[86] F. G. Lemoine, S. Goossens, T. J. Sabaka, J. B. Nicholas, E. Mazarico, et al., "High-Degree Gravity Models from GRAIL Primary Mission Data," *Journal of Geophysical Research*, vol. 118, pp. 1676–1698, 2013.

[87] M. Emilio, J. R. Kuhn, R. I. Bush, and I. F. Scholl, "Measuring the Solar Radius from Space During the 2003 and 2006 Mercury Transits," *Astrophysical Journal*, vol. 750, article 135, 8 pages, 2012.

[88] B. A. Archinal, M. F. A'Hearn, E. Bowell, A. Conrad, G. J. Consolmagno, et al., "Report of the IAU Working Group on Cartographic Coordinates and Rotational Elements: 2009," *Celestial Mechanics and Dynamical Astronomy*, vol. 109, pp. 101–135, 2011.

[89] L. Iorio, H. I. M. Lichtenegger, M. L. Ruggiero, and C. Corda, "Phenomenology of the Lense–Thirring Effect in the Solar System," *Astrophysical Space Science*, vol. 331, pp. 351–395, 2011.

[90] J. Baer and S. R. Chesley, "Astrometric Masses of 21 Asteroids and an Integrated Asteroid Ephemeris," *Celestial Mechanics and Dynamical Astronomy*, vol. 100, pp. 27–42, 2008.

[91] J. Baer, S. R. Chesley, and R. D. Matson, "Astrometric Masses of 26 Asteroids and Observations on Asteroid Porosity," *Astronomical Journal*, vol. 141, article 143, 12 pages, 2011.

[92] F. Marchis, D. Hestroffer, P. Descamps, J. Berthier, C. Laver, and I. de Pater, "Mass and Density of Asteroid 121 Hermione from an Analysis of Its Companion Orbit," *Icarus*, vol. 178, pp. 450–464, 2005.

[93] P. Descamps, F. Marchis, T. Michalowski, F. Vachier, F. Colas, et al., "Figure of the Double Asteroid 90 Antiope from Adaptive Optics and Light-Curve Observations," *Icarus*, vol. 187, pp. 482–499, 2007.

[94] F. Marchis, P. Descamps, M. Baek, A. W. Harris, M. Kaasalainen, et al., "Main Belt Binary Asteroidal Systems with Circular Mutual Orbits," *Icarus*, vol. 196, pp. 97–118, 2008.

[95] F. Marchis, P. Descamps, J. Berthier, D. Hestroffer, F. Vachier, et al., "Main Belt Binary Asteroidal Systems with Eccentric Mutual Orbits," *Icarus*, vol. 195, pp. 295–316, 2008.

[96] D. K. Yeomans, P. G. Antreasian, J.-P. Barriot, S. R. Chesley, D. W. Dunham, et al., "Radio Science Results During the NEAR-Shoemaker Spacecraft Rendezvous with Eros," *Science*, vol. 289, pp. 2085–2088, 2000.

[97] M. Pätzold, T. P. Andert, S. W. Asmar, J. D. Anderson, J.-P. Barriot, et al., "Asteroid 21 Lutetia: Low Mass, High Density," *Science*, vol. 334, pp. 491–492, 2011.

[98] A. S. Konopliv, J. K. Miller, W. M. Owen, D. K. Yeomans, J. D. Giorgini, et al., "A Global Solution for the Gravity Field, Rotation, Landmarks and Ephemeris of Eros," *Icarus*, vol. 160, pp. 289–299, 2002.

[99] C. T. Russell, C. A. Raymond, A. Coradini, H. Y. McSween, M. T. Zuber, et al., "Dawn at Vesta: Testing the Protoplanetary Paradigm," *Science*, vol. 336, pp. 684–686, 2012.